NWC TP 6307

Effect of Turbulent Fluctuations on Infrared Radiation From a Tactical Missile Plume

Final Report for Period 29 April 1980 Through 9 February 1981

by
Blaine E. Pearce
Ashok K. Varma
Aeronautical Research Associates of Princeton, Inc.
for the
Ordnance Systems Department

FEBRUARY 1982

NAVAL WEAPONS CENTER
CHINA LAKE, CALIFORNIA 93555

Approved for public release; distribution unlimited

Naval Weapons Center

AN ACTIVITY OF THE NAVAL MATERIAL COMMAND

FOREWORD

This report presents results of an analytical investigation to assess the effects of turbulent fluctuations on the infrared thermal emission from a rocket exhaust plume. The work reported herein was conducted from 29 April 1980 through 9 February 1981 by Aeronautical Research Associates of Princeton, Inc., under Contract No. N60530-80-C-0165 to the Naval Weapons Center.

The effort described herein was supported by the Naval Air Systems Command under the Missile Propulsion Technology Block Program (AIRTASK A03W3300/008B/0F31300000). Mr. Lee N. Gilbert is the NWC technology manager for this program.

Mr. A. C. Victor, the technical coordinator for this contract, has reviewed this report for technical accuracy. This report is released for information at the working level and does not necessarily reflect the views of NWC.

Approved by
C. L. SCHANIEL, *Head*
Ordnance Systems Department
28 January 1982

Under authority of
J. J. LAHR
Capt., U.S. Navy
Commander

Released for publication by
R. M. HILLYER
Technical Director

NWC Technical Publication 6307

Published by ..... Technical Information Department
Collation ..... Cover, 51 leaves
First printing ..... 290 unnumbered copies

UNCLASSIFIED

SECURITY CLASSIFICATION OF THIS PAGE (When Data Entered)

REPORT DOCUMENTATION PAGE	READ INSTRUCTIONS BEFORE COMPLETING FORM
1. REPORT NUMBER: NWC TP 6307	2. GOVT ACCESSION NO.: AD-A117 013
	3. RECIPIENT'S CATALOG NUMBER:
4. TITLE (and Subtitle): EFFECT OF TURBULENT FLUCTUATIONS ON INFRARED RADIATION FROM A TACTICAL MISSILE PLUME. FINAL REPORT FOR PERIOD 29 APRIL 1980 THROUGH 9 FEBRUARY 1981	5. TYPE OF REPORT & PERIOD COVERED: Final Report, 29 April 1980–9 February 1981
	6. PERFORMING ORG. REPORT NUMBER: ARAP Report No. 445
7. AUTHOR(s): Blaine E. Pearce, Ashok K. Varma	8. CONTRACT OR GRANT NUMBER(s): N60530-80-C-0165
9. PERFORMING ORGANIZATION NAME AND ADDRESS: Aeronautical Research Associates of Princeton, Inc., Princeton, New Jersey	10. PROGRAM ELEMENT, PROJECT, TASK AREA & WORK UNIT NUMBERS: AIRTASK A03W3300/008B/0F31300000
11. CONTROLLING OFFICE NAME AND ADDRESS: Naval Weapons Center, China Lake, California 93555	12. REPORT DATE: February 1982
	13. NUMBER OF PAGES: 100
14. MONITORING AGENCY NAME & ADDRESS(if different from Controlling Office)	15. SECURITY CLASS. (of this report): UNCLASSIFIED
	15a. DECLASSIFICATION/DOWNGRADING SCHEDULE

16. DISTRIBUTION STATEMENT (of this Report)

Approved for public release; distribution unlimited.

17. DISTRIBUTION STATEMENT (of the abstract entered in Block 20, if different from Report)

18. SUPPLEMENTARY NOTES

19. KEY WORDS (Continue on reverse side if necessary and identify by block number)

Infrared Radiation
Radiation Transfer
Rocket Plumes
Turbulent Fluctuations

20. ABSTRACT (Continue on reverse side if necessary and identify by block number)

See back of form.

DD FORM 1 JAN 73 1473 EDITION OF 1 NOV 65 IS OBSOLETE
S/N 0102-LF-014-6601

UNCLASSIFIED

SECURITY CLASSIFICATION OF THIS PAGE (When Data Entered)

(U) *Effect of Turbulent Fluctuations on Infrared Radiation From a Tactical Missile Plume. Final Report for Period 29 April 1980 Through 9 February 1981*, by Blaine E. Pearce and Ashok K. Varma, Aeronautical Research Associates of Princeton, Inc. China Lake, Calif., Naval Weapons Center, February 1982. 100 pp. (NWC TP 6307, publication UNCLASSIFIED.)

(U) Predictions of the effect of turbulent fluctuations of temperature and species concentrations on the infrared thermal emission from an afterburning exhaust plume of a tactical missile are summarized. The high spectral resolution emissions from portions of the 4.3 μm CO_2 band are examined. A consistent set of mean flow and turbulence properties in the plume obtained from a second-order closure model of the turbulent flow is used in the calculation. A precise closure model of the turbulent flow is used in the calculation. A precise formulation of the mean radiance is given which includes contributions of second-order turbulence correlations and explicitly identifies the contribution of two-point spatial correlations along the line of sight. These correlations are shown to affect the structure of individual spectral lines for non-optically thin paths. Total plume intensities in narrow 5 cm^{-1} wide spectral intervals in the CO_2 blue and red spike regions are not significantly augmented by the turbulent fluctuations for this class of afterburning plumes. Turbulence augmentation is most important in the lower temperature outer edges of the plume and regions of downstream decay. The situations where turbulence augmentation could be an important contributor to total plume intensities and to exhaust plume diagnostics are identified.

CONTENTS

Figures (Contd.)

Figures (Contd.)

Figures (Contd.)

Figures (Contd.)

Tables:

ACKNOWLEDGMENT

This work was performed for the Naval Weapons Center, China Lake, CA under Contract No. N60530-80-R-0165 monitored by Mr. A.C. Victor. We thank our A.R.A.P. colleagues Dr. Guido Sandri and Dr. Robert McCullough for helpful discussions, and Ms. Susan Schiller for her careful preparation of the Manuscript. Dr. R.P. Rhodes of A.R.O., kindly made a copy of Reference 13 available before publication.

INTRODUCTION

This report summarizes the results of a study to assess the effects of turbulent fluctuations on the infrared thermal emission from a rocket exhaust plume. The propellant composition, length scales, and flight conditions are typical of those for a small tactical missile. We consider emission from the CO_2 molecule in the 4.3 μm wavelength region. This chemical species is formed in the afterburning region where the high velocity, high temperature, fuel rich rocket exhaust mixes with the ambient air. The region where the plume and ambient air mix is highly turbulent, with random fluctuations in temperature and radiating species concentration. The goal of this study was to determine how these fluctuating properties affect the gaseous thermal emission from this class of flows.

Our approach was to utilize the available turbulent flowfield computational capability that has evolved from the higher-order turbulence modeling efforts at Aeronautical Research Associates of Princeton.[1-3] The computational codes developed during these studies predict the second-order correlations of the fluctuating temperature and chemical species in addition to the mean (time-averaged) properties of the flow. These predictions allow the time-averaged radiance to be evaluated with contributions from these fluctuations as well as the mean properties of the exhaust plume flow.

The results of the study are presented in the following sequence. A brief background and motivation for the work is provided in the remainder of the Introduction. The second section presents a discussion of the flowfield calculations, which includes a systematic comparison of the higher-order closure results with those obtained from the BOAT

[1]Donaldson, C. duP., "Atmospheric Turbulence and Dispersal of Atmospheric Pollutants," Environmental Protection Agency, March 1973. (EPA-R4-73-016a, publication UNCLASSIFIED.)

[2]Fishburne,E.S., R.A.Beddini, and A.K. Varma, "The Computation of Afterburning Rocket Exhaust Plumes," Aeronautical Research Associates of Princeton, Inc., July 1976. (A.R.A.P. Report No. 283, publication UNCLASSIFIED.)

[3]Varma, A.K., E.S. Fishburne, and R.A. Beddini, "A Second-Order Closure Analysis of Turbulent Diffusion Flames," NASA Langley Research Center, June 1977. (NASA CR-145226, publication UNCLASSIFIED.)

module of the JANNAF Standard Plume Flowfield code (SPF).[4] This comparison is included because the SPF will be the industry-wide tool for predicting exhaust plume flows. The SPF predictions provide a reference against which the more detailed, second-order closure results can be compared. We also include in this section an assessment of the importance of the turbulent fluctuations on the chemical reactions. A derivation of the equation for the fluctuation augmented radiance is given in the third section. The results of the radiance predictions are given and discussed in the fourth section. In all cases, the radiance with fluctuations is compared with that ignoring the fluctuations. A summary and the conclusions are given in the final section.[5]

BACKGROUND

Infrared signature codes currently available for routine use, now[5] or in the near future,[6] account only for emission from the mean properties of the flow. However, the highly non-linear dependence of the emission and absorption on temperature suggests that the true, time-averaged* radiance should be different from that evaluated at the mean properties:

$$\overline{N}_\omega(T,c) \neq N_\omega(\overline{T},\overline{c}) \qquad (1)$$

A simple quantitative example is easy to construct. Assume that the temperature dependence of the Planck function $B_\omega(T)$ can be approximated by a simple power law of the form aT^m ($m = 4$ exactly for the total radiance, and $2 < m < 10$ for the spectral radiance, depending on the wavelength region and temperature). The time-averaged radiance,

[4]Dash, S.M., et al., "Operational Instructions for a Preliminary Version of the JANNAF Standard Plume Flowfield Model (SPF/1)," June 1980. (A.R.A.P. Report No. 415, publication UNCLASSIFIED.)

[5]Pergament, H.S., et al., "The Naval Weapons Center Target Signature Code," February 1979. (A.R.A.P. Report No. 380, publication UNCLASSIFIED.)

[6]Ludwig, C. et al., "Development and Validation of a Standardized Infrared Radiation Model (SIRRM)," JANNAF Standard Plume Model Workshop, U.S. Army Missile Command, Huntsville, AL, 2-3 April 1981. (paper, UNCLASSIFIED.)

*Averaged over times long compared to the time scale of the turbulent fluctuations.

accounting for the fluctuations T' about the mean temperature $\bar{T}$ is, approximately,

$$\bar{N}_\omega(T)/N_\omega(\bar{T}) = 1 + 1/2\ m(m-1)\ \frac{\overline{T'^2}}{\bar{T}^2} + \frac{O(\overline{T'^4})}{\bar{T}^4} + \ldots \quad . \qquad (2)$$

For afterburning rocket plumes, and many other turbulent flows, $\overline{T'^2}/\bar{T}^2 \sim 0.1$, suggesting that the temperature fluctuations alone can substantially enhance the radiance over that evaluated at the mean temperature. For example, if m = 5, the spectral mean radiance is doubled by the temperature fluctuations. Of course, the actual situation in a partially transparent volume of molecular emitters is more complicated. The species and temperature sensitivity of the molecular absorption can be either positive or negative, and there are spatial correlations between fluctuations along the line of sight that both augment and diminish the radiance. A precise evaluation of the net change in radiance requires that these additional factors be included. That is the goal of this study.

FLOWFIELD CALCULATIONS

REVIEW OF AVAILABLE CODES

Two state-of-the-art computer programs for the calculation of turbulent reacting flows are available to us for predicting the flowfield properties of missile plumes of interest. The studies are restricted to flowfields involving constant pressure mixing and reactions. One is the BOAT[7] code - the constant pressure turbulent mixing module of the JANNAF Standard Plume Model. The other code is the A.R.A.P. reacting shear layer (RSL) code.[2] The program has also been called the multi-equation turbulent reacting code (METREC) in some previous publications.[8] Some features of the two codes of interest in the current study are described below.

[7]Dash, S.M., and H.S. Pergament, "A Computational Model for the Prediction of Jet Entrainment in the Vicinity of Nozzle Boattails (The BOAT Code)," NASA Langley Research Center, 1978. (NASA CR-3175, publication, UNCLASSIFIED.)

[8]Fishburne, E.S., and A.K. Varma, "Investigations of Chemical Reactions in a Turbulent Media," Acta Astronautica, Vol. 6, 1979, pp. 297-308.

BOAT COMPUTER PROGRAM

The BOAT code solves a parabolic axisymmetric, steady viscous flow in which the turbulence is described by a two-equation, turbulence kinetic energy model. The code is capable of handling multi-species, multi-step chemistry. However, it does not calculate the correlations between the various fluctuating scalar quantities such as, species concentrations and between species concentrations and temperature that are expected to be important in turbulence-chemistry and turbulence-radiation interactions. The program calculates only two turbulence quantities; the turbulent kinetic energy, $1/2q^2 = 1/2(\overline{u'^2} + \overline{v'^2} + \overline{w'^2})$, and the dissipation rate, ε. The chemistry calculations in BOAT neglect the effect of the turbulent fluctuations on the reactions, and only the mean species and temperatures are used to calculate the chemical source terms.

RSL COMPUTER PROGRAM

The RSL code solves a parabolic, two-dimensional (planar or axisymmetric), steady, viscous flow that includes the conservation equations for the mean properties and all the independent second-order correlations for a simple reacting system. The code has been designed to handle a total of three chemical species undergoing a one-step forward reaction, $\alpha + \beta \rightarrow \gamma$. The use of the basic shear layer assumptions leads to a set of 23 independent, coupled, partial differential equations; equations for the mean variables, ρ, u_i, H, α, and β, and the second-order correlations. The computer program actually solves a total of 29 equations for a three-species system. The additional equations provide a check on the mass conservation in the program and on the accuracy of the numerical scheme.

A major objective of the RSL code development was to provide a research tool to study the interactive effects of turbulence and chemistry. In the current application, the effect of all the second-order correlations on the chemical source term for the one-step reaction can be included in the calculation. The interaction effects can also be ignored and only the mean variables used in the chemistry calculation. A comparison of the two procedures will provide a measure of the importance of the turbulence-chemistry interaction for the flow under study.

COMPARISON OF COMPUTER PROGRAMS

The two programs have different strengths and weaknesses as far as the objectives of the current study are concerned. The objective is to evaluate the effect of turbulent fluctuations of species and temperature on the mean gaseous radiation from an afterburning plume. The BOAT code

can handle the multi-step chemistry of the large number of species in a tactical missile plume with the neglect of turbulence-chemistry interaction effects. However, the BOAT code is unable to directly provide the values of various scalar correlations of species and temperature in the flow which have to be known to calculate their effect on the radiation. In the two-equation turbulence model approach, these scalar correlations will have to be estimated in some consistent manner from $1/2q^2$ and ε. The RSL code solves modeled equations for these scalar correlations and, therefore, directly provides their values across the flowfield, without the need for additional assumptions. However, the RSL code has been designed for a simple one-step chemical reaction. A modeling approach for multi-species, multi-step chemistry has been formulated for use within the framework of the RSL code,[2] but the approach requires many assumptions, and has not been extensively tested. It was decided that the salient features of turbulence-chemistry and turbulence-radiation interactions can be studied in a simple chemically reacting flow that models one aspect of afterburning in a real plume. The reaction parameters and flow conditions were chosen to simulate properties of the actual plume of interest. With the use of a simple one-step chemical reaction, it is possible to compare the results of the BOAT and RSL codes for the same flow conditions.

COMPARISON OF RESULTS OF THE TWO CODES FOR NONREACTING FLOWS

We emphasize that the comparison of predictions from these two codes was not a primary objective of this study. The decision was made to use the RSL code to provide both the mean and fluctuating properties of the plume because we believe that to be the best available code that provides all these quantities. In addition, it was an initial objective to provide predictions from the current codes in use throughout the industry for comparison, for both the flowfield and radiation. An initial calculation of a turbulent reacting axisymmetric jet of carbon monoxide (CO) in a coflowing air stream with the BOAT and RSL codes showed very significant differences between the results from the two codes. The parameter of the flow and the results are discussed later in this section. The differences between the codes for the reacting flow necessitated a more extensive comparison of the two codes for simpler flows, and a number of such flowfields were studied in order to isolate the reasons for these differences and also to compare the predictions with measurements. The results of these tests are discussed below. We include this comparison here because it serves at least two useful purposes. It establishes the validity of the mean flow predictions from RSL for this type of plume by comparison with the results from the more familiar SPF/1. Secondly, the overall validity of both codes is assessed by comparison with experiment.

Constant Density Axisymmetric Jet Into Still Air

The data selected for this test was that obtained by Maestrello and McDaid, and was Test Case 6 of the NASA Free Turbulent Shear Flows Conference.[9] The initial mean velocity profile was measured at a location 1 jet diameter ($x/r_j = 2$) downstream of the exit, and was used to start both the codes. The BOAT code used the standard k-ε* turbulence model. The q^2 and ε profiles at the initial station are derived with the use of a mixing length model. The RSL code is normally started with a cosine shaped profile for the turbulence kinetic energy, $q^2/2$, with an arbitrary maximum value of $.003(u_j - u_\infty)^2$. The length scale, Λ, is related to the shape of the q^2 profile; for an axisymmetric jet it is calculated as a constant times the distance from the jet axis to the point where q^2 is 25% of its maximum value. The standard value of the constant is 0.2. The results from the two codes are shown in Figure 1 along with the experimental results for the decay of the jet velocity on the centerline. Predictions from both the codes are reasonably satisfactory for this flow. The RSL code predicts a shorter core, but shows better agreement farther downstream.

The results for the two codes shown in Figure 1 are based on different initial turbulence levels and scales. It is feasible to match the initial turbulence levels and profiles in the two codes, but in the current formulation it is not possible to match the turbulence scales over the entire flowfield. Currently, RSL does not incorporate a transport equation for the scale. The scale is algebraically related to the local q^2 profile, and is constant across the profile at every axial station. A number of RSL runs were made after matching the mean velocity and turbulence kinetic energy profiles to the results obtained from the BOAT code at $x = 4r_j$. The ε profile was used to estimate the average turbulence scale $[(q^2/2)^{3/2}/\varepsilon]$ and indicated the proper constant to be ~ 0.13 at the initial station. It must be remembered that the value of the scale constant will have to be changed at other stations to continue to match the scale being used in the BOAT code, and this cannot be accomplished in the current RSL code. The RSL runs used three scale constants, 0.1, 0.15, and 0.2. The results are shown in Figure 2. The results show that by selecting a smaller scale constant that is in line with the scale in the BOAT code, the RSL code results for the length of the core are in good agreement with the BOAT code. Farther downstream, it appears that the scale constant should increase towards 0.2, the nominal value used in standard RSL runs.

---

[9]Free Turbulent Shear Flows, Vols. I & II, NASA Langley Research Center, July 1972. (NASA SP-321, publication UNCLASSIFIED.)

*The common terminology for the turbulence kinetic energy is $k = 1/2q^2$. Two-equation turbulence model codes are therefore referred to as k-ε models.

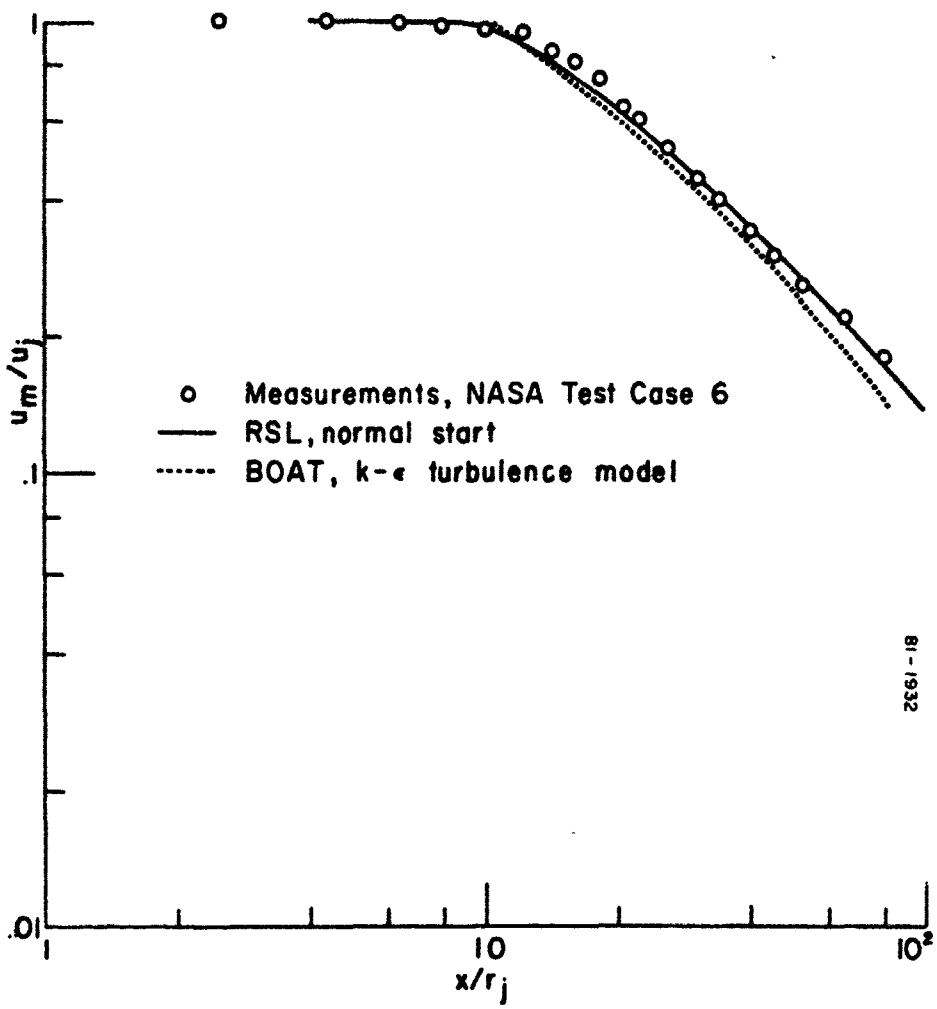

FIGURE 1. Predictions and Measurements of the Axis Velocity in a Constant Density, Low Speed, Inert Jet Exhausting into Still Air. NASA Test Case 6, u_j = 211 m/sec, r_j = .031 m.

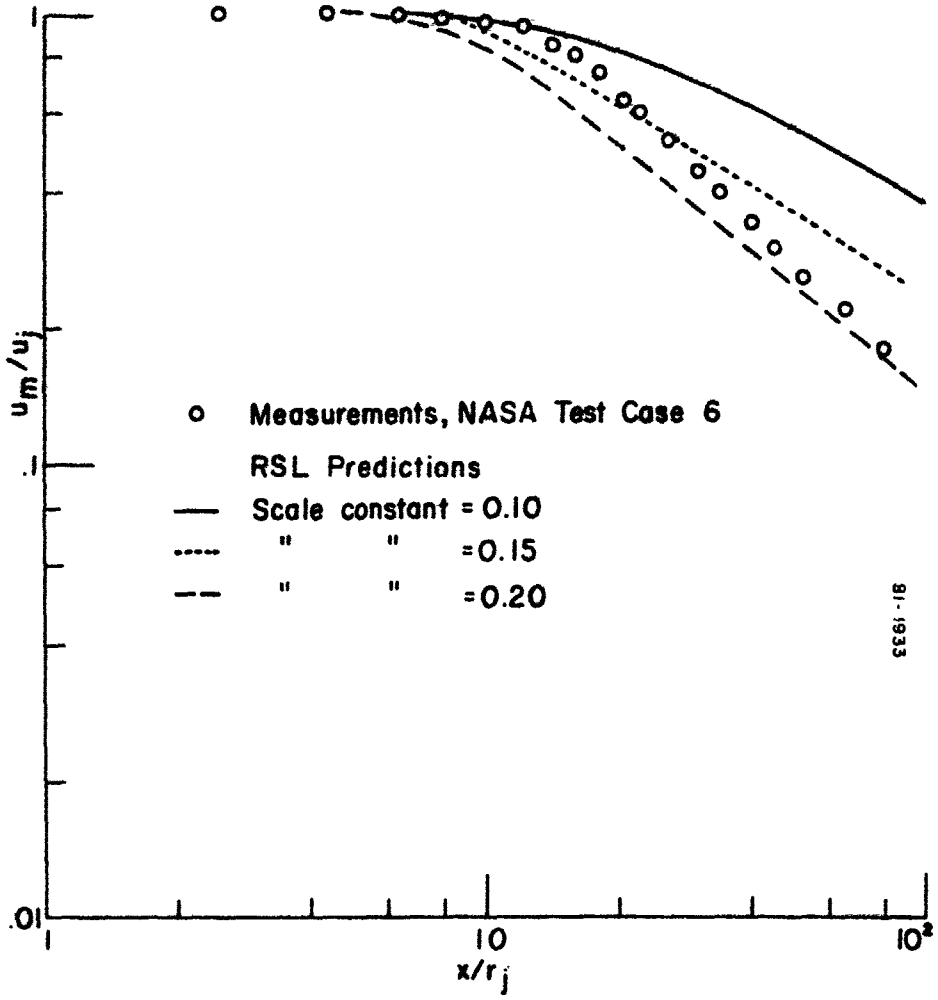

FIGURE 2. Effect of Varying the RSL Turbulence Length Scale Constant on Axial Velocity Decay. Initial Turbulence Level Matched to BOAT Run at $x = 4r_j$. Constant Density, Low Speed, Inert Jet Exhausting into Still Air.

In summary, both the codes are in reasonably good agreement with the experimental data for low speed isothermal jets when they each use their normal start procedures for the turbulence parameters. The results of the two codes also appear to be consistent with one another when the basic differences in the length scales used in the programs are taken into account.

Heated Axisymmetric Jet Into Still Air

Measurements of the decay of the axial velocity in heated axisymmetric jets into still air are reported in Abramovich.[10] The initial ratio of jet temperature to the ambient is 3.25. Both the codes were started with basically top hat mean profiles at the exit plane of the jet.* The length scale Λ is the same as in the isothermal jet study; 0.2 times the distance from the jet axis to the point where q^2 drops to 25% of its maximum value. This procedure will overestimate the scale to some degree in the potential core region where the turbulence is restricted to the shear layer region, but the scale specification will be correct farther downstream. The results from the two codes are shown in Figure 3. The RSL results are in better agreement with the data for this flow. The BOAT code predicts a much smaller effect of the lower density of the jet fluid compared to the results for the isothermal, constant density flow.

The major reason for the differences in the results obtained from the two codes for this flow is the different choices for the initial turbulence intensity and length scale. Some of the differences are also due to different modeling of density fluctuation terms in the full second-order closure turbulence model and the two-equation model. Some RSL runs were started with the initial conditions for the mean velocity, mean temperature, and turbulence kinetic energy matched to the results from the BOAT code at $x = 15.32r_j$, after the end of the potential core. The average Λ across the profile at this axial position in the BOAT results corresponds to the use of a scale constant of 0.25 in RSL instead of the normal value of 0.2 used in RSL for axisymmetric jet problems. RSL runs were made with the scale constant set equal to 0.2 and 0.25, and the results are shown in Figure 4. The results of these RSL runs with initial conditions matched to BOAT at $x = 15.32r_j$ show much better agreement with the downstream results obtained from BOAT, than the results shown earlier in Figure 3. The RSL run with the scale constant of 0.25, that approximately matches the initial scales in the two codes, deviates somewhat from the BOAT results, while much better

[10] Abramovich, G.N., The Theory of Turbulent Jets, The MIT Press, Cambridge, MA, 1963, Chapter 7.

*The initial q^2 profile in RSL was chosen to be sharply peaked near the jet radius, with a maximum value of $.003(u_j - u_\infty)^2$.

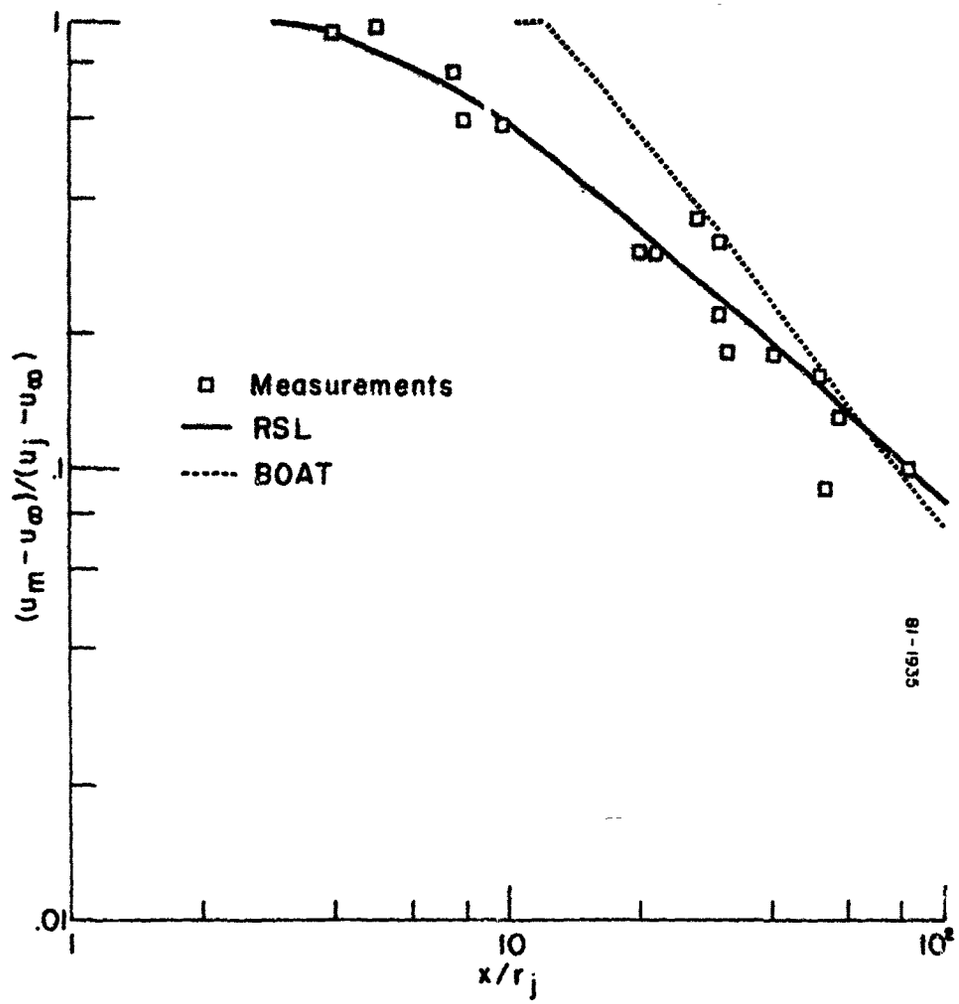

FIGURE 3. Axis Velocity in a Heated, Low Speed Jet, $T_j/T_\infty = 3.25$, $u_j = 7$ m/sec.

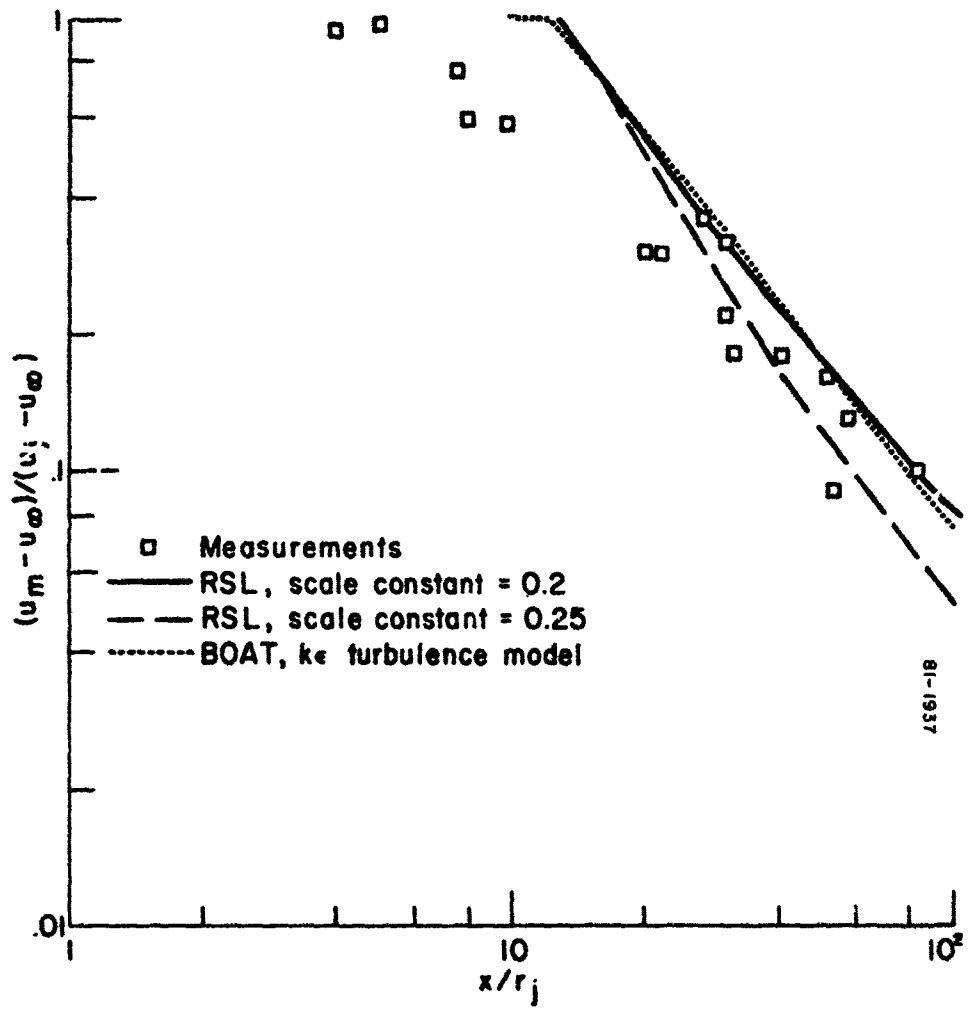

FIGURE 4. Effect of Varying Turbulence Length Scale Constant in a Heated, Low Speed Jet. BOAT, RSL Matched at $x/r_j = 15.32$. $T_j/T_\infty = 3.25$, $u_j = 7$ m/sec.

agreement is shown by the run with scale constant of 0.2. The differences between the RSL and BOAT runs with the matched initial scales may be due to a) differences in turbulence models in the codes, b) lack of agreement among the scales at downstream locations, or c) differences due to scale variation across the profile in BOAT, while RSL currently uses a constant scale across the profile for a jet flow.

In summary, the RSL code demonstrates significantly better agreement with the experimental data when it uses its normal start procedure. The BOAT code shows a very small effect of the density variation on the axial velocity decay profile, and is not in good agreement with the data.

Hydrogen Axisymmetric Jet Into A Moving Air Stream

Eggers[9] made measurements of mixing in relatively high speed streams of hydrogen and air. The centerline variation of the axial velocity and hydrogen mass fraction was measured. The initial velocity profile at the nozzle exit shows the presence of wall boundary layers, and has a substantial velocity defect. The RSL code has some difficulties starting from this initial profile due to the problem of specifying the proper turbulence scale distribution. A BOAT run was carried out from the initial profile, and then an RSL run was started using the results of the BOAT code at an axial station 4 radii downstream from the nozzle exit. The RSL run matched the mean velocity, mean species concentration, and the turbulent kinetic energy profile at the initial station. The average turbulent length scale across the profile at this axial station in the BOAT results corresponds to the use of a scale constant of 0.2 in RSL. The axis velocity and hydrogen mass fractions obtained from the BOAT and RSL codes (C = 0.2) are shown in Figures 5 and 6, respectively along with the experimental data. The BOAT code predictions are in good agreement with the data. The RSL results start out in good agreement with the BOAT results (as expected for matched initial conditions) but then deviate from them. We compared the length scales in the two codes at $x/r_j = 40$ and found that the average scale across the flow in BOAT was 50% higher than that in RSL. Farther downstream, at $x/r_j = 100$, the scales in the two codes are again comparable. We made another RSL run using a scale constant C = 0.3, and these results are also plotted in the figures. The velocity decay data is bounded by the RSL results with the two length scales. The species mass fraction is overpredicted at large distances, even with the larger scale constant. It is clear from these comparisons that much of the difference between the mean flow predictions of these two codes for this particular test case is due to the different length scales. Due to limitations in the length scale model currently being used in RSL, the RSL results for this flow are not very satisfactory. The results of the BOAT code for this flow are in good agreement with the data.

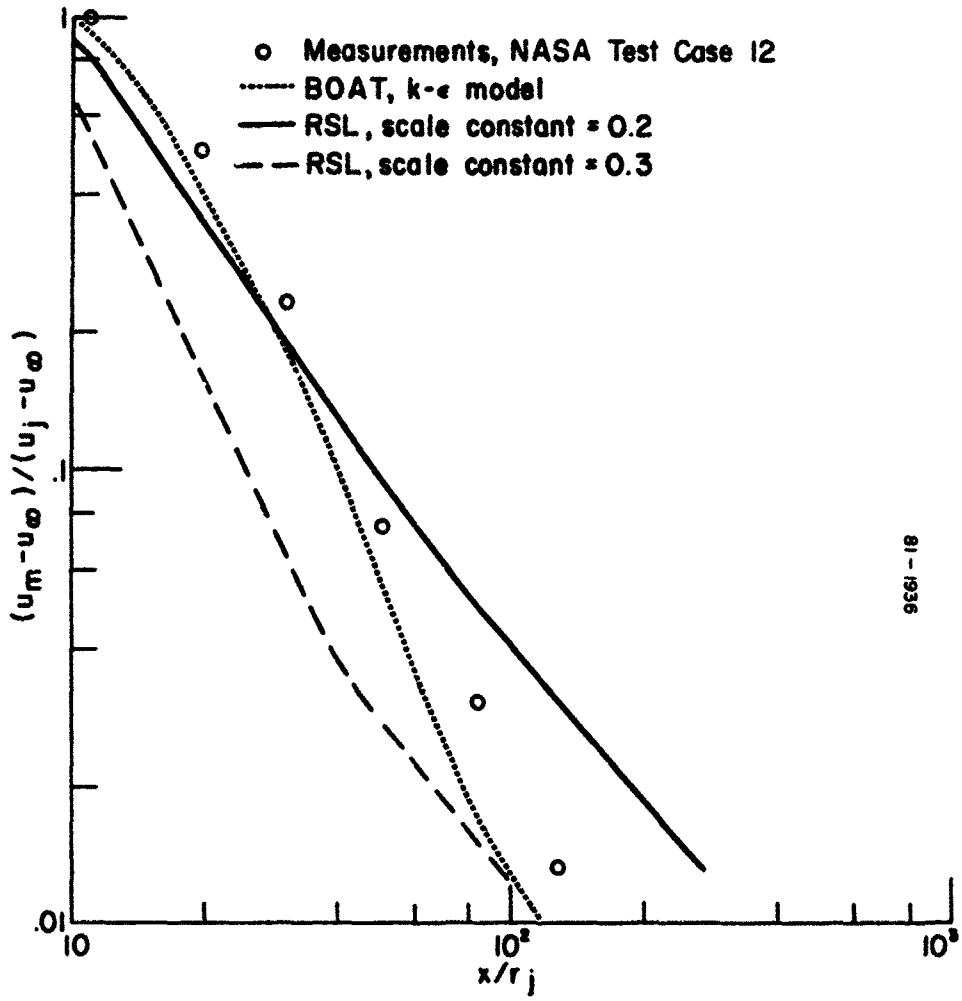

FIGURE 5. Axis Velocity in a Hydrogen Jet in a Coflowing Stream. NASA Test Case 12, u_j = 1074 m/sec, r_j = .0058 m, u_∞ = 394 m/sec.

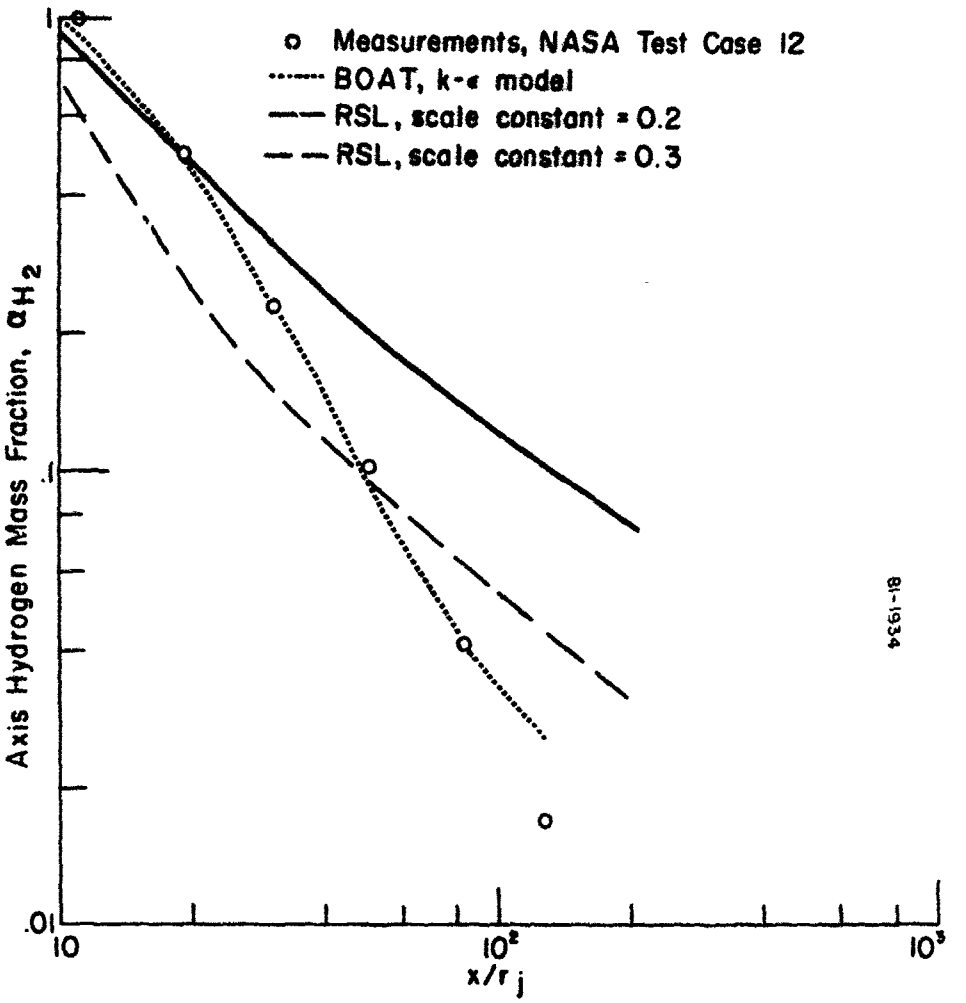

FIGURE 6. Axis Hydrogen Mass Fraction in a Hydrogen Jet in a Coflowing Stream. NASA Test Case 12.

Summary of RSL -- BOAT Comparisons For Non-Reacting Flows

The three test cases carried out here show mixed results. Both the codes are satisfactory for the constant density jet flow, but for the two variable density flows, RSL does better for the heated jet experiments while BOAT performs better for the light species jet. Further tests on more complex flows will have to be carried out to document the superiority of one code over the other. The predictions of the codes are in reasonable agreement with each other when the initial conditions for the turbulence scale and turbulent kinetic energy are matched.

REACTING FLOW CALCULATIONS

The two computer codes were used to calculate the flowfield properties of a turbulent reacting axisymmetric jet of carbon monoxide in a coflowing stream of air.* The initial conditions for the calculations were as follows:

TABLE 1. Initial Conditions for Model Afterburning Plume

Jet Stream	External Stream
u_j = 2500 m/sec	u_∞ = 300 m/sec
D = 0.13 m	T_∞ = 300°K
T_j = 1200°K	
Species Mass Fraction	**Species Mass Fraction**
CO = 0.25	O_2 = 0.23
N_2 = 0.75	N_2 = 0.77

*chosen to simulate the exhaust plume from a small (5000 lb_f thrust) tactical missile using a non-aluminized solid propellant.

For both cases, the initial velocity and species profiles were cosine curves between the jet and external stream values. The initial temperature profile had a peak temperature of 1836 K in the mixing region to ignite the CO jet. The BOAT code used its conventional start procedure (a mixing length model) to calculate the initial profiles of turbulence kinetic energy, $1/2q^2$, and the dissipation rate, ε. The BOAT code incorporates an empirical compressibility correction model to be used for high speed flows, and the calculations for the CO jet were made both with and without the use of this correction. The RSL code was also started with its normal start procedure. A cosine shaped profile for the turbulence kinetic energy $1/2q^2$ is used with a maximum value of $.003(u_j - u_\infty)^2$. The length scale, Λ is based on the q^2 profile with a scale constant of 0.2.

The carbon monoxide reaction with atmospheric oxygen is assumed to be an overall one-step irreversible reaction

$$\alpha + \beta \overset{k_f}{\rightarrow} \gamma \tag{3}$$

with α the air species (N_2,O_2),

β the plume species (CO,N_2),

γ the products (CO_2,N_2).

$$k_f = 2 \times 10^{13} \exp(-15000/RT) \tag{4}$$

This reaction mechanism is a significant simplification of the multi-step elementary reactions that are believed to take place. The chemical source terms in the BOAT code are calculated using the mean species concentrations and the mean temperature, and neglecting the effect of turbulent fluctuations on the chemistry. RSL calculations were carried out in two different ways; one using only the mean values, and the other including the effect of second-order species fluctuation correlations and mean square temperature fluctuations on the chemical source terms.

The axial variation of the maximum temperature in the flow obtained from the BOAT and RSL computer programs is plotted in Figure 7. The use of the compressibility correction in the BOAT predictions decreases the rate of mixing and extends the reaction zone to some degree. The RSL calculations shown here used only the mean scalar variables to calculate the chemical source terms, that is, the same procedure as in the BOAT code. The predictions of the RSL run with the normal value of the scale constant, $C = 0.2$ for axisymmetric jet flows, are significantly

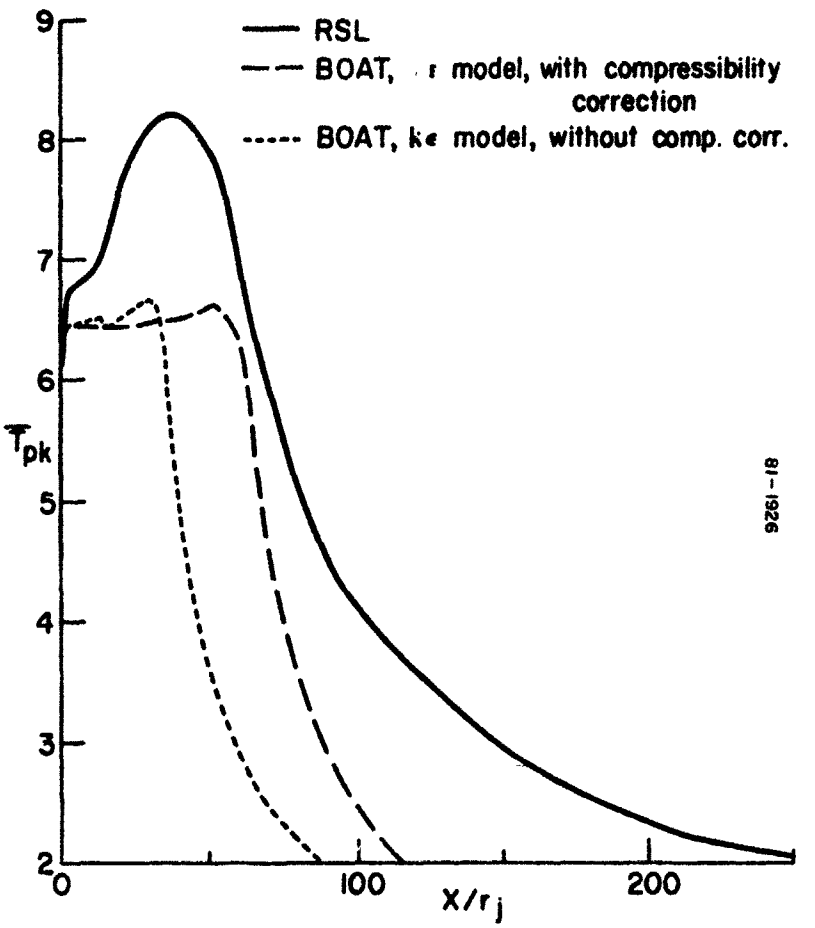

FIGURE 7. Peak Temperature in the Model Afterburning Exhaust Plume. Temperature Normalized by a Reference Temperature of 300 K.

different from both the BOAT predictions. A comparison of the values of the turbulence scale in the two codes at different axial stations was carried out, and the results are tabulated below.

TABLE 2 - Average Turbulence Scale Constants, $\Lambda/2r_j$

BOAT			RSL		
			scale constants		
x/r_j	with comp	w/o comp	C=0.15	C=0.2	C=0.25
0	0.10	0.10	0.13	0.17	0.21
20	0.33	0.37	0.15	0.21	0.27
40	0.66	0.58	0.19	0.31	0.47
100	1.08	0.87	0.36	0.72	1.12

At the initial station, the RSL scale length is larger, but at other axial stations, within the afterburning region ($x/r_j < 100$), the scale length is significantly smaller. At around $x/r_j = 100$, the difference becomes less than at earlier stations. Additional RSL runs were made with the scale constant set at 0.15 and 0.25 to attempt to resolve the discrepancy between the RSL and BOAT results. The complete set of results for the RSL cases is shown in Figure 8.

The scale in RSL runs with C = 0.25 is closer to the BOAT scale in the region from 10 to 50 diameters, and so are the predictions for the peak temperature. Still, there are other differences between the two results that cannot be explained by the different scales, but certainly matching the scales improves the agreement between the predicted results from the two codes.

For the purposes of the current study, we need the consistent set of species and temperature correlations provided by the RSL code. In the absence of experimental data on reacting afterburning plume flows to fix the empirical value of the scale constant, we will retain the standard value of 0.2 that we use for nonreacting axisymmetric jet flows.

TURBULENCE-CHEMISTRY INTERACTION

The non-linear dependence of the chemical reaction rate on temperature [Eq. (4)] suggests that, like the radiant emission, the time-averaged chemical species production is different from that evaluated at the mean temperature and species concentrations.

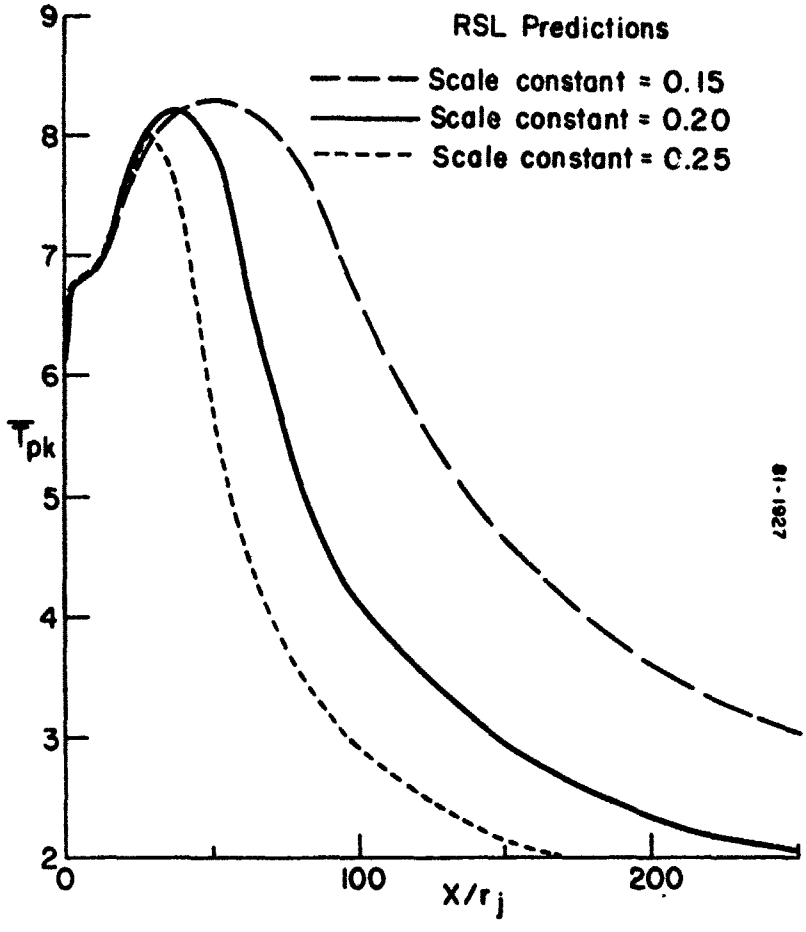

FIGURE 8. Peak Temperature in the Model Afterburning Exhaust Plume for Various Length Scale Constants. Peak Temperature Normalized by a Reference Temperature of 300 K.

Expansions of the species production rate, keeping terms up to the second-order correlations are included in RSL. The rate of formulation of product species, γ, is

$$d\gamma/dt = k_f \alpha \beta \tag{5}$$

If each term is expanded in terms of a mean and fluctuating part, $k_f = \bar{k}_f + k_f'$, $\alpha = \bar{\alpha} + \alpha'$, $\beta = \bar{\beta} + \beta'$, then

$$d\bar{\gamma}/dt = \bar{k}_f \bar{\alpha}\, \bar{\beta}(1 + \overline{\alpha'\beta'}/\bar{\alpha}\,\bar{\beta} + \ldots) \quad . \tag{6}$$

where

$$\bar{k}_f = k_f(\bar{T})[1 + \hat{E}(\hat{E}/2 - 1)\overline{T'^2}/\bar{T}^2 + \ldots] \quad . \tag{7}$$

The neglected terms involve second-order correlations of k_f' with α', β', and all third- and higher-order correlations. $\overline{\alpha'\beta'}/\bar{\alpha}\,\bar{\beta}$ is the "unmixedness correlation" which defines the effect of species fluctuations on the reaction rate. In a diffusion flame where the reactants are initially separated (as the case for afterburning rocket plume), this correlation is negative. Limiting cases are:[8]

fast chemistry: $\overline{\alpha'\beta'}/\bar{\alpha}\,\bar{\beta} \to -1.0$

slow chemistry: $\overline{\alpha'\beta'}/\bar{\alpha}\,\bar{\beta} \to -0.2$.

RSL runs have been made using the above expression for the chemical source term as well as using only the mean variables; that is, $d\gamma/dt = k_f(T)\alpha\,\beta$. The two results are shown in Figure 9. The calculations show that in this simulation of an afterburning plume, the chemical reactions are virtually completed at 50 radii downstream of the nozzle exit. The fuel (CO) mass concentration has decreased from an initial value of 0.25 to about 0.02 at this station. Further downstream, the flow is simply the mixing and cooling of a hot axisymmetric jet. The turbulence-chemistry interaction effects will only be important in the initial reacting region, and the inclusion of the species fluctuations, as expected, acts to reduce the reaction rate, and leads to a slightly lower peak temperature. Due to the small extent of the reaction zone, turbulence-chemistry interactions are not very important in this flowfield. The axial profile of the peak temperature is virtually identical for the two runs beyond 50 radii.

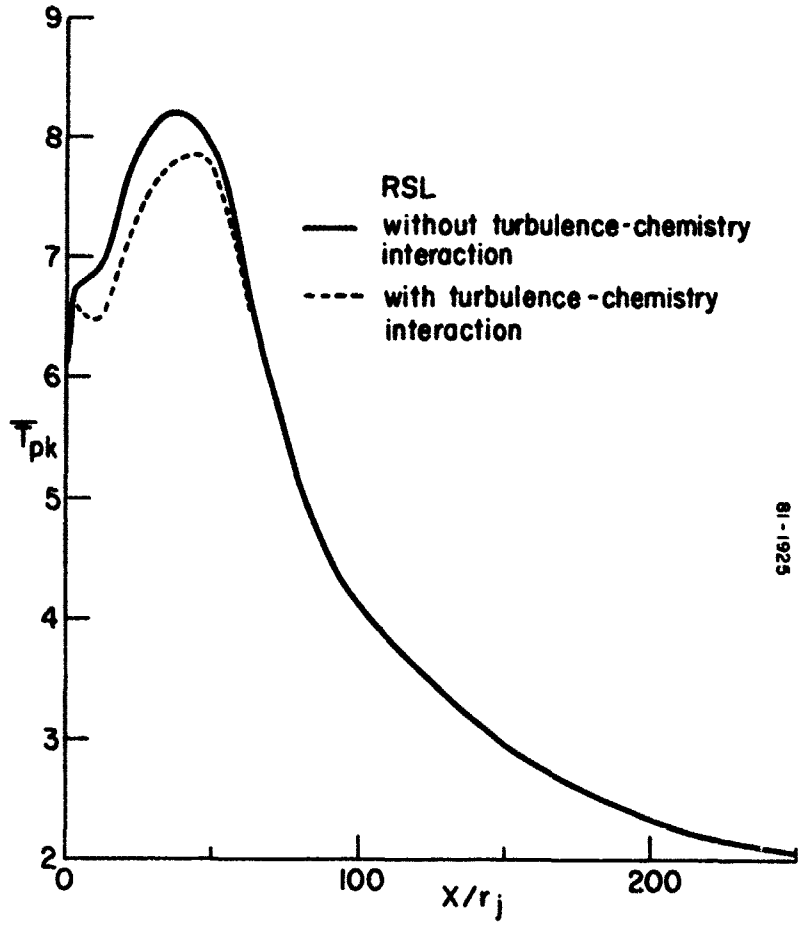

FIGURE 9. Effect of Turbulent Fluctuations on Peak Temperature in the Model Afterburning Exhaust Plume. Peak Temperature Normalized by a Reference Temperature of 300 K.

The fact that the turbulence-chemistry interaction is not a major factor in this particular flow can be explained by two effects. One is that the magnitude of the "unmixedness correlation" is insufficient to substantially reduce the reactant production below its nominal time-averaged value. Moreover, the effect of the temperature fluctuations acts in the opposite direction to increase the rate constant (for exothermic reactions). These two effects, unmixedness and temperature fluctuations, therefore tend to cancel each other. It is important to note also that this result is highly dependent on the specific reactions because the augmentation by temperature fluctuations depends on activation energy.[8] For the case considered here, $\hat{E} = E/\overline{RT} \leq 7.5$ in the reacting layer and $\overline{T'^2}/\overline{T}^2 \leq 0.1$. For these conditions, the rate constant is at most tripled, which is insufficient to significantly change the mean flow properties even if there were no compensating unmixedness correction. The detailed results for the exhaust plume certainly support these qualitative arguments. We caution that each flow situation and chemical system must be individually examined for the relative importance of these effects. More importantly, the conclusions here are based on a global reaction scheme. It is possible that a more precise specification of the chemistry, in terms of the elementary reactions involving all the trace species, will be more sensitive to the turbulence.

COMPARISON OF TURBULENCE QUANTITIES

The final comparison between the RSL and BOAT code predictions is between the radial profiles of mean temperature, and the turbulence quantity predicted by both codes; the turbulence kinetic energy. The mean square temperature fluctuation $\overline{T'^2}$ and product species fluctuation $\overline{\gamma'^2}$* from the RSL code are also shown. The radial mean temperature profiles at $x/r_j = 40$ and $x/r_j = 100$ and radial profiles of the turbulence kinetic energy, temperature and species correlations are plotted in Figures 10 and 11. The profiles for the mean temperature and the turbulence kinetic energy at the same axial stations from the BOAT code are shown in Figures 12 and 13 without and with the compressibility correction, respectively. Due to the extended reaction zone in the BOAT predictions with the compressibility correction, the mean temperature profiles at $x/r_j = 40$ are quite different. The turbulence level with the compressibility correction is increased over that without the

*This quantity is a mean square mass fraction fluctuation. The radiation formulation requires mole fractions. The conversion from mass fraction to mole fraction in this case is $c' = \gamma' c/\gamma$, approximately. In the most general case, conversion from fluctuating mass fraction to mole fraction involves correlations between all species. The largest error in neglecting the fluctuations occurs in mixtures with species with disparate molecular weights (e.g., hydrogen containing mixtures). The error is negligible for the mixture considered here.

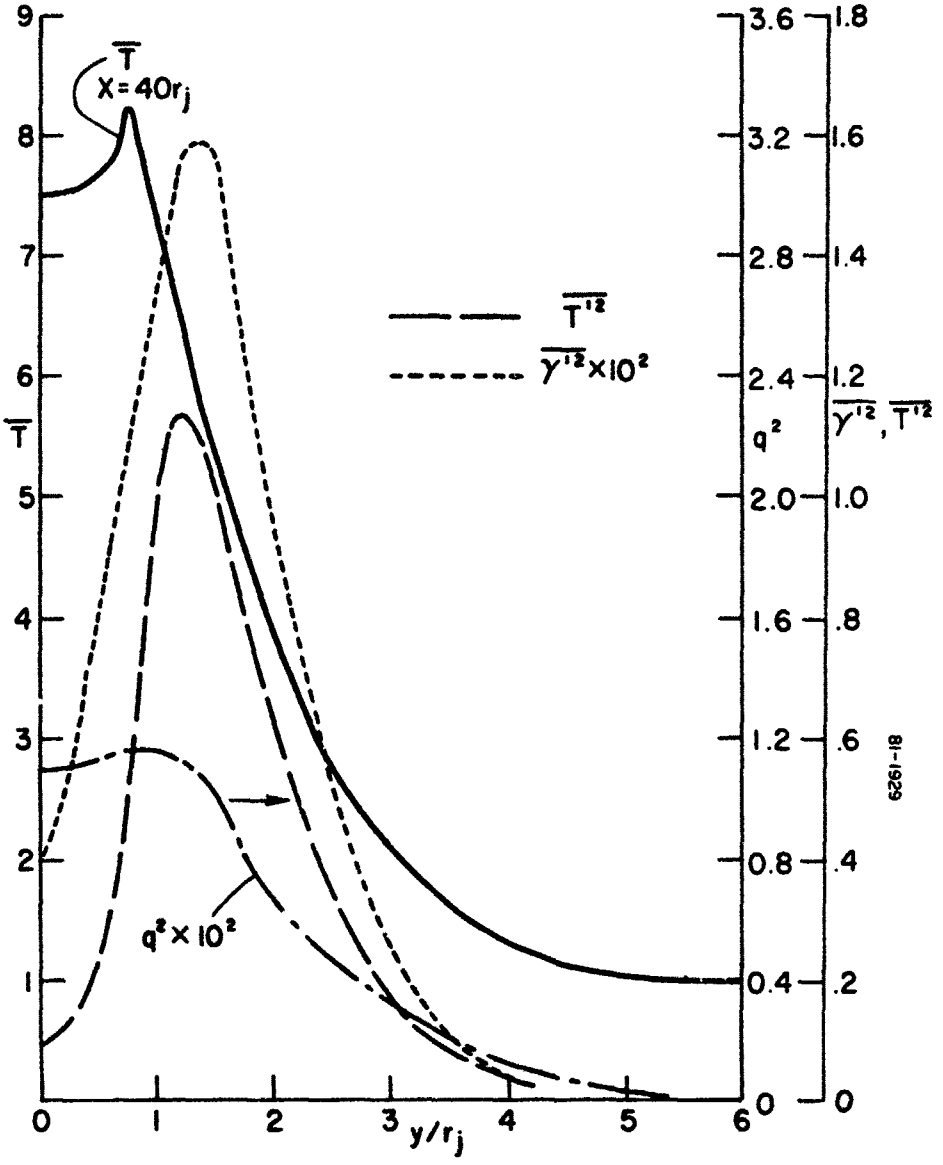

FIGURE 10. Radial Distribution of Mean and Fluctuating Properties Predicted by RSL Code for the Model Afterburning Exhaust Plume at $x/r_j = 40$. Temperature and Velocity Normalized by Reference Values of 300 K and 2500 m/sec, Respectively.

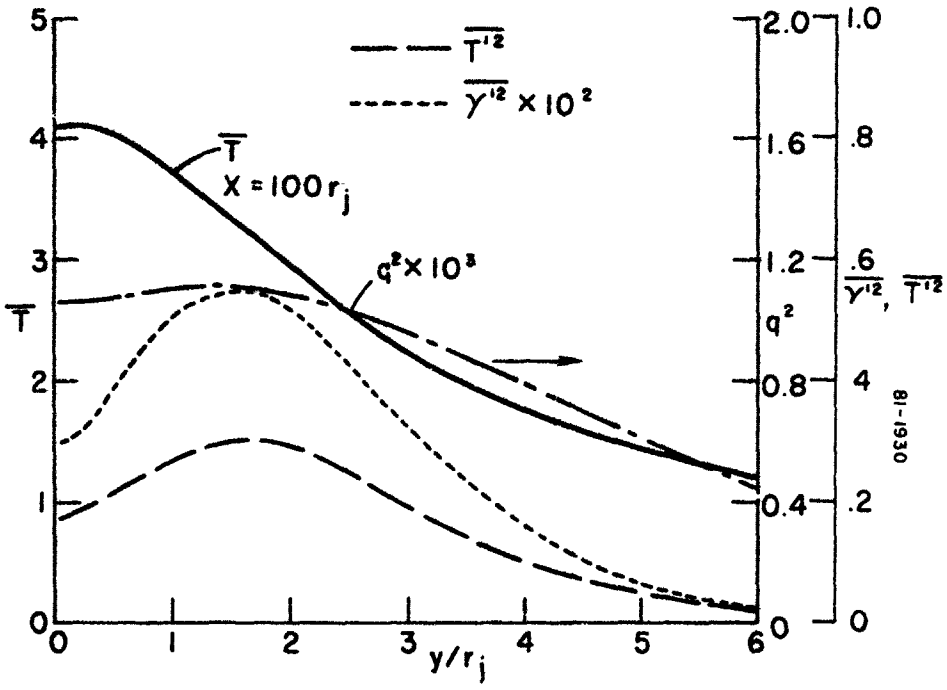

FIGURE 11. Radial Distribution of Mean and Fluctuating Properties Predicted by RSL Code for the Model Afterburning Exhaust Plume at $x/r_j = 100$. Temperature and Velocity Normalized by Reference Values of 300 K and 2500 m/sec, Respectively.

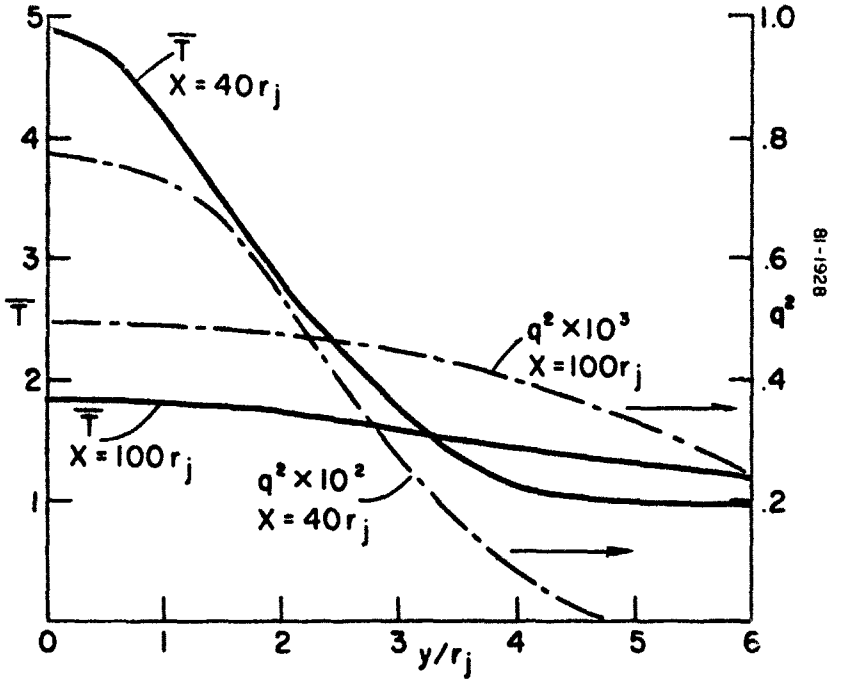

FIGURE 12. Radial Profiles of Mean and Fluctuating Properties Predicted by the BOAT Code <u>without</u> a Compressibility Correction for the Model Afterburning Exhaust Plume at $x/r_j = 40$ and 100. Temperature and Velocity Normalized by Reference Values of 300 K and 2500 m/sec, Respectively.

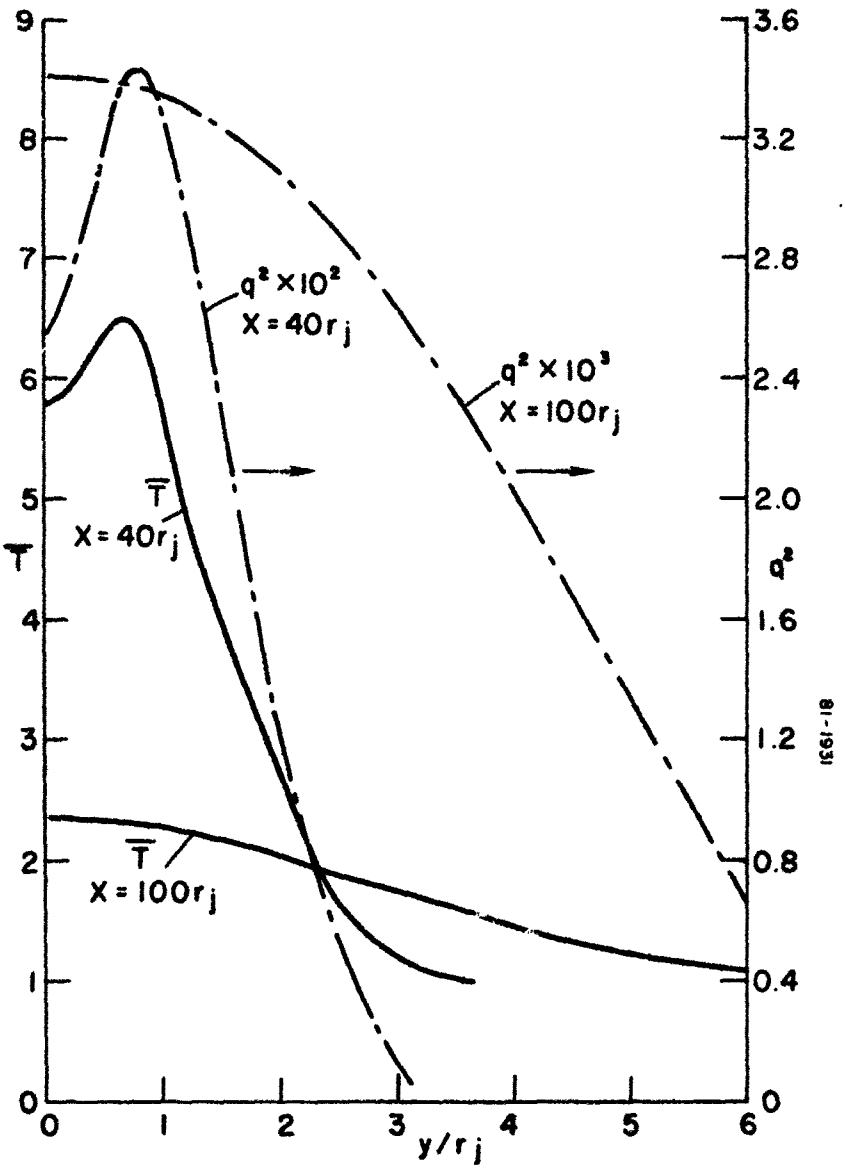

FIGURE 13. Radial Profile of Mean and Fluctuating Properties Predicted by the BOAT Code with a Compressibility Correction for the Model Afterburning Exhaust Plume at x/r_j = 40 and 100. Temperature and Velocity Normalized by Reference Values of 300 K and 2500 m/sec, Respectively.

correction, and is larger than that predicted by the RSL code.

The turbulent kinetic energy levels predicted by the RSL code are comparable to the levels in the BOAT predictions without the compressibility corrections in spite of the differences in the mean properties. This agreement is not a verification of the predictions from either code, but it is an encouraging result, particularly since the other turbulence correlations predicted by RSL are to be used to study the effect of fluctuations on the radiation from the hot reaction products without benefit of a similar comparison. The differences in the predictions of the mean properties in the two codes for reacting flows require further investigation and detailed comparison with experimental measurements to assess the relative performance of the two codes.

The RSL results for the scalar correlations, $\overline{\gamma'^2}$ and $\overline{T'^2}$, and the velocity correlation q^2, show that these radial profiles are quite different. It is not correct to directly relate these other scalar correlations to the turbulent kinetic energy alone. Thus, the coupling of turbulence and chemistry and/or turbulence and radiation that requires information about many second-order correlations, cannot be adequately studied with a flowfield code using simply the two-equation, k-ε turbulence model alone. Additional turbulence equations and model assumptions will have to be used for this task. For example, three-equation, k-ε-g turbulence models, algebraic stress modeling (quasi-equilibrium models), or complete second-order closure models as used in the RSL code are required.

RADIATION FROM A FLUCTUATING FLAME

We begin with the integrated equation of transfer for the spectral radiance along a given optical path through the plume

$$N_\omega = \int_0^L B_\omega(T)\, k_\omega(T) c \left[\exp - \int_0^s k_\omega c\, ds' \right] ds \quad . \tag{8}$$

k_ω is the spectral absorption coefficent which is due to the summation of the contribution from many rotational lines in a vibration-rotational band. The spectral dependence of this absorption is very complicated; it varies by an order of magnitude within spectral intervals comparable to a line width ($< .05\ cm^{-1}$), and there may be hundreds of lines of varying strength contributing to the absorption at a given wavenumber. In the typical spectral resolution of low-resolution radiance predictions ($5 - 25\ cm^{-1}$), there may be contributions from thousands of lines. There are two ways of dealing with this computational

problem: one is to perform the calculation on a purely monochromatic basis (line-by-line approach) and accept the computational penalty; the other is to use a band model approach in which the absorption is spectrally averaged over many lines before the spatial integration is performed. For homogeneous optical paths, this interchanging of the spectral and spatial integration is exact. However, for non-homogeneous paths, it is exact only for optically thick or optically thin paths. Intermediate optical depths are essentially an interpolation between these two limits that requires spatial averages of two parameters: the absorption coefficient, and the ratio of average line width to spacing.[11,12] These spatial averages make application of the band model calculation difficult to apply when the optical path is to include the fluctuating quantities.*[13] The line-by-line approach was therefore chosen for this study. This permits the direct expansion of the radiance in terms of known mean and second-order correlations of the fluctuating properties provided by the turbulent flowfield solution.

There is a disadvantage to choosing the line-by-line formulation. The required tabulation of line properties (spectral positions, strengths, and quantum states) is incomplete. Vibrational transitions between energy states that become populated only at high temperatures ($> 600^{o}K$) are absent from the available compilation.[14] However, an alternative source for these "hot lines" has been devised for the linear

[11]Ludwig, C.B., et al., Handbook of Infrared Radiation from Combustion Gases, 1973. (NASA SP-3080, publication UNCLASSIFIED.)

[12]Young, S.J., "Nonisothermal Band Model Theory," The Aerospace Corporation, September 1976. (SAMSO-TR-76-207, publication UNCLASSIFIED.)

*Rhodes[13] used the clever approach of defining an ensemble average of the radiance over many realizations of the optical path. Properties at each point were chosen by random selection from an assumed probability density distribution. The mean radiance was obtained by arithmetrically averaging the radiance for each realization of the optical path.

[13]Rhodes, R.P., "The Effect of Turbulent Fluctuations on the Infrared Radiation from Rocket Plumes," 12th JANNAF Plume Technology Meeting, CPIA Publication 332, Vol. III, December 1980, pp. 81-97. (paper, UNCLASSIFIED.)

[14]McClatchey, R.A., et al., "AFCRL Atmospheric Absorption Line Parameters Compilation," Air Force Geophysics Lab., January 1973. (AFCRL-TR-73-0096, publication UNCLASSIFIED.)

CO_2 molecule.[15] In the optically thin limit, the band model and line-by-line computations are equivalent. The temperature sensitivity of emission from the 4.3 μm CO_2 band has recently been described in this limit for the band model formulation.[16] However, the need in the present study was for an approach that was uniformly valid for any optical depth. Therefore, the line-by-line formulation was chosen. Because the pressure is atmospheric and the temperatures are moderate, we assumed a Lorentz line shape and considered only collision broadening.

A precise evaluation of the radiance from a fluctuating optical path requires a joint probability density function, PDF(T, c_i, $\vec{x}$), for the temperature and composition at every point in the plume, $\vec{x}$, along the optical path. However, the properties available are the mean values $\bar{T}$, $\bar{c}_i$, and second-order correlations, $\overline{T'^2}$, $\overline{c_i'T'}$, and $\overline{c_i'c_j'}$ at each point. The fluctuating radiance calculated here can use only these quantities. The approach was to decompose each variable into its mean and fluctuating part. For primary variables, these two components are obtained directly from the turbulent flowfield solution. Secondary quantities such as the Planck function and absorption coefficient were expanded about their values at the mean temperature and composition to express their fluctuations in terms of the fluctuating species and temperature.

$$B_\omega(T) = B_o + B' = B_\omega(\bar{T}) + \bar{T}\, dB/dT\, T'/\bar{T} + 1/2\bar{T}^2\, d^2B/dT^2\, T'^2/\bar{T}^2 + \ldots \tag{9}$$

$$k_\omega(T) = k_o + k' = k_o(\bar{T},\bar{c}) + \bar{T}\, \partial k/\partial T\, T'/\bar{T} + \partial k/\partial c\, c'$$

$$+ 1/2\, \bar{T}^2\, \partial^2 k/\partial T^2\, T'^2/\bar{T}^2 + \bar{T}\, \partial^2 k/\partial T \partial c\, c'T'/\bar{T} + 1/2\, \partial^2 k/\partial c^2\, c'^2 + \ldots \tag{10}$$

These two expansions, along with $T = \bar{T} + T'$ and $c = \bar{c} + c'$ were used in Eq. 8, which was expanded, retaining only terms up to and including the second-order correlations $\overline{T'^2}$, $\overline{c'T'}$, and $\overline{c'^2}$. The algebra is tedious,

[15]McCullough, R.W., "Compilation of CO_2 Rotational Lines Including Transitions That Are Important at Temperatures up to 2000°K, Aeronautical Research Associates of Princeton, Inc., unpublished, December 1980. (paper, UNCLASSIFIED.)

[16]Draper, J.S., L.S. Bernstein, and W.K. Cheng, "Fluctuating Emission from Molecular Vibrational-Rotational Bands," J. Quart. Spectrosc. and Radiat. Transfer, Vol. 23, 1980, pp. 323-326.

and only the final result is given here.

The particular property of the fluctuating radiance we chose to evaluate was the time-averaged value, $\bar{N}_\omega(T,c)$. This quantity is what would be measured by a sensor that has a temporal response that is slow compared to the frequencies of the plume fluctuations. There are other quantities of interest which define the effect of turbulent fluctuations, such as the mean square radiance fluctuation, $\overline{(N_\omega - \bar{N}_\omega)^2}$. However, this quantity does not indicate the direction in which the fluctuations act on the radiance; enhancing or diminishing the average radiance from the value that was obtained using only mean flow properties.

The final result for the average radiance is given below. The steps taken in its derivation were:

1) expand each term in the integral in terms of its mean and fluctuating component,

2) expand the transmittance integral about the mean optical path, separating out the optical depth of the mean flow; and then expand the fluctuating part:

$$\exp\left(-\int_0^s k\,c\,ds'\right) = \exp\left(-\int_0^s k_o\bar{c}\,ds'\right)\exp\left(\int_0^s F(c',T',\ldots)\,ds'\right)$$

$$= \exp\left(-\int_0^s k_o\bar{c}\,ds'\right)\left\{1 - \int_0^s F(c',T',\ldots)ds' + 1/2\left[\int_0^s F(c',T'\ldots)ds'\right]^2 + \ldots\right\} \tag{11}$$

where $F(c',T'\ldots)$ denotes terms involving the fluctuating properties.

Note that the square of the integral within the expansion can be expressed as a double integral over the square domain with area s^2.

3) Perform the multiplications and discard all higher-order terms beyond the second-order correlations,

4) time-average the result.

In the time-average, all terms involving c' and T' alone have zero

averages (from the definition of the fluctuations). All terms involving products, T'^2, $c'T'$, c'^2, give the second-order correlations $\overline{T'^2}$, $\overline{c'T'}$, and $\overline{c'^2}$. A special case of the second-order correlations occurs in evaluating the integral terms. The following forms of integrals must be averaged.

$$\overline{\int_0^L A(s)\, T'(s) \int_0^s B(s')\, T'(s')\, ds\, ds'} \tag{12a}$$

$$\overline{\int_0^L C(s) \int_0^s \int_0^s A(s')\, T'(s')\, B(s'')\, T'(s'')\, ds'\, ds''\, ds} \tag{12b}$$

where A(s), B(s), and C(s) are terms involving derivatives of B_ω and k evaluated at the mean flow properties at the point s. We express these time-averages as,

$$\overline{\int_0^L \int_0^s A(s)\, T'(s)\, B(s')\, T'(s')\, ds'\, ds} = \int_0^L \int_0^s A(s)\, B(s')\, \overline{T'(s)\, T'(s')}\, ds'\, ds \tag{13a}$$

$$\overline{\int_0^L C(s) \int_0^s \int_0^s A(s')\, B(s'')\, T'(s')\, T'(s'')\, ds'\, ds''\, ds} =$$

$$= \int_0^L C(s) \int_0^s \int_0^s A(s')\, B(s'')\, \overline{T'(s')T'(s'')}\, ds'\, ds''\, ds\,. \tag{13b}$$

These averages give the two-point correlation of the turbulent fluctuations along the optical path. In the subsequent analysis, these correlations are expressed in terms of the correlation coefficients,

$$\overline{T'(s)\,T'(s')} = [\overline{T'^2}(s)]^{1/2}\,[\overline{T'^2}(s')]^{1/2} r_{TT}(s,s') \quad (14)$$

There are similar correlations between c' and T', and between c' and c'. In all cases, we use an exponential form of the correlation

$$r_{TT}(s,s') = \exp\left(-|s - s'|/\ell\right) \quad (15)$$

where ℓ is a correlation length which we take to be the same for all the scalar correlations. It was our original intent to choose different functional forms for the correlation to test the sensitivity of the mean radiance to these terms. However, this particular form admits a convenient transformation that gives an accurate numerical quadrature, and so this form was maintained throughout the study. We argue that this term always appears as an integral and therefore, the sensitivity to the precise form of the integrand is reduced. The correlation length, ℓ, is a parameter that was varied over a wide range.

Following the procedure outlined above gives the equation for the time averaged spectral radiance from a turbulent flow. As in most radiative transfer problems, we have taken the step of using the mean optical path length rather than the geometric path length as the variable of integration

$$\tau = \int_0^s k_o \bar{c}\, ds' \quad (16)$$

$$\int_0^L F(s)\, k_o \bar{c} \exp\left(-\int_0^s k_o \bar{c}\, ds'\right) ds = \int_0^{\tau_L} F[s(\tau)]\, e^{-\tau}\, d\tau \quad . \quad (17)$$

The full equation for the time-averaged radiance is

$$\bar{N}_\omega = \int_0^{\tau_L} B_o e^{-\tau} d\tau + \tag{18a}$$

$$+ \int_0^{\tau_L} \left[\left(\frac{1}{2} \bar{T}^2 B_o k_{TT}/k_o + \bar{T}^2 B_T k_T/k_o + \frac{1}{2} \bar{T}^2 B_{TT} \right) \overline{T'^2}/\bar{T}^2 \right. \quad *$$

$$+ \left(\bar{T} B_o k_T/k_o + \bar{T} B_T k_c/k_o + \bar{T} B_o k_T/k_o \bar{c} + \bar{T} B_T/\bar{c} \right) \overline{c'T'}/\bar{T}$$

$$\left. + \left(\frac{1}{2} B_o k_{cc}/k_o + B_o k_c/k_o \bar{c} \right) \overline{c'^2} \right] e^{-\tau} d\tau + \tag{18b}$$

$$- \int_0^{\tau_L} B_o \int_0^s \frac{1}{2} \bar{T}^2 k_{\sim T} \bar{c}\, \overline{T'^2}/\bar{T}^2 + \left(\bar{T} k_{cT} \bar{c} + \bar{T} k_T \right) \overline{c'T'}/\bar{T} + \left(\frac{1}{2} k_{cc} \bar{c} + k_c \right) \overline{c'^2}\, ds'\, e^{-\tau} d\tau \tag{18c}$$

$$- \int_0^{\tau_L} \left(\bar{T} B_o k_T/k_o + \bar{T} B_T \right) \left(\overline{T'^2}/\bar{T}^2 \right)^{1/2} \int_0^s \bar{T} k_T \bar{c} \left(\overline{T'^2}/\bar{T}^2 \right)^{1/2} r_{TT}(s,s')\, ds'\, e^{-\tau} d\tau \tag{18d}$$

$$- \int_0^{\tau_L} \left(\bar{T} B_o k_T/k_o + \bar{T} B_T \right) \left(\overline{T'^2}/\bar{T}^2 \right)^{1/2} \int_0^s \left(k_o \bar{c} + k_o \right) \left(\overline{c'^2} \right)^{1/2} r_{cT}(s,s')\, ds'\, e^{-\tau} d\tau \tag{18e}$$

$$- \int_0^{\tau_L} \left(B_o k_c/k_o + B_o/\bar{c} \right) \left(\overline{c'^2} \right)^{1/2} \int_0^s \bar{T} k_T \bar{c} \left(\overline{T'^2}/\bar{T}^2 \right)^{1/2} r_{cT}(s,s')\, ds'\, e^{-\tau} d\tau \tag{18f}$$

$$- \int_0^{\tau_L} \left(B_o k_c/k_o + B_o/\bar{c} \right) \left(\overline{c'^2} \right)^{1/2} \int_0^s \left(k_c \bar{c} + k_o \right) \left(\overline{c'^2} \right)^{1/2} r_{cc}(s,s')\, ds'\, e^{-\tau} d\tau \tag{18g}$$

$$+ \frac{1}{2} \int_0^{\tau_L} B_o \int_0^s \int_0^s \left[\bar{T} k_T \bar{c} \left(\overline{T'^2}/\bar{T}^2 \right)^{1/2} \right]_{s''} \left[\bar{T} k_T \bar{c} \left(\overline{T'^2}/\bar{T}^2 \right)^{1/2} \right]_{s'} r_{TT}(s',s'')\, ds'\, ds''\, e^{-\tau} d\tau \tag{18h}$$

$$+ \int_0^{\tau_L} B_o \int_0^s \int_0^s \left[\bar{T} k_T \bar{c} \left(\overline{T'^2}/\bar{T}^2 \right)^{1/2} \right]_{s''} \left[\left(k_c \bar{c} + k_o \right) \left(\overline{c'^2} \right)^{1/2} \right]_{s'} r_{cT}(s',s'')\, ds'\, ds''\, e^{-\tau} d\tau \tag{18i}$$

$$+ \frac{1}{2} \int_0^{\tau_L} B_o \int_0^s \int_0^s \left[\left(k_c \bar{c} + k_o \right) \left(\overline{c'^2} \right)^{1/2} \right]_{s''} \left[\left(k_c \bar{c} + k_o \right) \left(\overline{c'^2} \right)^{1/2} \right]_{s'} r_{cc}(s',s'')\, ds'\, ds''\, e^{-\tau} d\tau \tag{18j}$$

*We use the shorthand subscript notation for derivatives, for example, $B_T = dB/dT$, $k_{TT} = \partial^2 k/\partial T^2$.

This expansion is uniformly valid for all optical depths, but it does require that the perturbations in the optical path are small compared to the mean optical path because of the expansion of the exponential [Eq. (11)]. The error in this expansion vanishes as $\tau_L \to 0$ and as $\tau_L \to \infty$. Numerical tests show that the relative error is maximum for $\tau_L = 0(1)$, but that it is at most 2 percent even if the perturbations in optical depth are as large as half the mean optical depth. The perturbations for the levels of fluctuations examined here were much smaller than that, and the expansion is adequate for the present application.

The physical interpretation of the terms in the radiance is given below:

Term	Physical Description
18(a)	Radiance from the source function B_0, evaluated at the mean temperature, and transmitted through the optical path evaluated at the mean properties.
18(b)	Radiance from the fluctuation augmented source function transmitted through the optical path evaluated at the mean properties.
18(c), 18(h) → 18(j)	Radiance from source function evaluated at mean temperature transmitted by fluctuating optical path.
18(d) → 18(g)	Radiance from fluctuating source function transmitted by fluctuating optical path.

Another viewpoint that may clarify the expansion is to view each term as a product of two factors: a local emission (source) term and a transmittance term. The expansion in Eq. 18 can then be schematically outlined as shown below.

Terms in Eq. (18)	Source	Transmittance
18(a)	mean	mean
18(b)	fluctuating	mean
18(c) + 18(h) + 18(j) + 18(k)	mean	fluctuating
18(d) + 18(e) + 18(f) + 18(g)	fluctuating	fluctuating

Each of these integral terms was evaluated numerically for the known distribution of mean and fluctuating properties across the axisymmetric exhaust plume. The numerical quadrature scheme is described in Appendix A. In addition, the values of the Planck function and the absorption coefficient, and their various derivatives, were evaluated at each point. The equations used for this purpose are given in Appendix B, along with some typical results to indicate the behavior of the derivative terms, which define the sensitivity of the absorption to temperature and species fluctuations.

This type of expansion clarifies the contribution of each term to the time-averaged radiance and suggests the order of the importance of the spatial correlations that are known to be required because of the propagational nature of the problem. Identification of the order of the spatial correlation contribution to the radiance is a unique feature of this study. Radiance from a fluctuating optical path with spatial correlations was formulated by Tan and Foster.[17] In fact, their formulation was evaluated exactly in closed form (without the need for a small perturbation expansion), when Gaussian probability density functions for the fluctuations were assumed. However, they pointed out that non-physical results (average transmittance > 1 at large optical depths) were possible with that assumption.*

EXAMINATION OF THE CORRELATION TERMS

The precise contribution of the terms involving the two-point correlations along the line of sight requires the detailed numerical evaluation to be given in the subsequent sections. However, it is possible to estimate their magnitude and dependence on correlation length and optical depth in advance. The integrals can be evaluated analytically for the special case where both the mean and fluctuating properties are uniform.

$$\int_0^{\tau_L}\left[\int_0^{s}\exp\left(-|s-s'|/\ell\right)ds'\right]e^{-\tau}\,d\tau = \ell\int_0^{\tau_L}\left[1-\exp(-s/\ell)\right]e^{-\tau}\,d\tau$$

[17] Tan, E., and P.J. Foster, "Radiation Through a Turbulent Medium," Sixth International Heat Transfer Conference, Toronto, Canada, V. 3, 1978, pp. 403-408. (paper, UNCLASSIFIED.)

*This nonphysically allowed result is due to the tails of the Gaussian distribution which admit small or negative values of the variable with finite probability, when in reality, there is a lower bound below which the probability density is zero.

$$= \ell\left\{(1 - e^{-\tau_L}) - \frac{k_o \ell}{1 + k_o \ell}\left[1 - \exp\left(-\tau_L(1 + 1/k_o \ell)\right)\right]\right\} \tag{19}$$

$$\int_0^{\tau_L}\int_0^{s}\int_0^{s} \exp(-|s' - s''|/\ell)ds'ds'' e^{-\tau} d\tau =$$

$$2\ell^2\int_0^{\tau_L} (s/\ell + \exp - s/\ell - 1)e^{-\tau} d\tau =$$

$$= 2\ell^2\left\{\frac{1}{k_c \ell}\left[1 - (\tau_L + 1)e^{-\tau_L}\right] + \frac{k_o \ell}{1 + k_o \ell}\left[1 - \exp\left(-\tau_L\left(1 + \frac{1}{k_o \ell}\right)\right)\right] - (1 - e^{-\tau_L})\right\} \tag{20}$$

The correlation coefficient has introduced an additional length scale into the formulation in addition to the total path length L, and the absorption length, k_o^{-1}. The nature of this additional length is perhaps more evident if we look at the limiting cases of small and large optical paths, τ_L. The asymptotic behavior of these integrals is given in the following table.

	Eq. (19)		Eq. (20)	
	$\ell << L$	$\ell >> L$	$\ell << L$	$\ell >> L$
$\tau_L \to 0$	$1/2\ k_o L^2$	(independently of ℓ)	$1/3\ k_o L^3$	(independently of ℓ)
$\tau_L \to \infty$	ℓ	k_o^{-1}	$2\ell k_o^{-1}$	$2k_o^{-2}$

These limits suggest that for optically thin flows, ($\tau_L \to 0$), the contribution of the correlation terms is independent of the correlation coefficient and depends only on the total optical depth, τ_L, and total geometric path length, L. In the optically thick limit ($\tau_L \to \infty$), the significance of the additional length scale, ℓ, becomes apparent. When ℓ is small, it defines the order of the contribution of the correlations. However, when ℓ becomes large (compared to L), the

absorption length, k_o^{-1}, defines the contribution, in agreement with the well-known limiting behavior of optically thick media. These order of magnitude arguments, in particular, the absence of an ℓ-dependence in the optically thin limit, are verified in the subsequent numerical examples.

It should be pointed out that we are dealing with one form of the correlation coefficient [Eq. (15)], and the precise form of the integrals and their dependence on the correlation length, ℓ are particular to this choice. However, we expect that the functional dependence suggested by the asymptotic limits in the above table are more general, and would hold for any physically meaningful correlation function.

RADIATION FROM A TURBULENT EXHAUST PLUME

ISOLATED SPECTRAL LINE

We anticipate that the predictions of the turbulence augmented radiance from the exhaust plume will depend on the particular line of sight through the flow (temperature and turbulence levels), the spectral location, the type of line (transition between low or high energy levels), and the spectral resolution. In order to examine these issues separately, we present the radiance for an isolated spectral line before dealing with the competing effects of many lines in a broader bandpass. Typical exhaust plume infrared signatures are usually low resolution (2 - 5 cm^{-1} at the highest), and do not resolve the features of a single line. However, combustion diagnostics can be high resolution, and the results for a single line are of interest for this application as well as illustrating more general features.

As a specific example, we choose a broadside observation of the plume at an axial location 40 radii downstream from the nozzle exit. The radial profiles of mean and fluctuating properties at this location are shown in Figure 14. This location is in the region of peak afterburning (Figure 7). Predictions of the spectral radiance from isolated lines with different strengths and energy levels were made for lines of sight passing through the middle of the plume and also displaced from the axis of symmetry ($r = 0.4\ r_p$). The latter line of sight emphasizes the region of increased turbulence and lower temperature that leads to the largest effect of the turbulent fluctuations. A typical result at $\omega = 2200\ cm^{-1}$ (4.5μm) is given in Figure 15. The line shapes for the radiance from the mean properties and from the turbulence augmented radiance are given in terms of the spectral displacement $\Delta\omega = \omega - \omega_o$ from the line center normalized by the half-width, α_o, at the reference temperature $T_o = 296$ K. Predictions of

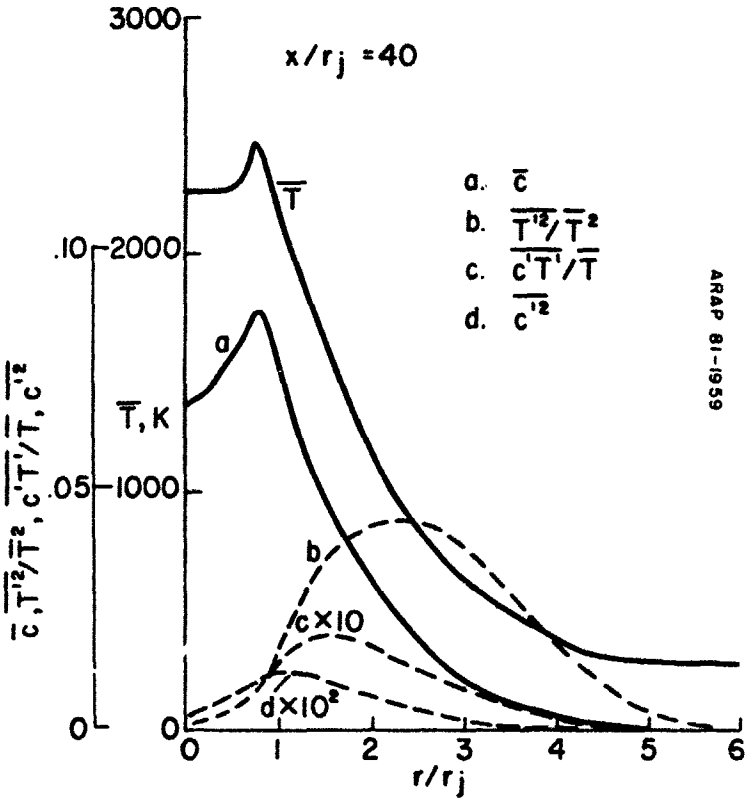

FIGURE 14. Radial Profiles of Mean and Fluctuating Properties in the Model Afterburning Plume at $x/r_j = 40$. RSL Predictions, Nominal Start Conditions and Turbulence Length Scale.

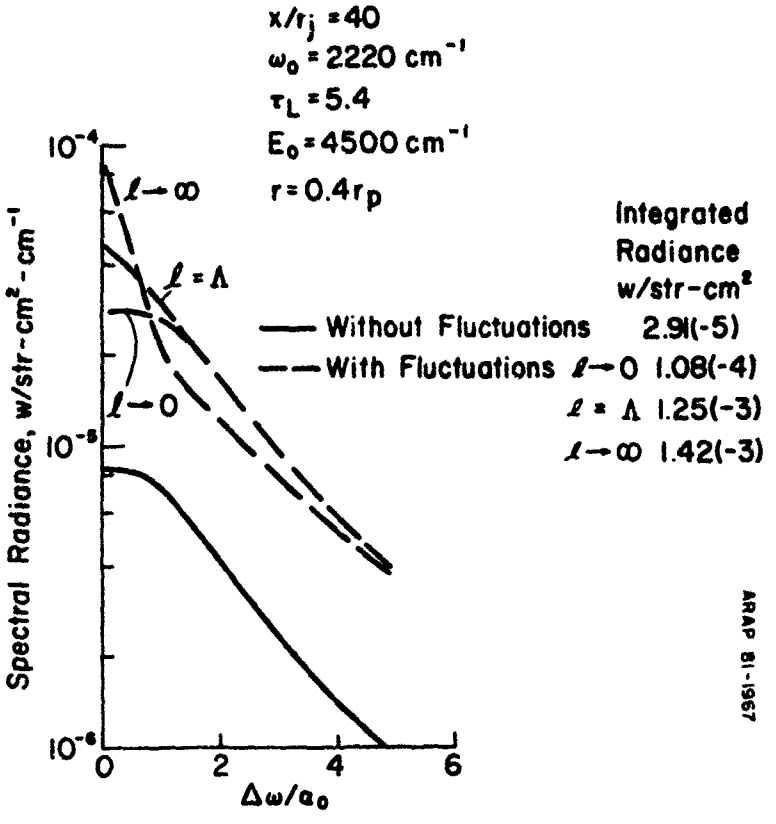

FIGURE 15. Spectral Structure of Isolated Lorentz Line. Broadside Line of Sight Off the Plume Axis at $x/r_j = 40$, $\Lambda = 4.03$ cm.

the turbulence augmented mean radiance are given for a very large correlation length (perfect correlation), a correlation length equal to the local integral velocity scale Λ, (our best estimate of the true correlation length), and a small correlation length (completely uncorrelated scalar fluctuations). These results are for a line of moderate strength with a lower energy state $E_o = 4500\ cm^{-1}$, typical of lines that become important at temperatures of 600 K or more. In this particular example, the turbulence augmented radiance integrated over the entire line width is more than a factor of four greater than that evaluated at the mean properties. An additional important result is that the integrated line radiance is not particularly sensitive to the correlation length, but the precise line shape is very strongly dependent on the correlation. This is a result that is potentially important for any measurement that relies on either the shape or peak intensity of single spectral lines (i.e., line reversal temperature measurements, or rotational temperature measurements from relative line intensities).

A similar prediction for a line of sight passing through the plume axis is given in Figure 16. This line, which is identical in strength to that used in Figure 15, is totally self-absorbed along this line of sight. Again, the integrated radiance is not significantly different for the range of correlation lengths, but the line structure is strongly affected. For this choice of line strength and lower energy level, the absorption is intense and the resulting radiance is localized to that region of the plume where the turbulence intensity and temperature combine to produce a line structure that is very different from that of a normal emission line, even when it is strongly self-absorbed.

Transition from completely correlated ($\ell \to \infty$) to totally uncorrelated scalar fluctuations is shown for these two lines of sight in Figure 17. In both these cases, the radiance from the mean properties is smaller than that with the fluctuations at all correlation lengths. This comparison also points out that the off-axis line of sight ($r = 0.4\ r_p$) through the cooler, more turbulent portion of the flow has a radiance that is more intensely augmented by the turbulent fluctuations, although its absolute level is reduced from that of the line of sight through the axis. That condition remains true for all calculations performed in this report, regardless of axial location or spectral resolution.

These predictions are for a relatively strong spectral line. Similar calculations for a much weaker line show no effect of correlation length, in agreement with the limiting cases of the correlation integrals identified for Eqs. (19) and (20). Moreover, for an optically thin plume, the line of sight through the axis shows essentially no contribution of the turbulent fluctuations to the radiance at axial positions where the peak turbulent fluctuations do not coincide with the peak temperature (i.e., Figure 14). In this

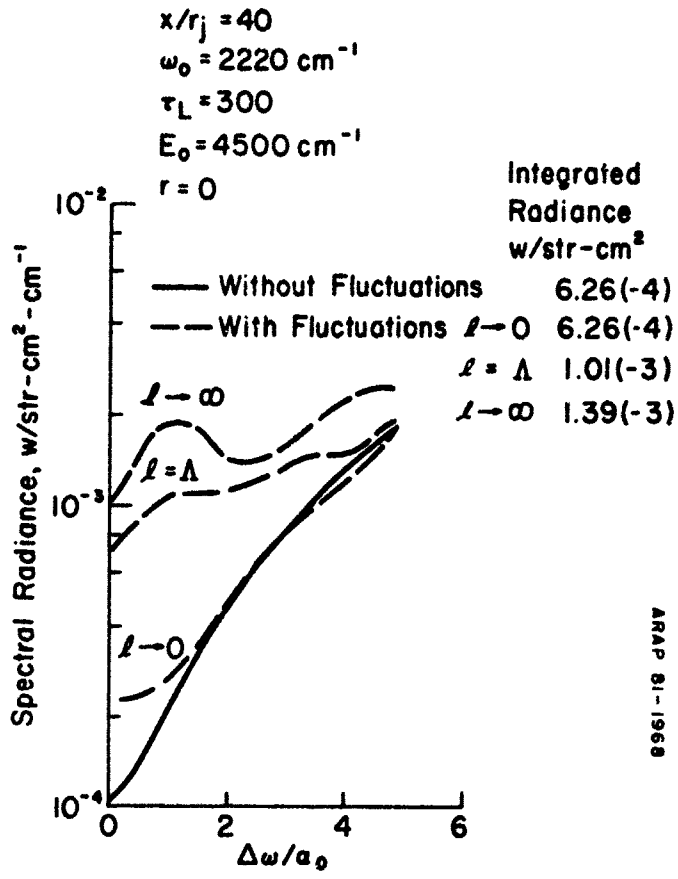

FIGURE 16. Spectral Structure of Isolated Lorentz Line. Broadside Line of Sight Through the Plume Axis at $x/r_j = 40$, $\Lambda = 4.03$ cm.

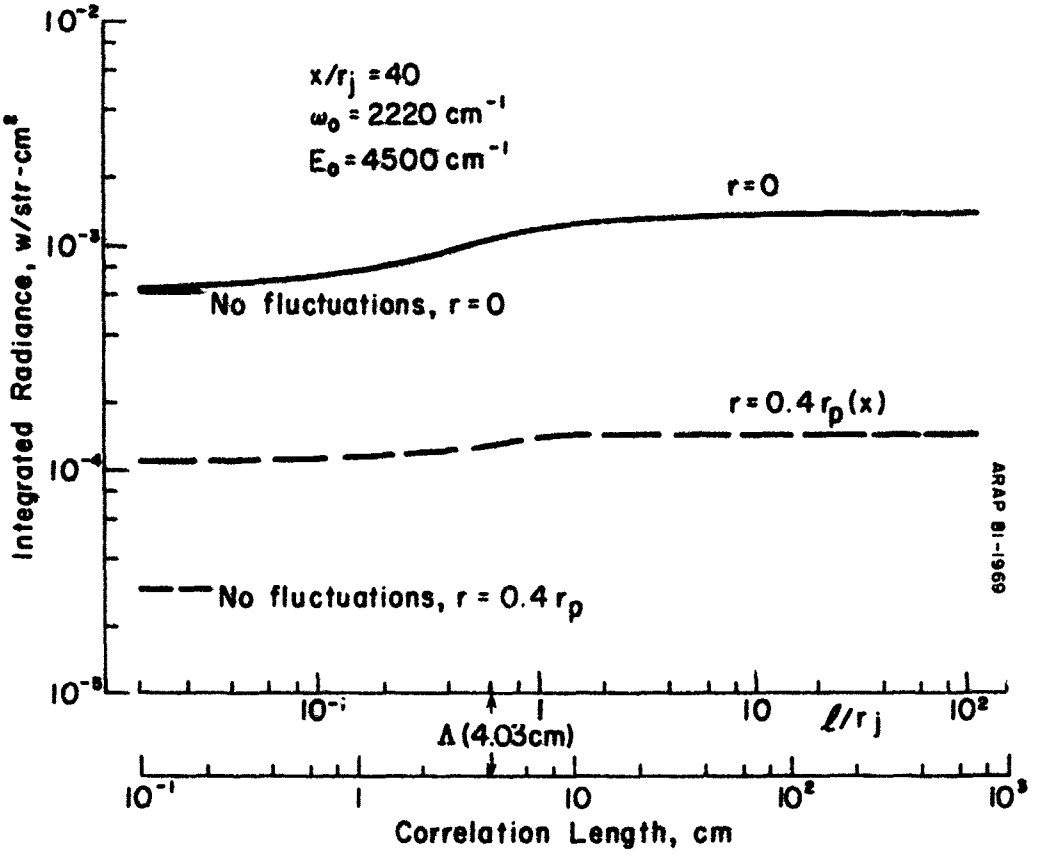

FIGURE 17. Integrated Radiance of an Isolated Spectral Line for Various Correlation Lengths. Broadside Line of Sight at $x/r_j = 40$. $r_p(x) = 0.429$ m.

situation, the essentially steady, but very intense radiance from the peak temperature region is affected very little by the contributions from the lower temperature outer region where the fluctuations are relatively more intense. A line of sight through the outer edge of the plume [say at $r = 0.4r_p(x)$] shows a substantial turbulence augmentation (factor of two for a weak line with the same lower energy level as that in Figures 15 and 16) independently of correlation length.

An additional parameter that is as important as the optical depth is the lower energy level of the particular spectral line. This affects the temperature sensitivity of the absorption. For example, the Boltzman factor defining the population of states with the energy level E_o is $\exp(-hc\tilde{E}_o/KT)$. The temperature derivatives of the absorption coefficient, $T\partial k/\partial T/k$, and $T^2\partial^2 k/\partial T^2/k$ (see Appendix B) therefore involve terms like $(hc\tilde{E}_o/KT)$ and $(hc\tilde{E}_o/KT)^2$ and the temperature sensitivity is increased with increasing E_o. Other factors, such as the line strength and temperature derivatives of the vibrational partition function are essentially the same for every line. Sample calculations of the temperature sensitivity for two typical energy levels and several temperatures are given in Appendix B. These calculations suggest that the temperature derivatives change magnitude and sign according to the particular lower energy state and temperature. These effects are somewhat obscured by a non-homogeneous path. However, the line shape and the effect of correlation length from a line with an energy level of $E_o = 1500\ cm^{-1}$ are shown in Figures 18 and 19, respectively, and are different from the similar predictions with $E_o = 4500\ cm^{-1}$. This low energy level line (typical of those which make up a large portion of the low temperature spectrum of CO_2 in the 4.3 μm region) is not particularly sensitive to turbulent fluctuations. Even in the optically thick region of the line center (Figure 18), the turbulent fluctuations have little effect on the line shape, in contrast to the lines that originate from transitions between higher energy levels (Figure 15).

Finally, we present an indication of the turbulence effect on a line with a high energy level, $E_o = 7000\ cm^{-1}$. The effect of the correlation length on the integrated line radiance is given in Figure 20 for the two lines of sight. For this class of lines, the temperature sensitivity is high, but the line strengths are weak, and so the optical depths are small. The sensitivity to the correlation length is therefore diminished. It is interesting to note that for this class of lines, the turbulence augmented integrated line radiance for an uncorrelated path ($\ell \to 0$) is actually less than that evaluated at the mean properties. However, the turbulence augmented radiance for the correct correlation length, $\ell = \Lambda$, is greater than that for the mean properties.

These few illustrations suggest the importance of the turbulence augmentation of the mean radiance from the individual spectral lines of CO_2 in a small afterburning missile exhaust plume. Both the line shape and integrated radiance are affected. The extent of the effects depends

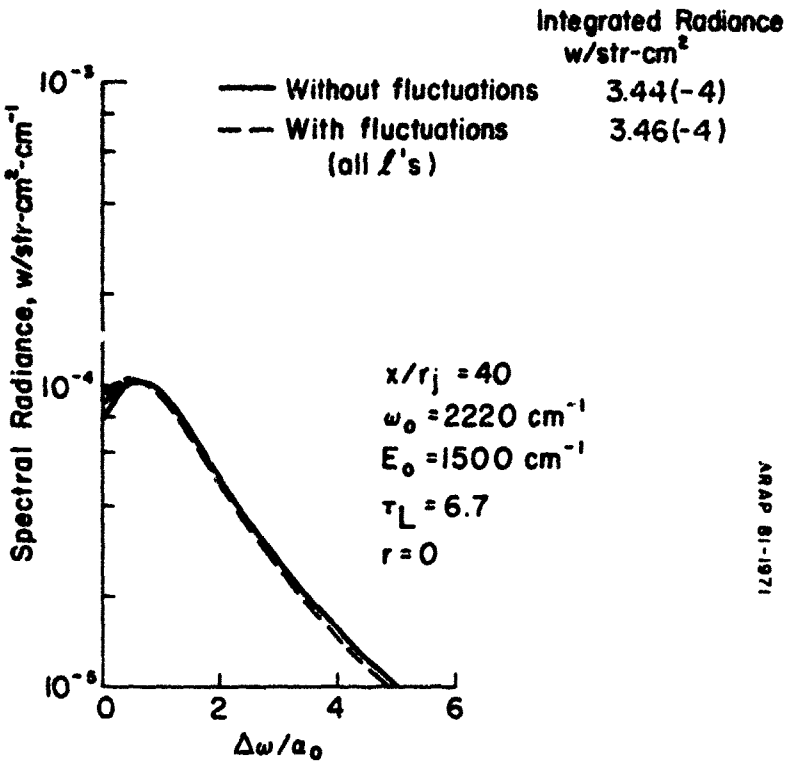

FIGURE 18. Spectral Structure of Isolated Lorentz Line. Broadside Line of Sight Through the Plume Axis at $x/r_j = 40$. $\Lambda = 4.03$ cm.

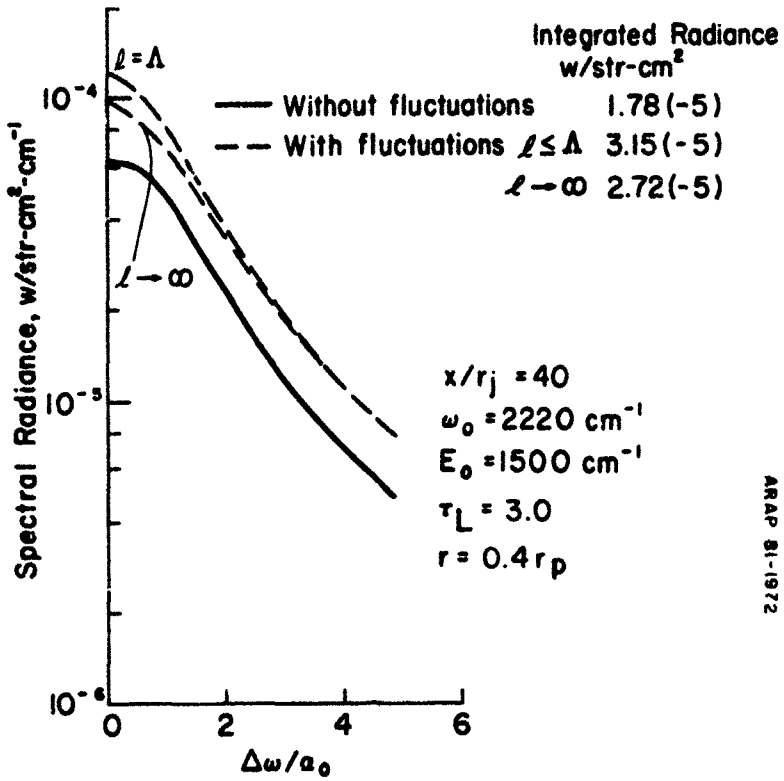

FIGURE 19. Spectral Structure of Isolated Lorentz Line. Broadside Line of Sight Off the Plume Axis at x/r_j = 40. Λ = 4.03 cm.

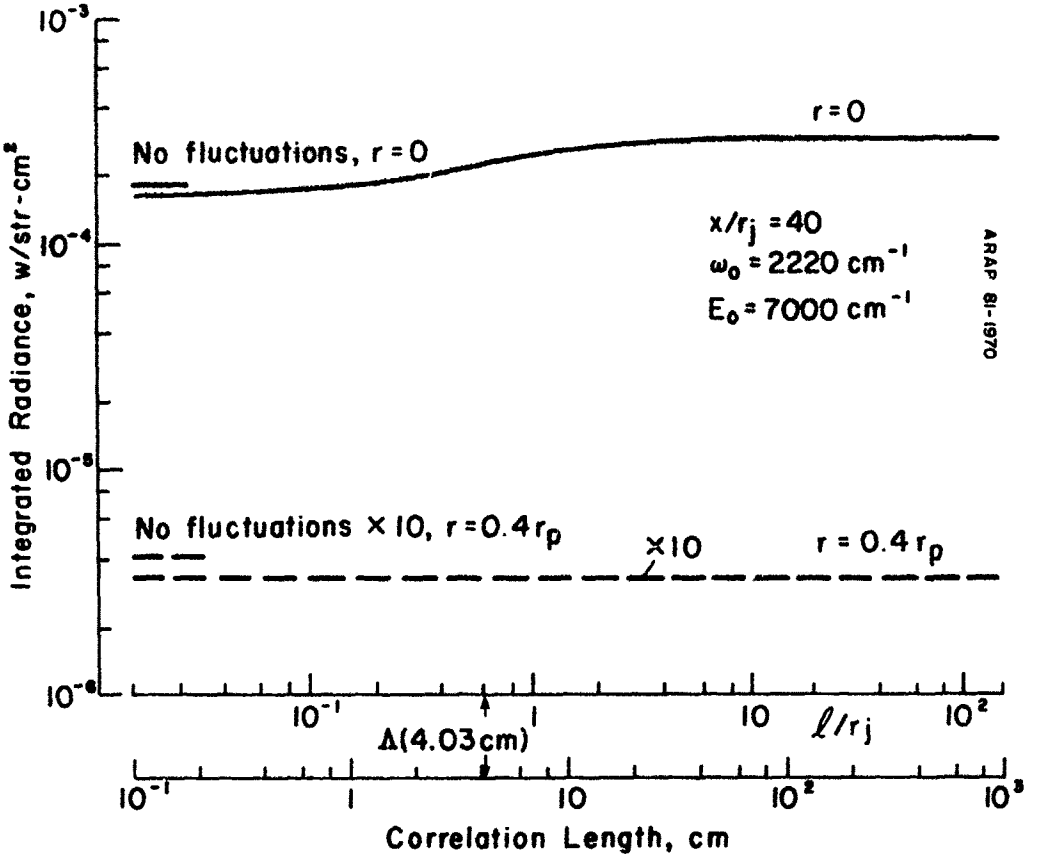

FIGURE 20. Integrated Radiance of an Isolated Spectral Line for Various Correlation Lengths. Broadside Line of Sight at $x/r_j = 40$, $r_p(x) = .429$ m.

on optical depth, the particular line (energy level), and the distribution of properties along the optical path and the extent of correlation of these quantities. The largest contribution to the augmentation comes from the additional fluctuating source terms [term b in Eq. (18)]. However, the correlations between scalar properties (T',c') along the line of sight can certainly be important. Past studies[13,16,17] have correctly identified the importance of the fluctuating source term; the present study has identified the explicit contribution of the correlations.

IN-BAND RADIANCE - CO_2 BLUE SPIKE

For exhaust plume signature applications, a spectral interval wider than a single line is of interest. The highest resolution band models deal only with 0.2 - 2.0 cm^{-1} resolution[18] and the most widely used compilation is 5 cm^{-1} resolution.[11] We chose a 5 cm^{-1} bandpass for use here.

An operationally important spectral region is the CO_2 blue spike, located between about 2380 and 2397 cm^{-1}. This emission propagates through long atmospheric paths and is a part of the spectral signature from all tactical missile exhaust plumes. However, it is not the most sensitive part of the spectral signature to the presence of turbulent fluctuations because of its reduced temperature sensitivity.[16] However, because of its technical importance, we have made predictions of the turbulence augmented emission in the 5 cm^{-1} bandpass between 2385 and 2390 cm^{-1}.

The prediction of the emission from more than a single spectral line requires a compilation for all the lines of interest for the given bandpass. In this region, we used the AFGL Line Atlas.[14] Normally, this compilation is incomplete for high temperatures. It does not contain the lines that become important at high temperatures ($E_o \gtrsim 3000$ cm^{-1}). However, these lines are adequate for this particular spectral region up to about 1500 K. (This was verified by comparing the average absorption computed with the AFGL Atlas over 5 cm^{-1} and 2 cm^{-1} intervals with that presented in References 11 and 18, respectively.) The use of this particular line atlas will underestimate the turbulence augmentation in the higher temperature regions, but it is adequate for the purpose of this assessment.

---

[18]Berstein, L.S., D.C. Robertson, and J.A. Conant, "Band Model Parameters for the 4.3 μm CO_2 Band from 200 to 3000°K - II. Predictions, Comparison to Experiment, and Application to Plume Emission - Absorption Calculations," J. Quart. Spectrosc. Radiative Transfer, Vol. 23, 1980, pp. 169-185.

Predictions of the tactical missile exhaust plume radiance and intensity in the 2385 - 2390 cm^{-1} bandpass were made for various axial locations in the plume. At each axial location, the correlation length was chosen to be the local turbulence length scale, Λ. The length scale and the plume radius at the axial locations at which these calculations were made are given below.

Table 3 - Axial Locations
and Plume Dimensions
for the Radiance Calculation
r_j = .065 m

x/r_j	Λ, m	$r_p(x)$, m
0	.022	0.13*
2	.024	.169
4	.025	.182
10	.0253	.247
20	.027	.299
40	.0403	.429
100	.093	.533
200	.114	.585
400	.114	.585

*Pressure equilibrated

Radial profiles of the mean and second-order correlations of the fluctuating properties have already been given for x/r_j = 40 in Figure 14. We include additional profiles at the axial locations x/r_j = 4, 20, 100, and 200 in Figures 21, 22, 23, and 24, respectively. These profiles are given to show the development and spread of the mean and turbulence quantities used in the subsequent radiance predictions.

Radial distributions of the in-band radiance in the 2385 - 2390 cm^{-1} bandpass are given at the three axial locations x/r_j = 10, 40, and 100 in Figures 25, 26, and 27, respectively. These locations are upstream, within, and downstream of the peak afterburning region. In all cases, the turbulent fluctuations have a negligible effect on the mean radiance near the plume axis. As mentioned earlier, the radiance in the region near the axis is dominated by the high temperature, relatively less turbulent part of the mixing region. The turbulence contribution becomes more important for the off-axis lines of sight and the downstream portion of the plume where the peak turbulence fluctuations and peak temperatures more nearly coincide. For the three axial locations shown, the station radiation (the radiation per unit plume length) is augmented by turbulence by the amounts of 22%, 20%, and 37%,

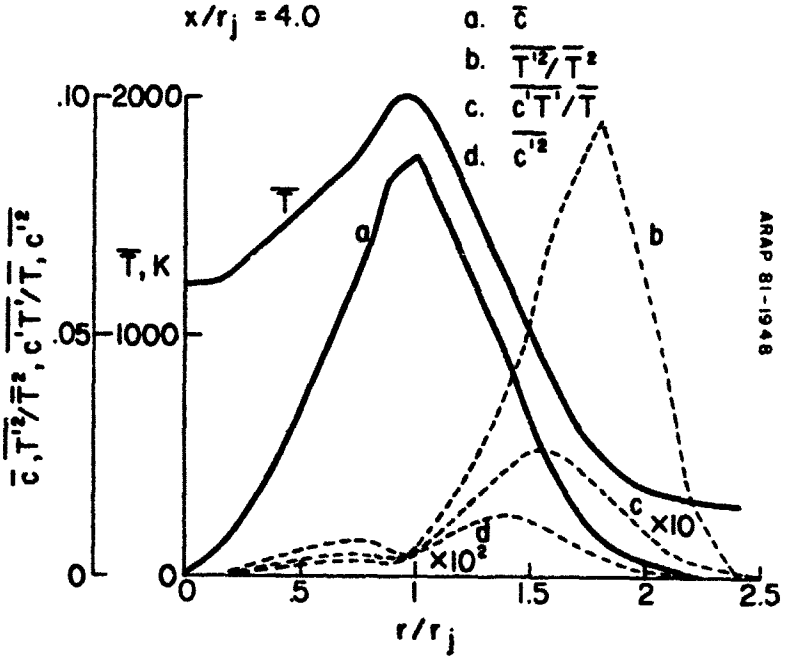

FIGURE 21. Radial Profiles of Mean and Fluctuating Properties in the Model Afterburning Plume at $x/r_j = 4.0$. RSL Predictions, Nominal Start Conditions and Turbulence Length Scale.

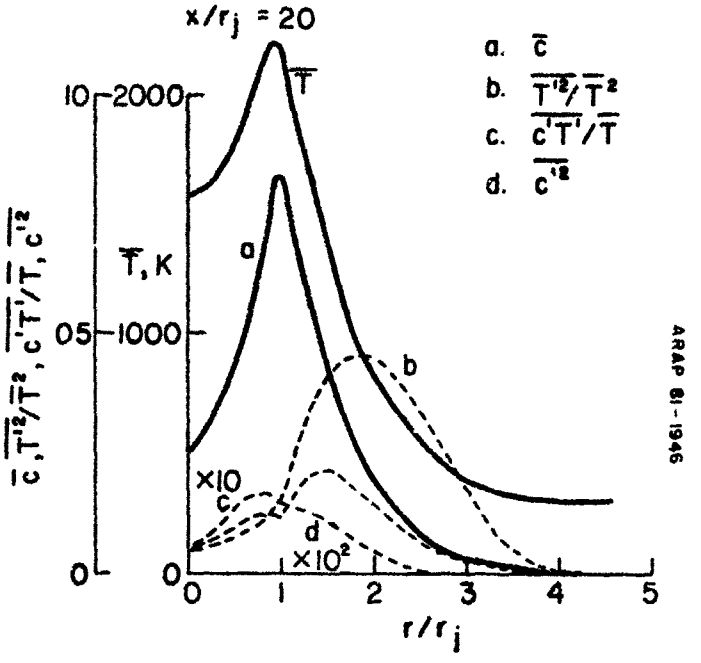

FIGURE 22. Radial Profiles of Mean and Fluctuating Properties in the Model Afterburning Plume at $x/r_j = 20$. RSL Predictions, Nominal Start Conditions and Turbulence Length Scale.

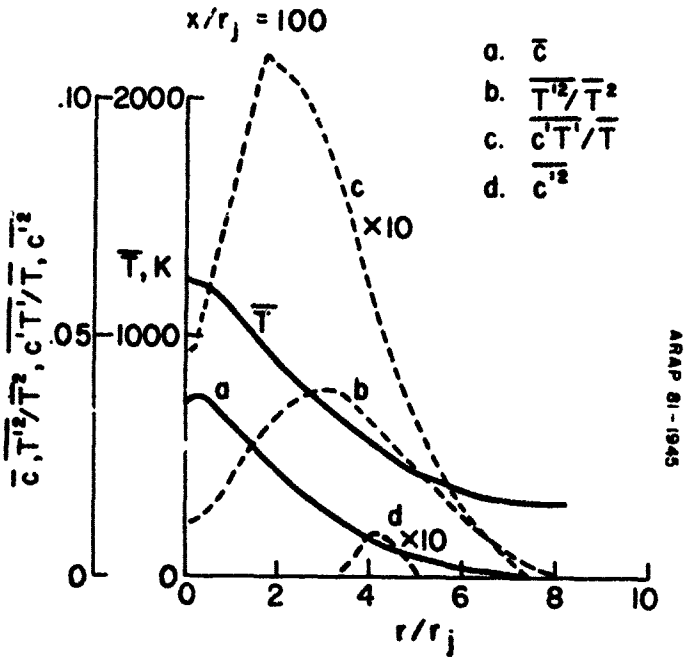

FIGURE 23. Radial Profiles of Mean and Fluctuating Properties in the Model Afterburning Plume at $x/r_j = 100$. RSL Predictions, Nominal Start Conditions and Turbulence Length Scale.

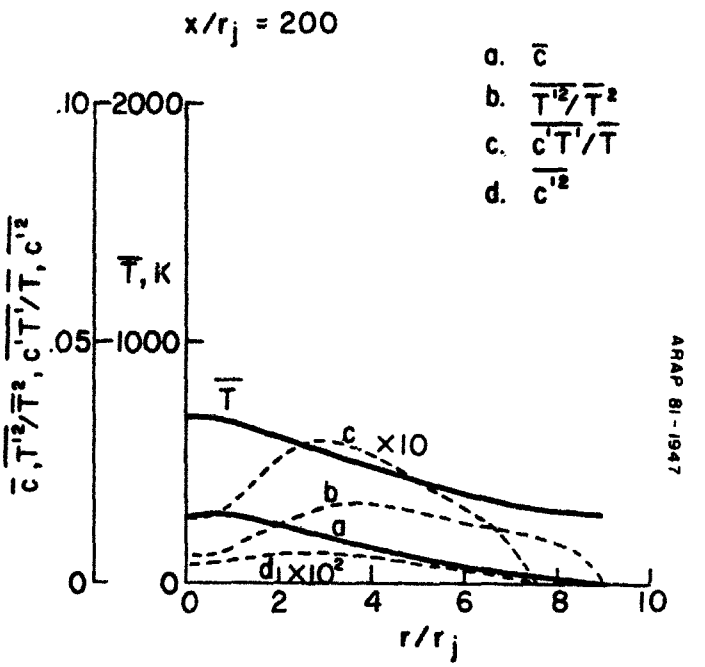

FIGURE 24. Radial Profiles of Mean and Fluctuating Properties in the Model Afterburning Plume at $x/r_j = 200$. RSL Predictions, Nominal Start Conditions and Turbulence Length Scale.

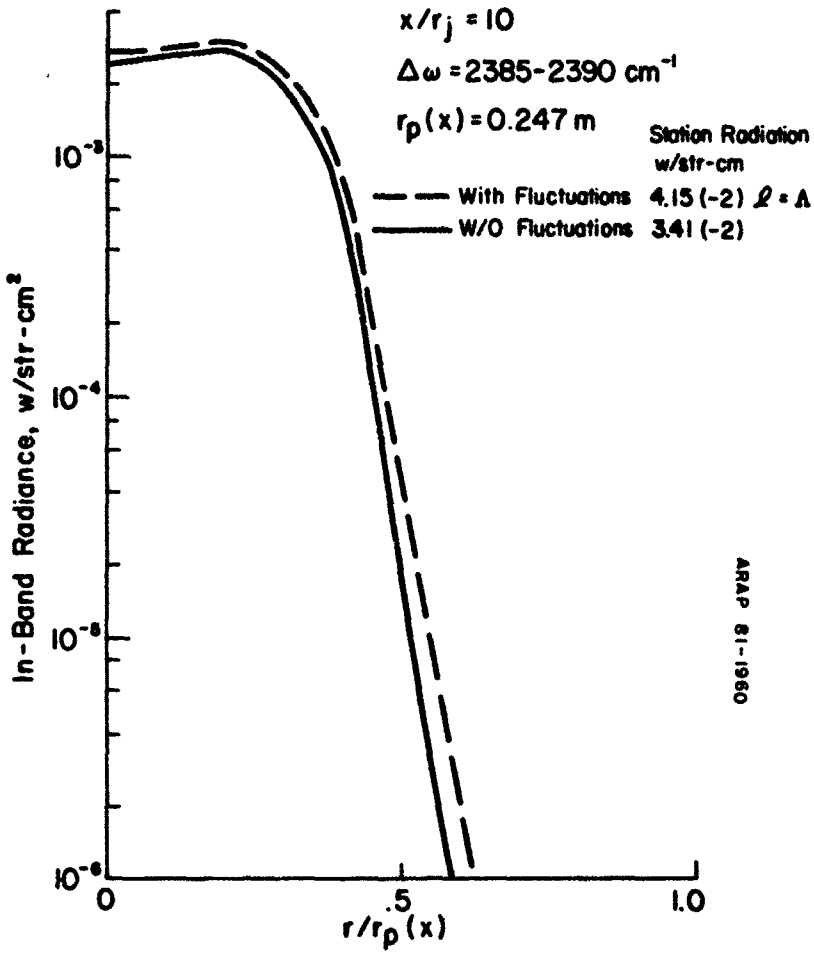

FIGURE 25. Radial Distribution of In-Band Source Radiance Across the Plume at $x/r_j = 10$.

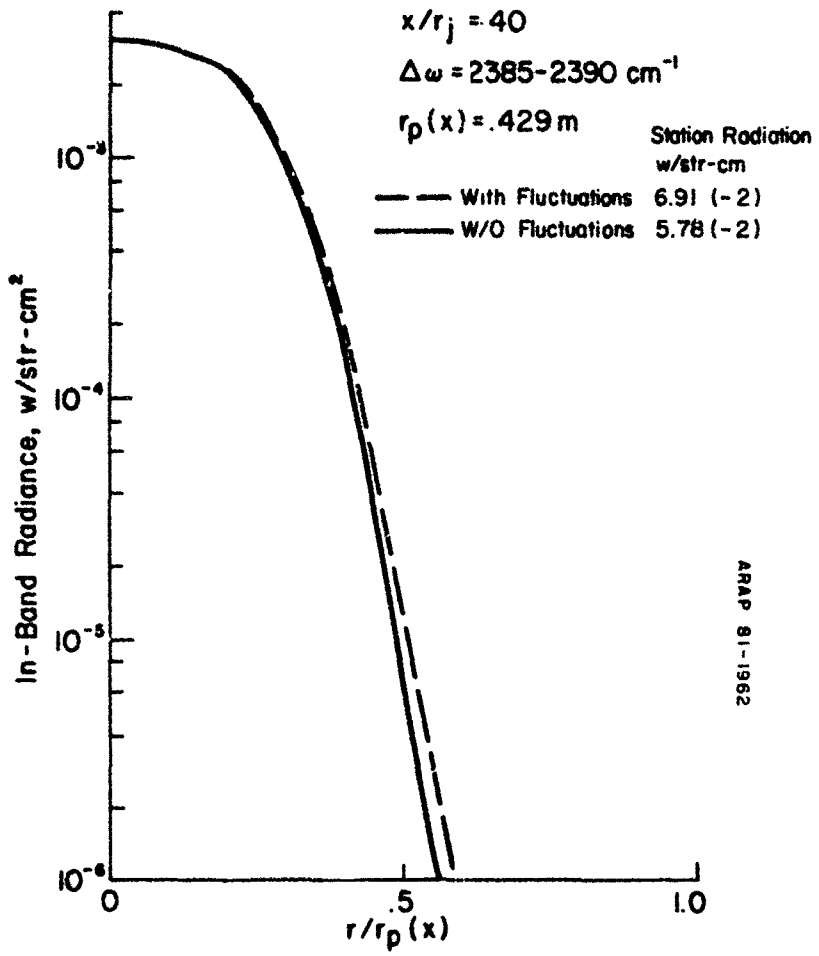

FIGURE 26. Radial Distribution of In-Band Source Radiance Across the Plume at x/r_j = 40.

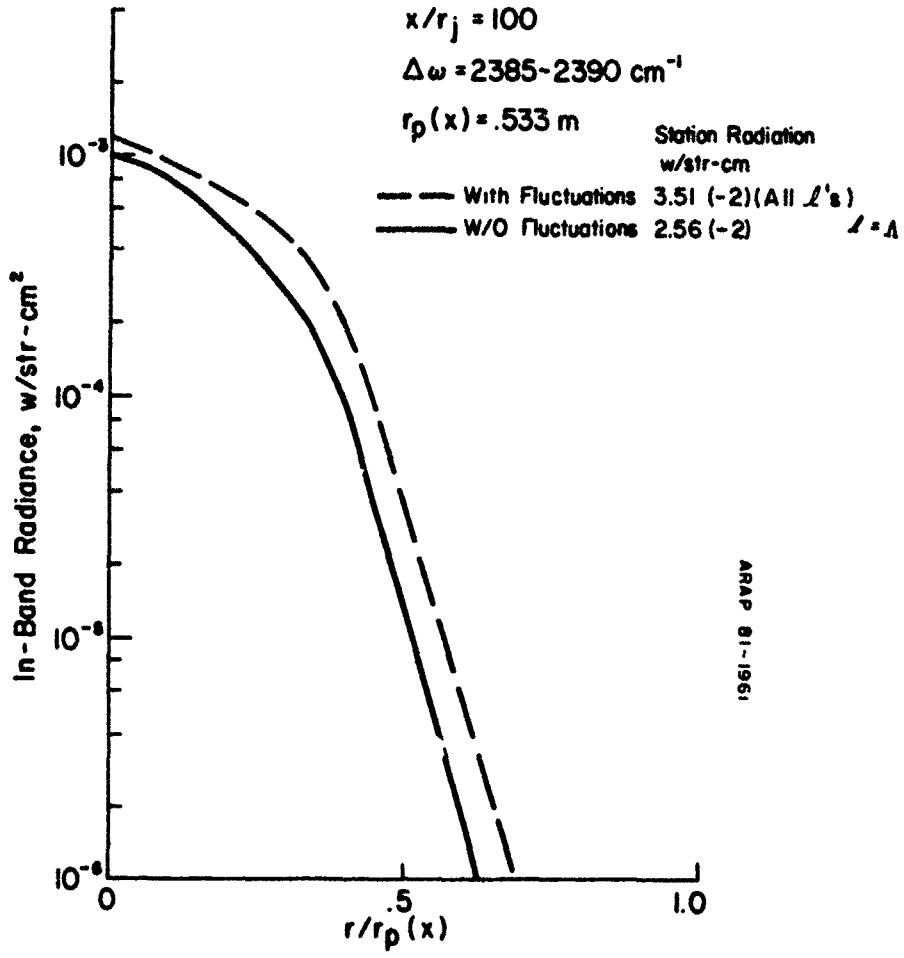

FIGURE 27. Radial Distribution of In-Band Source Radiance Across the Plume at $x/r_j = 100$.

at x/r_j = 10, 40, and 100, respectively.

The increased radiance over the entire plume length is indicated by the axial distribution of station radiation in Figure 28. This clearly shows the increasing relative importance of the turbulence on plume emission with increasing axial distance. For this particular exhaust plume and the 2385 - 2390 cm^{-1} bandpass, the turbulence augmented mean intensity is only 24 percent greater than that calculated using only the mean plume temperature and species distribution. This augmentation is comparable to the uncertainties usually associated with total plume signature predictions under the most favorable circumstances.

The turbulence augmentation assumes a potentially more important role in a spatially resolved signature. The true, turbulence augmented radiance is significantly larger than that evaluated at the mean properties near the outer edge of the plume. This result was emphasized for the single spectral lines discussed previously, and it is equally true for a wider bandpass. The spectral radiance in the 5 cm^{-1} bandpass is shown for an off-axis line of sight ($r = 0.4r_p$) at the four axial locations x/r_j = 10, 20, 40, and 100 in Figures 29, 30, 31, and 32, respectively. At these locations, the in-band radiance is increased by 72, 45, 100, and 250 percent, respectively over that evaluated without the contributions of the fluctuation. The in-band radiance is substantially enhanced for the outer edges of this particular exhaust plume. Moreover, we expect this conclusion to hold for all afterburning plumes. We point out that for plumes at higher altitude where afterburning is reduced, the entire plume is essentially a chemically frozen shear flow resembling the outer edge or downstream decaying region of an afterburning plume. The turbulence augmentation is potentially a much larger contribution to the total plume signature in that case. We suggest that this is the situation for which Rhodes[13] obtained such a large effect of turbulence (factor of 200 increase in station radiation) on the signature in the 2.7 μm water vapor band.

Predictions like these were made with both very large and very small correlation lengths in addition to our best estimate of $\ell = \Lambda$. The results were insensitive to the correlation length. The reason for this is suggested by the results for a single spectral line. The correlation effect is important in the turbulence augmented line structure, but not in determining the integrated radiance. Also, the lines with lower energy levels (Figures 18 and 19) are less sensitive to the correlation effect. In the 2385 - 2390 cm^{-1} spectral region, most of the lines are of this class. The importance of the correlation of fluctuations along the line of sight is therefore not important in this particular spectral region, and the turbulence augmentation is due entirely to the additional fluctuation induced source terms [Term b in Eq. (18)].

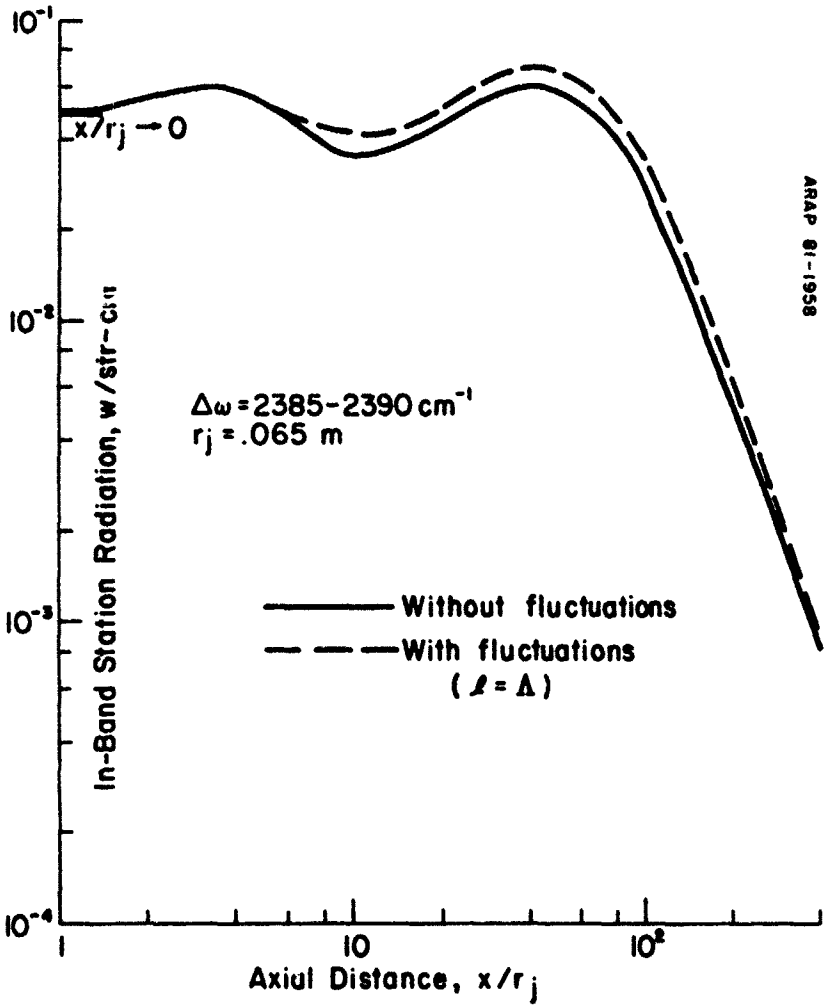

FIGURE 28. Axial Distribution of In-Band Source Station Radiation for the Model Afterburning Exhaust Plume. CO_2 Blue Spike Region.

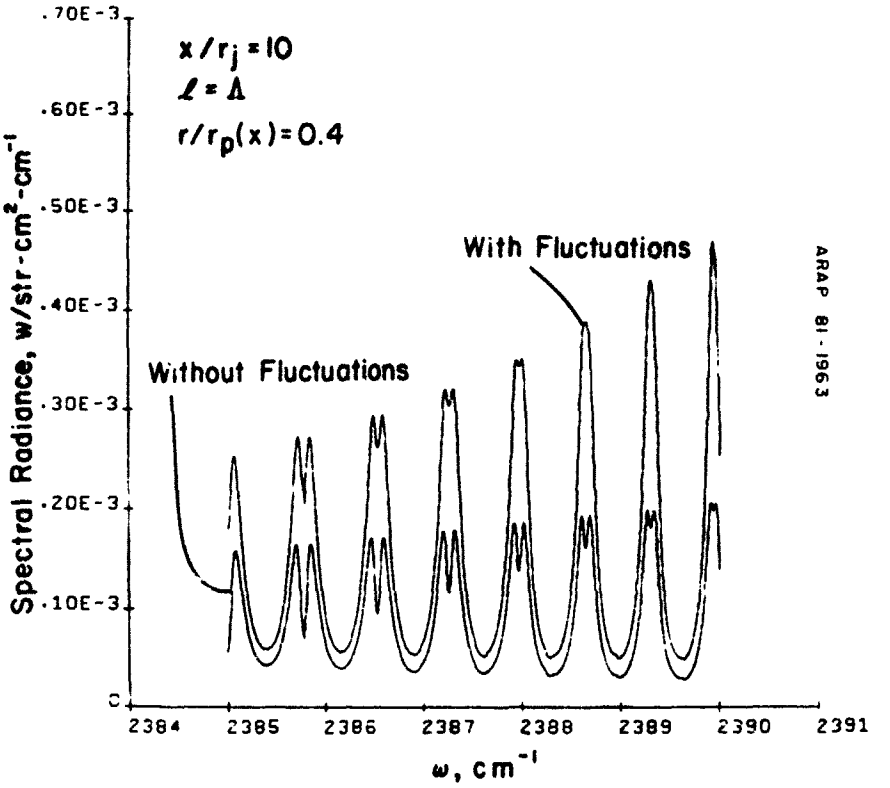

FIGURE 29. Source Spectral Radiance for a Line of Sight at the Axial Location x/r_j = 10 and Off the Plume Axis at r = $0.4r_p$. CO_2 Blue Spike Region.

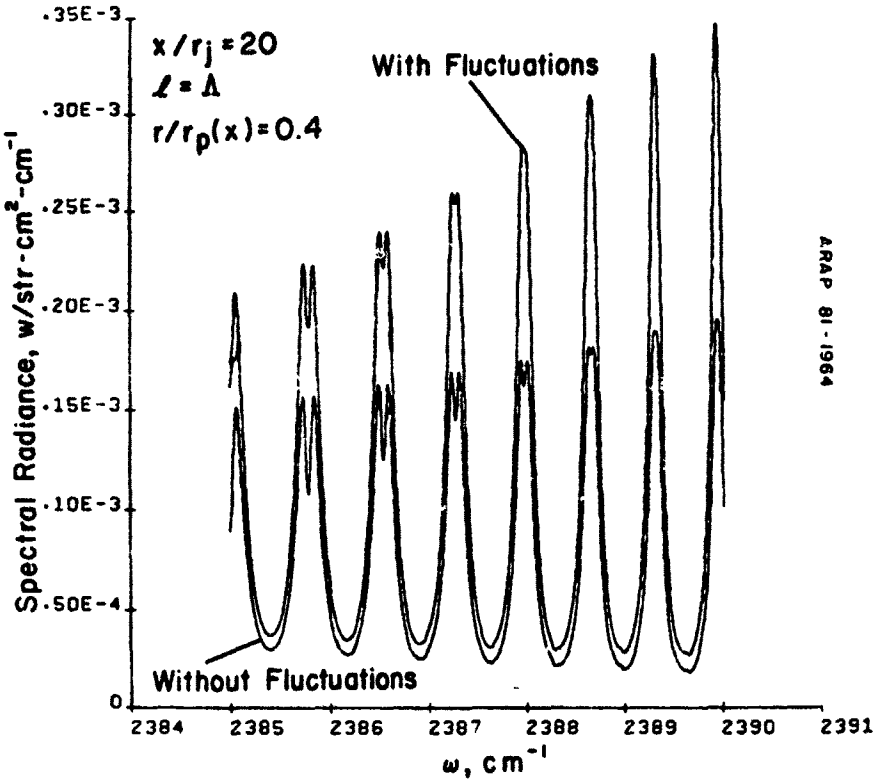

FIGURE 30. Source Spectral Radiance for a Line of Sight at the Axial Location $x/r_j = 20$ and Off the Plume Axis at $r = 0.4r_p$. CO_2 Blue Spike Region.

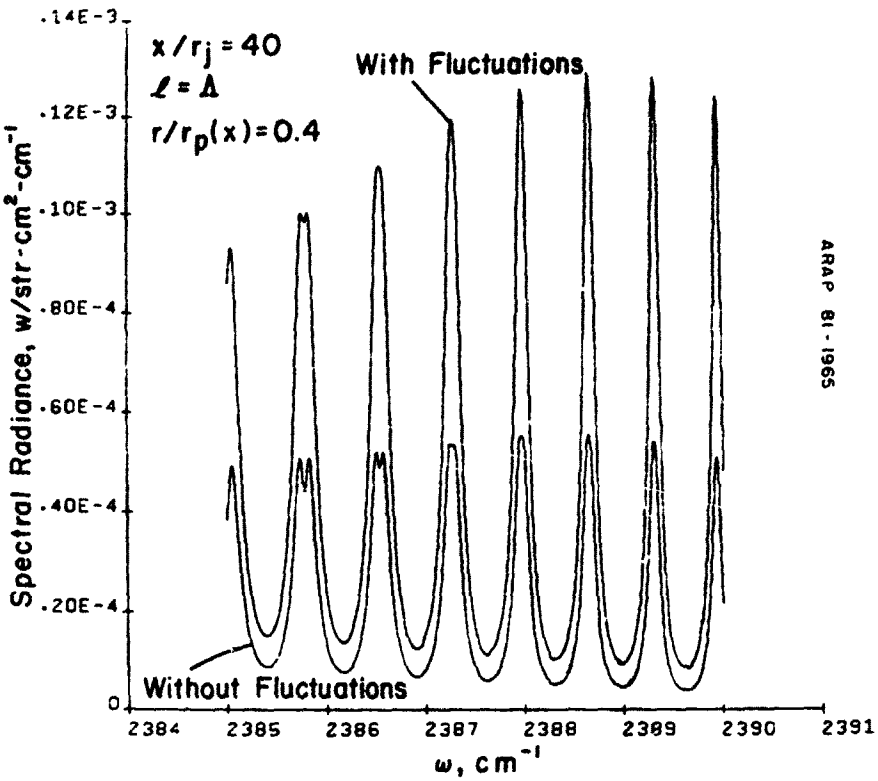

FIGURE 31. Source Spectral Radiance for a Line of Sight at the Axial Location $x/r_j = 40$ and Off the Plume Axis at $r = 0.4r_p$. CO_2 Blue Spike Region.

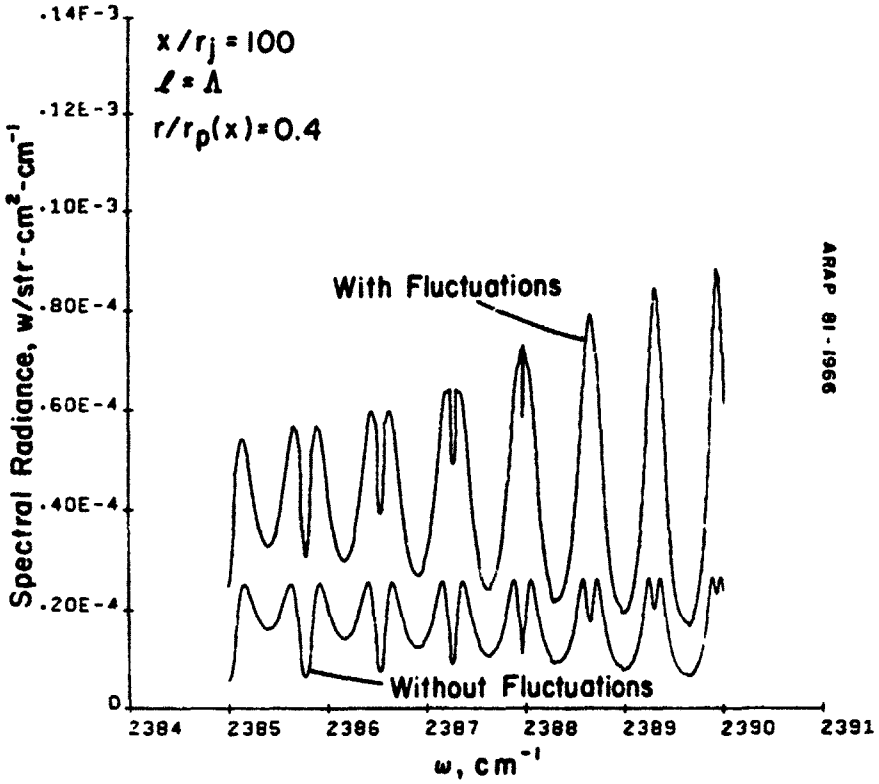

FIGURE 32. Source Spectral Radiance for a Line of Sight at the Axial Location $x/r_j = 100$ and Off the Plume Axis at $r = 0.4r_p$. CO_2 Blue Spike Region.

Even for this least sensitive spectral region, the effect of the turbulent fluctuations is very important on both the magnitude and spectral detail of the emission from the edges and downstream portion of the flow. The line shape and relative intensities of the spectral lines are altered by the turbulence. These effects are potentially important for spatially resolved signature applications and in diagnostic techniques relying on line shape or relative intensities.

IN-BAND RADIANCE - CO_2 RED SPIKE

An additional spectral interval of the CO_2 4.3 μm band of technical interest is the long wavelength side of the band near 4.5 μm (2200 cm^{-1}). This is the spectral location of the peak radiance that is transmitted through the atmosphere. We chose the 5 cm^{-1} spectral interval between 2220 and 2225 cm^{-1}. In this spectral region, the AFGL Atlas is inadequate. Bernstein[19] has shown that lines originating from energy levels of 15,000 cm^{-1} or more and line densities of 1000 per unit wavenumber are necessary to provide the correct absorption at high temperatures in this spectral region. We utilized a synthetic line atlas for this narrow spectral region that was developed at A.R.A.P.[15] This formulation is more approximate than that developed by Bernstein. It does not go to as high energy levels or contain as many lines. However, the absorption averaged over 2 cm^{-1} and 5 cm^{-1} computed with this synthetic compilation compared favorably with Bernstein, et al.[18] and the NASA compilation[11] up to temperatures of 1500 K. At higher temperatures, it underestimates the absorption and the temperature sensitivity of the absorption. Predictions given here, like those for the 2385 - 2390 cm^{-1} blue spike region, will therefore underestimate the radiance and the sensitivity of the radiance to turbulent fluctuations in the higher temperature regions of the flow.

Predictions for the 2220 - 2225 cm^{-1} bandpass were made at the same axial locations as those shown earlier for the blue spike region. A radial distribution of the in-band radiance at $x/r_j = 100$ is given in Figure 33. Like the blue spike region, the turbulent fluctuations have no effect on the mean radiance near the plume axis. This portion of the radiance is primarily from the high temperature, relatively less turbulent central portion of the plume. The relative importance of the turbulent fluctuations increases towards the outer edge of the plume, but the absolute level is sufficiently reduced that the contribution of the outer edges to the station radiation is small. For example, the station radiation at the three axial positions x/r_j = 10, 40, 100 is increased only by 10, 0, and 24 percent, respectively. These increases are even less than those found for the blue spike region.

19. Bernstein, L.S., "Band Model Parameters for the Parallel Bands of Linear Triatomic Molecules - I. Theory," J. Quart. Spectrosc. Radiative Transfer, Vol. 23, 1980, pp. 157-167.

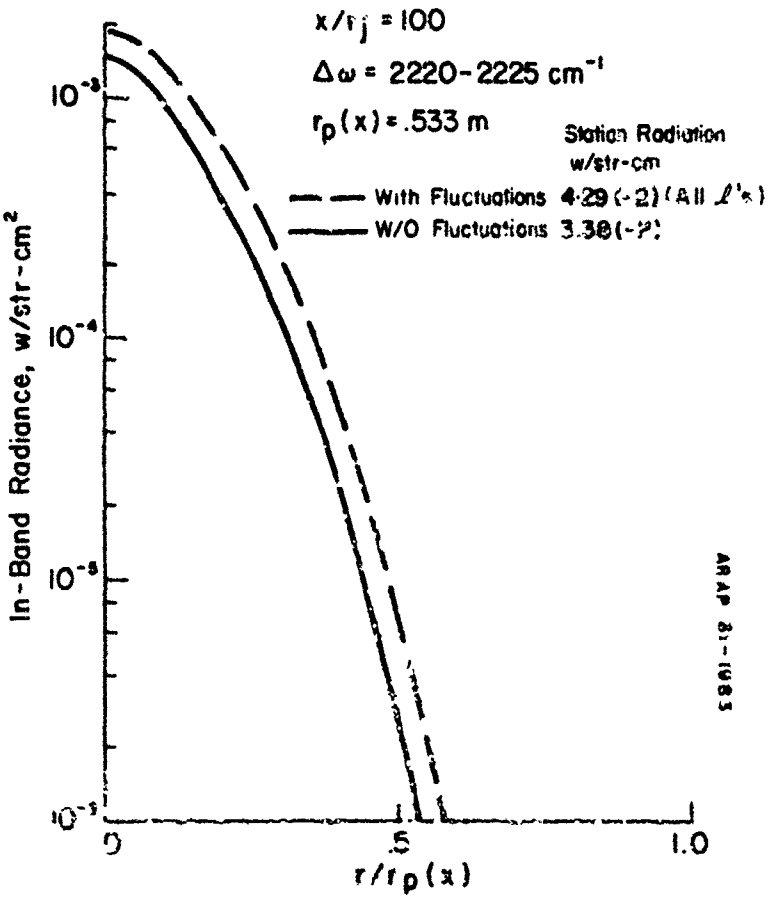

FIGURE 33. Radial Distribution of In-Band Source Radiance Across the Plume at $x/r_j = 100$.

The augmentation of the plume radiance off the axis of the plume is larger in the 2220 - 2225 cm^{-1} bandpass than for the blue spike region. For example, at $r = 0.4r_p$, the in-band radiance is increased by factors of 3.1, 2.4, and 2.4 for the three axial locations x/r_j = 10, 40, and 100. The augmentation due to turbulence is nearly three times greater in the 2220 - 2225 cm^{-1} bandpass, as expected from the greater temperature sensitivity of this region of the spectrum at temperature levels that correspond to afterburning exhaust plumes. However, the mean radiance also has this sensitivity and the radiance near the plume axis is sufficiently large to make the turbulence augmentation a small addition in this particular wavelength and for the tactical missile class of plumes.

The relative importance of the turbulent fluctuations over the entire plume length for the 2220 - 2225 cm^{-1} bandpass is shown in Figure 34. In this particular example, the total plume mean intensity with the turbulent fluctuations is only 6 percent greater than that calculated without the contributions from the fluctuations. This rather small increase is the result of the dominant contribution by the less turbulent, higher temperature inner regions of the plume (i.e., Figures 14, 22, and 23).

At the outer edges, the turbulent fluctuations provide an enhanced radiance. Spectral distributions in the 2220 - 2225 cm^{-1} bandpass at x/r_j = 10, 20, 40, and 100 are given in Figures 35, 36, 37, and 38, respectively. In these spectra, calculated at 0.01 cm^{-1} intervals, both the intensity and structure of the lines are changed by the turbulence, although the individual features of the spectral lines are not as evident as in the blue spike region. In this spectral region, there are many more lines contributing to the radiance (an order of magnitude or more, depending on temperature), and the individual features are obscurred. As mentioned previously, the augmentation of the in-band radiance for these off axis lines of sight is greater for the 2220 - 2225 cm^{-1} spectral interval. As with the 2385 - 2390 cm^{-1} spectral interval, the augmentation for lower temperature, non-afterburning plumes would be more like these results for the edges of the plume and the total signature would be increased more than that calculated here. However, we expect that the slight increase in total signature predicted here for a particular tactical missile plume to be generally true for all low altitude, intense afterburning plumes. We emphasize again that the augmentation at the outer edges, while not important for the total signature, is potentially important in spatially resolved signatures and diagnostic measurements.

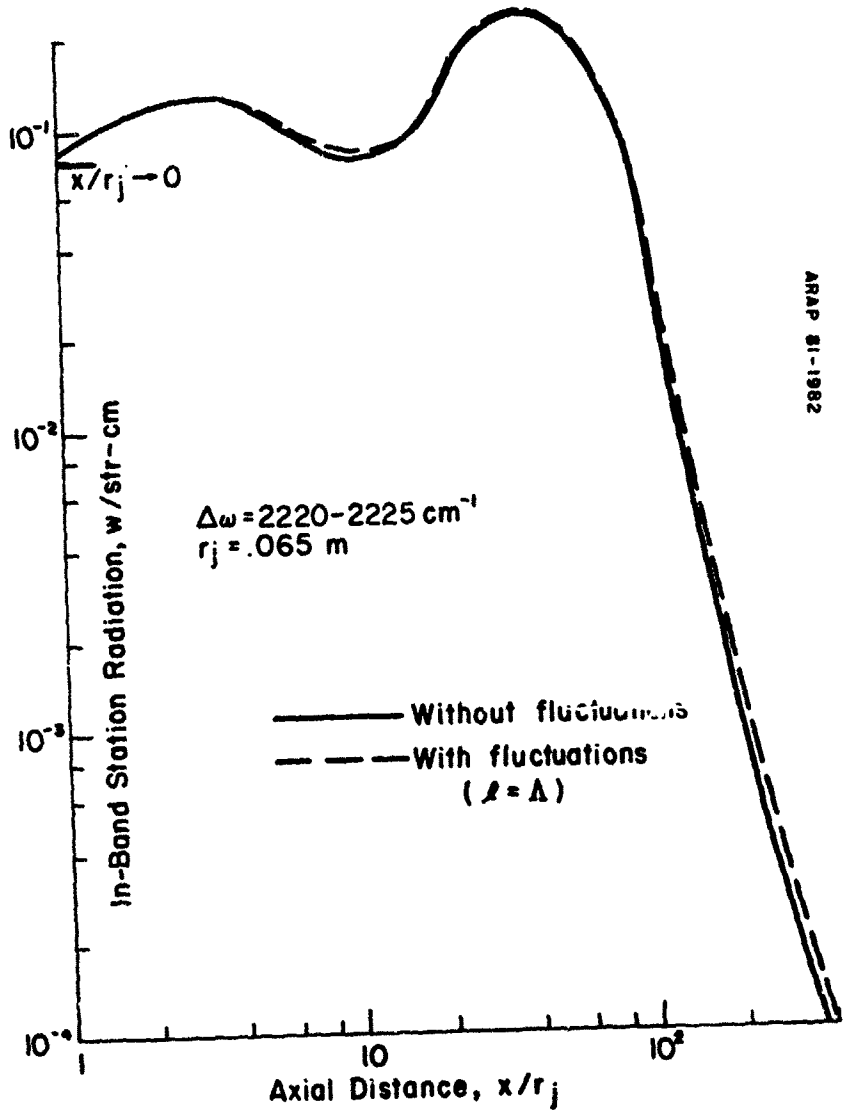

FIGURE 34. Axial Distribution of In-Band Source Station Radiation for the Model Afterburning Exhaust Plume. CO_2 Red Spike Region.

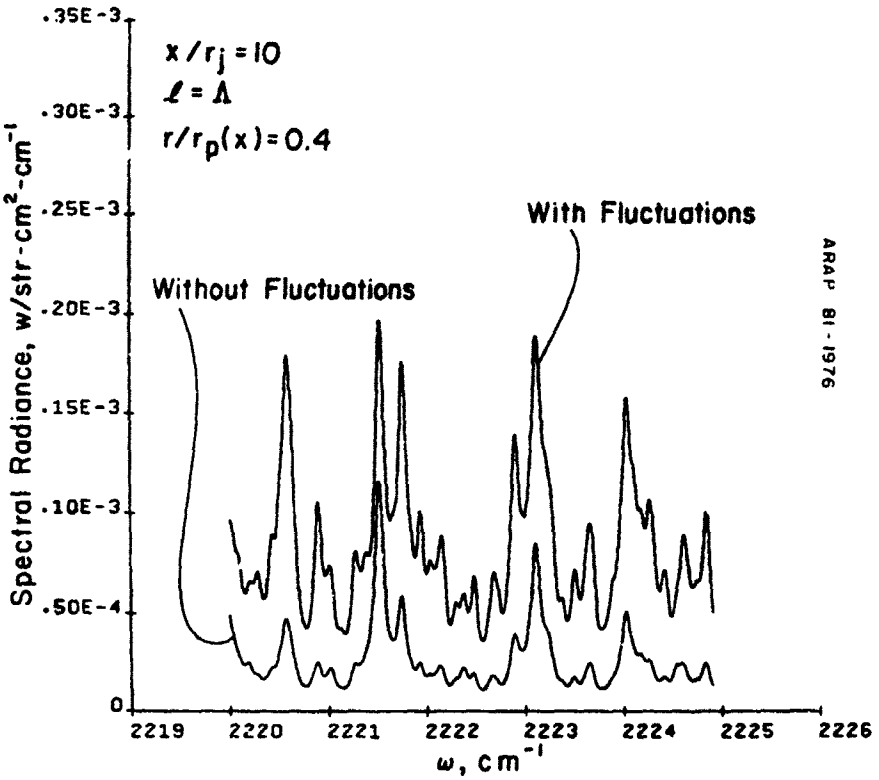

FIGURE 35. Source Spectral Radiance for a Line of Sight at the Axial Location $x/r_j = 10$ and Off the Plume Axis at $r = 0.4r_p$. CO_2 Red Spike Region.

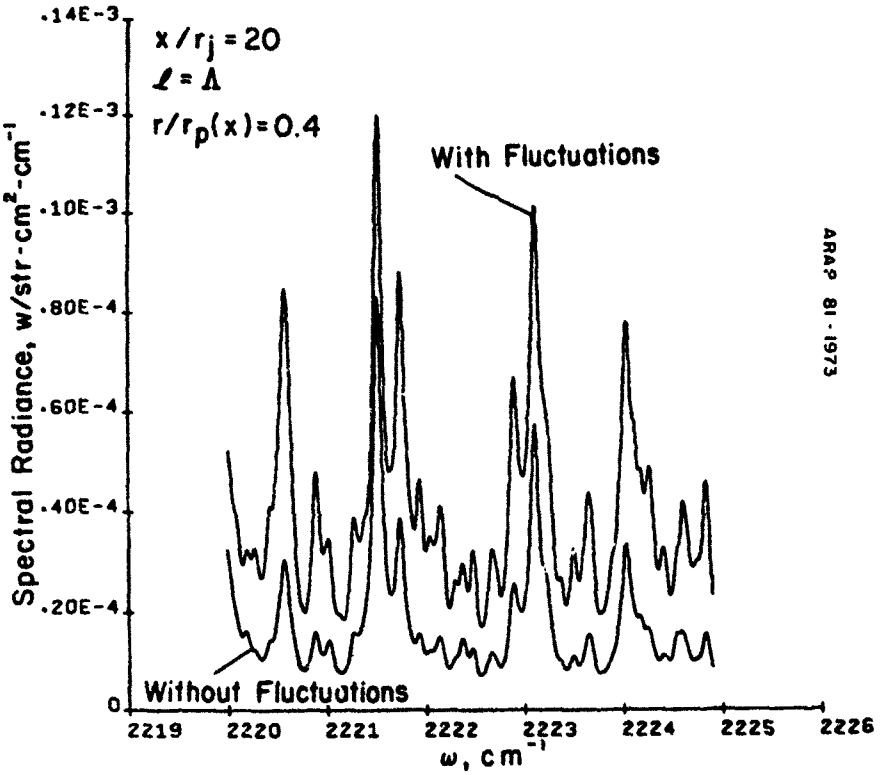

FIGURE 36. Source Spectral Radiance for a Line of Sight at the Axial Location x/r_j = 20 and Off the Plume Axis at r = $0.4r_p$. CO_2 Red Spike Region.

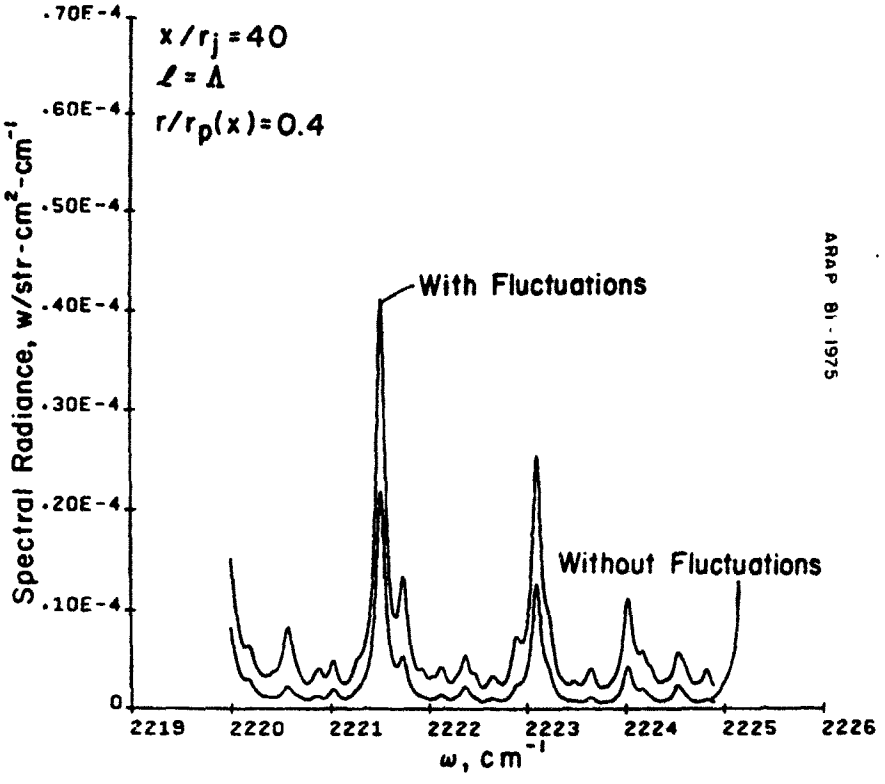

FIGURE 37. Source Spectral Radiance for a Line of Sight at the Axial Location $x/r_j = 40$ and Off the Plume Axis at $r = 0.4r_p$. CO_2 Red Spike Region.

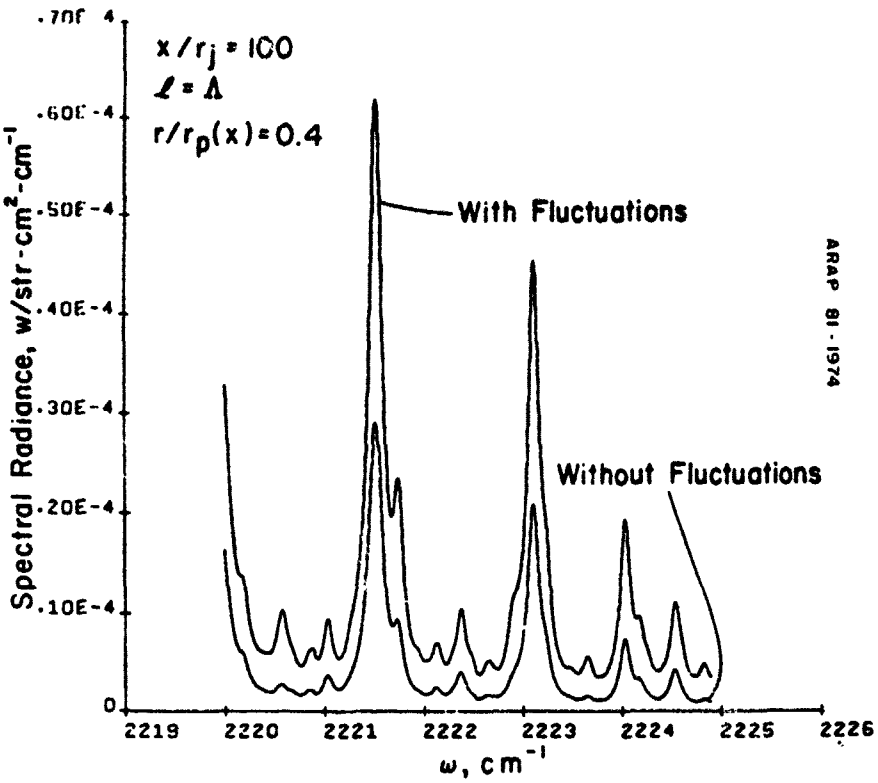

FIGURE 38. Source Spectral Radiance for a Line of Sight at the Axial Location $x/r_j = 100$ and Off the Plume Axis at $r = 0.4r_p$. CO_2 Red Spike Region.

SUMMARY AND CONCLUSIONS

This report has presented a set of predictions for the mean radiance from a turbulent, afterburning exhaust plume using a consistent set of predictions for the mean and turbulence properties in the flow, and a precise formulation for the turbulence augmented mean radiance.

The turbulent flow properties were obtained from A.R.A.P.'s RSL code, which predicts the mean and second-order correlation of turbulent fluctuations using a second-order closure model. Comparisons between these predictions and those for a two-equation, turbulence kinetic energy model (the constant pressure turbulent mixing portion of the JANNAF Standard Plume Flowfield Model) are in essential agreement for constant density, low speed flows. Differences between these predictions begin to occur for flows with density differences due either to temperature or light species. A major reason for different predictions is the different length scale models used in the two calculations, and there is some effect due to different choices of initial turbulence levels and the treatment of density fluctuations in variable density flows. For the application at hand, a primary result is that the common turbulence quantity predicted by the two codes, the turbulence kinetic energy, is comparable. An additional result is that the fluctuations of other scalar quantities, such as temperature and species concentrations develop differently from the turbulence kinetic energy. Therefore, applications such as radiance predictions from turbulent flows require that these additional scalar fluctuations be properly modeled in addition to the turbulent velocity fluctuations.

For the particular flow examined here, and with the global model for the afterburning reaction, we found that the effect of the turbulent fluctuations on the chemical reactions has only a small influence on the temperature and species concentrations in the afterburning region.

A formulation for the mean spectral radiance accounting for the additional fluctuating source and transmittance terms created by fluctuations in temperature and chemical species was derived. It is essentially a direct expansion of the monochromic radiance, up to and including second-order correlations between the fluctuations. It is uniformly valid for all optical depths but requires that the turbulent fluctuation remain small compared to their mean values, a condition that is satisfied by the flowfield used here. A unique feature is that the contributions of spatial correlations between fluctuating properties along the line of sight are explicitly obtained.

The spectrally resolved mean radiance with and without the contributions from the fluctuations was computed for two regions in the 4.3 μm CO_2 vibrational-rotational band for lines with a Lorentz line shape. The spectral information for the line strengths and positions

was taken from the AFGL compilation in the 2385 - 2390 cm^{-1} spectral region and from a synthetic compilation in the 2220 - 2225 cm^{-1} bandpass. Both compilations were verified to be adequate up to about 1500 K, but underpredict the absorption at higher temepratures.

Predictions for isolated spectral lines were used to determine the importance of the correlation between fluctuating properties along the line of sight. For optically thin paths, there is no effect of correlation. However, at intermediate and large optical depths, the correlations affect the line structure, but do not strongly affect the integrated line radiance. An important parameter governing the sensitivity of the line to the turbulent fluctuations is the lower energy state of the particular line. The sensitivity increases with an increasing lower energy level, suggesting that the least sensitive absorption is due to the lines that determine the low temperature spectra, and that the most sensitive lines are those which contribute at the higher temperatures. These observations have implications to plume diagnostics that utilize properties of the individual line shape or relative intensities of single lines.

In-band radiance for wider bandpasses (5 cm^{-1}), was predicted for the CO_2 blue spike (2385 - 2390 cm^{-1}) and red spike (2220 - 2225 cm^{-1}) spectral regions. For the blue spike region, the station radiation in the afterburning and downstream region was increased by at most 37 percent, and the total plume intensity for broadside observation was increased by 24 percent by the turbulent fluctuations. The small augmentation is because the predominant contribution to the signature comes from those lines of sight passing near the plume axis, for which the turbulent augmentation is very small. The outer edges of the plume are substantially augmented by the turbulence, by factors as much as 2.5 times the radiance without the fluctuations. These outer regions do not contribute significantly to the total plume intensity, but could be important in a spatially resolved signature.

In-band radiance in the red spike region, 2220 - 2225 cm^{-1}, has essentially the same behavior as that in the blue spike, except that the center portion of the plume is even more dominant and the augmentation by the fluctuations to the total plume intensity is even less; only 6 percent for the example used here. For this bandpass the station radiation is increased by at most 33 percent, but only downstream, where the effect on the total intensity is small. The augmentation of the radiance at the edges of the plume is substantial, but not important for the total plume intensity.

The effect of the spatial correlations of the temperature and species concentrations was very small for the radiance in these two bandpasses. The correlations affect the line structure but not the line strength and, therefore, a broader bandwidth radiance is much less sensitive to the correlation. The turbulence augmentation of the wider

bandpass radiance is due primarily to the additionl radiance source terms created by the single point correlations of turbulent fluctuations, and not to the fluctuation augmented transmittance, to which the two-point spatial correlations contribute.

We conclude that, for this specific case of a typical low altitude, afterburning exhaust plume from a tactical missile, turbulent fluctuations are not important contributors to the total plume intensity in either the CO_2 blue spike or red spike spectral regions. The predicted augmentations in these spectral regions of 24 and 6 percent, respectively, are well within the uncertainty of contemporary flowfield and signature predictions. We expect this conclusion to hold for the entire class of tactical missile plumes at low altitude.

However, the turbulence augmentation could be substantial for non-afterburning plumes such as higher altitude rocket plumes and for aircraft plumes. For this class of plumes, the flow is more like the outer edges and downstream portions of an afterburning plume, for which the predicted turbulence augmentation was a factor of from two to three. Turbulence could then substantially increase the total plume intensity from these types of exhaust plumes. For the same reasons, turbulent augmentation of radiation observed in the forward hemisphere is expected. In cases of forward hemisphere observation, much of the afterburning region of the plume is blocked by the missile structure, and only the outer edges and downstream portions contribute to the observed signature.

RECOMMENDATIONS

The results of this study suggest several extensions. There are clear implications of these results for high spectral resolution diagnostic techniques such as temperature measurements by line reversal techniques and rotational temperature measurements from the distribution of line intensities. It would be worthwhile to examine the results of these types of measurements in experiments where the flow is turbulent with the turbulent augmentation included.

An important contemporary plume diagnostic that would be affected by the predicted turbulence augmentation in the wider bandpass (~ 5 cm^{-1}) is the emission/absorption inversion technique used to infer temperature and radiating species profiles from axisymmetric flows. In these measurements, the entire transverse profiles of emission and transmission are utilized. The substantial turbulence augmentations at the outer edges of the plume suggest that the actual inferred properties are radiation weighted mean temperature and species concentrations that could differ from the presumed normal mean properties. An examination

of experimental measurements with some indication of the augmentation of the emission might indicate the effect on the inferred temperature. This application would require a prediction of the time-averaged fluctuation augmented transmittance, which was not given here explicitly, but could be easily derived.

Finally, we argue that it is probably feasible to include a prediction of the turbulence augmented radiance in the normal signature predictions. The missing element is a formulation of the turbulence augmentation for band models. Rhodes's ensemble averaging approach is probably too time consuming for most applications.[13] This capability would be most valuable for higher altitude rocket plumes or aircraft plumes. For line-by-line predictions, the formulation presented here is directly applicable. In all these applications, however, the primary requirement is a plume flowfield prediction that includes reliable models for the scalar fluctuating quantities that affect the plume emission.

REFERENCES

1. Donaldson, C. duP., Atmospheric Turbulence and Dispersal of Atmospheric Pollutants, Environmental Protection Agency, EPA-R4-73-016a, March 1973.

2. Fishburne, E.S., R.A.Beddini, and A.K. Varma, "The Computation of Afterburning Rocket Exhaust Plumes," Aeronautical Research Associates of Princeton, Inc., A.R.A.P. Report No. 283, July 1976.

3. Varma, A.K., E.S. Fishburne, and R.A. Beddini, "A Second-Order Closure Analysis of Turbulent Diffusion Flames," NASA Langley Reseach Center, NASA CR-145226, June 1977.

4. Dash, S.M., et al., "Operational Instructions for a Preliminary Version of the JANNAF Standard Plume Flowfield Model (SPF/1)," A.R.A.P. Report No. 415, June 1980.

5. Pergament, H.S., et al., "The Naval Weapons Center Target Signature Code," A.R.A.P. Report No. 380, February 1979.

6. Ludwig, C. et al., "Development and Validation of a Standardized Infrared Radiation Model (SIRRM)," JANNAF Standard Plume Model Workshop, U.S. Army Missile Command, Huntsville, AL, 2-3 April 1981.

7. Dash, S.M., and H.S. Pergament, "A Computational Model for the Prediction of Jet Entrainment in the Vicinity of Nozzle Boattails (The BOAT Code)," NASA Langley Research Center, NASA CR-3175, December 1978.

8. Fishburne, E.S., and A.K. Varma, "Investigations of Chemical Reactions in a Turbulent Media," Acta Astronautica, Vol. 6, 1979, pp. 297-308.

9. Free Turbulent Shear Flows, Vols. I & II, NASA Langley Research Center, July 1972. (NASA SP-321, publication, UNCLASSIFIED.)

10. Abramovich, G.N., The Theory of Turbulent Jets, The MIT Press, Cambridge, MA, 1963, Chapter 7.

11. Ludwig, C.B., et al., Handbook of Infrared Radiation from Combustion Gases, NASA SP-3080, 1973.

12. Young, S.J., "Nonisothermal Band Model Theory," The Aerospace Corporation, SAMSO-TR-76-207, September 1976.

13. Rhodes, R.P., "The Effect of Turbulent Fluctuations on the Infrared Radiation from Rocket Plumes," 12th JANNAF Plume Technology Meeting, CPIA Publication 332, Vol. III, December 1980, pp. 81-97.

14. McClatchey, R.A., et al., "AFCRL Atmospheric Absorption Line Parameters Compilation," Air Force Geophysics Lab., AFCRL-TR-73-0096, January 1973.

15. McCullough, R.W., "Compilation of CO_2 Rotational Lines Including Transitions That Are Important at Temperatures up to 2000°K, Aeronautical Research Associates of Princeton, Inc., unpublished, December 1980. (paper, UNCLASSIFIED.)

16. Draper, J.S., L.S. Bernstein, and W.K. Cheng, "Fluctuating Emission from Molecular Vibrational-Rotational Bands," J. Quart. Spectrosc. and Radiat. Transfer, Vol. 23, 1980, pp. 323-326.

17. Tan, E., and P.J. Foster, "Radiation Through a Turbulent Medium," Sixth International Heat Transfer Conference, Toronto, Canada, Vol. 3, 1978, pp. 403-408.

18. Bernstein, L.S., D.C. Robertson, and J.A. Conant, "Band Model Parameters for the 4.3 μm CO_2 Band from 200 to 3000°K - II. Predictions, Comparison to Experiment, and Application to Plume Emission - Absorption Calculations," J. Quart. Spectrosc. Radiative Transfer, Vol. 23, 1980, pp. 169-185.

19. Bernstein, L.S., "Band Model Parameters for the Parallel Bands of Linear Triatomic Molecules - I. Theory," J. Quart. Spectrosc. Radiative Transfer, Vol. 23, 1980, pp. 157-167.

Appendix A
NUMERICAL EVALUATION OF INTEGRALS

There are two types of integrals to be evaluated in the expression for the time-averaged radiance. One is the integral over the optical path, and the second is the integral of the correlation coefficient over the geometric distance along the line of sight. The two integrals are treated similarly, but the numerical quadratures are different. Each will be described separately.

INTEGRAL OVER THE PATH

This integral is of the form

$$I = \int_0^L F(s) k_o \bar{c} \exp\left(-\int_0^s k_o \bar{c} ds'\right) ds \qquad \text{(A-1)}$$

where F(s) is any form of the integrand [even including other integrals, i.e., Eq. (18)]. The independent variable is transformed to optical depth

$$\tau = \int_0^s k_o \bar{c} ds' \qquad \text{(A-2)}$$

$$I = \int_0^{\tau_L} F(\tau) \exp(-\tau) d\tau \qquad \text{(A-3)}$$

The optical path can vary between very small and very large values, $0 < \tau < \infty$. Because of the exponential weighting, a single quadrature scheme may not be uniformly accurate. For example, if $\tau_L << 1$, then the entire optical path makes a contribution to the integral, while if $\tau_L >> 1$, only the thin layer of plume closest to the observer determines the radiance. In order to correctly account for these effects in a uniformly accurate manner, the numerical evaluation of Eq. (A-3) was performed with two quadrature schemes, depending on the value of the total optical depth.

	Limits of Integration	Integration Scheme
$\tau_L < 10$	$0 \leq \tau \leq \tau_L$	Lobatto
$\tau_L > 10$	$0 \leq \tau \leq \infty$	Laguerre

In the case where $\tau_L < 10$, the variable of integration is $\xi = \tau/\tau_L$, and the integral is

$$I = \int_0^{\tau_L} F(\tau)\ e^{-\tau}\ d\tau = \tau_L \sum_{i=1}^{N} F(\tau_i)\exp(-\xi_i \tau_L) w_i \quad . \qquad \text{(A-4)}$$

where ξ_i are the roots, and w_i the weights of the integration. For the large optical path limit,

$$I = \int_0^{\infty} F(\tau)\ e^{-\tau}\ d\tau = \sum_{i=1}^{N} F(\tau_i)\ w_i \ . \qquad \text{(A-5)}$$

In both cases, N = 16 points [half of a 30 point scheme for the finite path length case, Eq. (A4)]. These numerical quadratures were highly accurate and gave essentially exact results for all optical depths when compared to cases that could be evaluated analytically [constant values for the integrand F(s)]. The results were insensitive to the choice of cut-off between the finite and infinite optical depth limits.

INTEGRALS OVER THE SPATIAL CORRELATION COEFFICIENT

These integrals are of the form

$$I = \int_0^{s} F(s')\ \exp(-\ |s - s'|/\ell) ds' \qquad \text{(A-6)}$$

Again, because of the exponential weighting, an arbitrary numerical quadrature (such as a trapezoidal rule) is not uniformly accurate unless the increments are always small compared to ℓ, the correlation length. To circumvent this inconvenience, the variable of integration was tranformed to

$$\xi = \exp(-\ |s - s'|/\ell) \quad , \text{ so that}$$

$$I = \ell \int_0^{\xi} F(\xi)\, d\xi \qquad \text{(A-7)}$$

This integral was evaluated by a normal, trapezoidal rule. The numerical evaluation gave essentially exact results for arbitrary values of ℓ. It is this convenient transformation that mitigated against us examining other forms of correlation coefficients.

Appendix B
DERIVATIVES OF THE PLANCK FUNCTION AND SPECTRAL ABSORPTION COEFFICIENT

PLANCK FUNCTION

$$B_\omega(T) = \frac{C_1\omega^3}{\exp(hc\omega/KT) - 1} \tag{B-1}$$

Let $X = hc\omega/KT$, then

$$T\ dB/dT = BXe^X/(\exp X - 1) \tag{B-2}$$

and

$$T^2\ d^2B/dT^2 = 2(T\ dB/dT)(T/B\ dB/dT - 1 - X/2) \tag{B-3}$$

ABSORPTION COEFFICIENT

The spectral absorption coefficient for a rotational line is

$$k_i = S_i(T)f(\alpha_i) \tag{B-4}$$

where $S_i(T)$ is the line strength, $f(\alpha)$ is the line shape function, and α_i the half-width for the i^{th} spectral line with center wavenumber at ω_{oi}. We assume a Lorentz line shape

$$f(\alpha_i) = 1/\pi\ \frac{\alpha i}{\alpha_i^2 + (\omega - \omega_{oi})^2} \tag{B-5}$$

The line strength is given by

$$S_i(T) = pN_o \frac{S_{oi}\exp(-hc\tilde{E}_o/KT)[1 - \exp(-hc\tilde{\omega}/KT)]Q_v(T_o)T_o/T}{Q_R(T)Q_v(T)\exp(-hc\tilde{E}_o/KT_o)[1 - \exp(-hc\tilde{\omega}/KT_o)]} \quad \text{(B-6)}$$

S_{oi} is the line strength at the reference temperature T_o, and E_o is the energy of the lower level of the particular vibrational-rotational transition which is responsible for the line. Q_R and Q_v are the rotational and vibrational partition functions, respectively. The first exponential term accounts for the distribution of molecules in the energy state E_o (the Boltzman factor), and the second exponential term accounts for stimulated emission. The temperature ratio T_o/T is explicitly included here to account for the fact that S_o is defined on a per molecule basis.* The temperature ratio is conventionally carried as a separate term.

The partial derivatives of the absorption coefficient are calculated in the following manner.

$$\partial k/\partial T = \partial S/\partial T\, f + S\partial f/\partial \alpha_i\, \partial \alpha_i/\partial T \quad \text{(B-7)}$$

$$\partial k/\partial c = S\partial f/\partial \alpha_i\, \partial \alpha_i/\partial c \quad \text{(B-8)}$$

$$\frac{\partial^2 k}{\partial T^2} = \frac{\partial^2 S}{\partial T^2} f + 2\frac{\partial S}{\partial T}\frac{\partial f}{\partial \alpha_i}\frac{\partial \alpha_i}{\partial T} + S\frac{\partial^2 f}{\partial \alpha_i^2}\left(\frac{\partial \alpha_i}{\partial T}\right)^2 + S\frac{\partial f}{\partial \alpha_i}\frac{\partial^2 \alpha_i}{\partial T^2} \quad \text{(B-9)}$$

$$\frac{\partial^2 k}{\partial T \partial c} = \frac{\partial S}{\partial T}\frac{\partial f}{\partial \alpha_i}\frac{\partial \alpha_i}{\partial c} + S\frac{\partial^2 f}{\partial \alpha_i^2}\frac{\partial \alpha_i}{\partial c}\frac{\partial \alpha_i}{\partial T} + S\frac{\partial f}{\partial \alpha_i}\frac{\partial^2 \alpha_i}{\partial c \partial T} \quad \text{(B-10)}$$

$$\frac{\partial^2 k}{\partial c^2} = S\frac{\partial^2 f}{\partial \alpha_i^2}\left(\frac{\partial \alpha_i}{\partial c}\right)^2 + S\frac{\partial f}{\partial \alpha_i}\frac{\partial^2 \alpha_i}{\partial c_i^2} \quad \text{(B-11)}$$

Each of these terms is defined below:

*$k(cm^{-1}) = \overline{k(molecule^{-1})} \cdot N = kN_o(N/N_o) = kN_o pT_o/T$ where N is the molecular number density and p the pressure. We define the absorption coeffcient to be $kN_o pT_o/T$.

$$f(\alpha_i) = \alpha_i/\pi(\alpha_i^2 + \Delta\omega^2) \tag{B-12}$$

$$\partial f/\partial\alpha_i = f(1 - 2\pi\alpha_i f)/\alpha_i \tag{B-13}$$

$$\partial^2 f/\partial\alpha_i^2 = 2\pi f^2(4\pi\alpha_i f - 3)/\alpha_i \tag{B-14}$$

$$\alpha_i = \alpha_o p(T_o/T)^{1/2}(\gamma_i c + \gamma_j c_j) \tag{B-15}$$

$$T\ \partial\alpha_i/\partial T = -\alpha_i/2 \tag{B-16}$$

$$T^2\ \partial^2\alpha_i/\partial T^2 = 3\alpha_i/4 \tag{B-17}$$

$$\partial\alpha_i/\partial c = \alpha_o p(T_o/T)^{1/2}\ (\gamma_i - \gamma_j) \tag{B-18}$$

$$\partial^2\alpha_i/\partial c\partial T = -1/2\ \partial\alpha_i/\partial c \tag{B-19}$$

γ_i and γ_j are constant coefficients which account for self and foreign gas broadening. In this work, $\gamma_i = 1.4$, $\gamma_j = 1.07$, and $c_j = 1 - c$. For these conditions,

$$\partial^2\alpha_i/\partial c^2 = 0\ . \tag{B-20}$$

Derivatives of the temperature dependent portion of the absorption coefficient are more complicated. First, the partition functions are (for CO_2):

rotation: $$Q_r(T) = T/T_o \tag{B-21}$$

vibration:

$$Q_v(T) = \frac{1}{(1 - \exp - h\bar{c}\omega_1/KT)^2(1 - \exp - h\bar{c}\omega_2/KT)(1 - \exp - h\bar{c}\omega_3/KT)} \tag{B-22}$$

where $\omega_1 = 667.379\ cm^{-1}$, $\omega_2 = 1388.187\ cm^{-1}$, $\omega_3 = 2349.146\ cm^{-1}$.

Normally, the stimulated emission term and Q_v at the reference temperature, T_o, (296°K), which are nearly unity, are not explicitly included in Eq. (B6).

For the purpose of evaluating the derivative of S(T), we define the following terms:

$$\begin{aligned} X_o &= hc\mathcal{E}_o/KT \quad , & y_o &= X_o e^{-X_o}/(1 - e^{X_o}) \\ X &= hc\omega/KT \quad , & y &= Xe^{-X}/(1 - e^{-X}) \\ X_1 &= hc\omega_1/KT \quad , & y_1 &= X_1 e^{-X_1}/(1 - e^{-X_1}) \\ X_2 &= hc\omega_2/KT \quad , & y_2 &= X_2 e^{-X_2}/(1 - e^{-X_2}) \\ X_3 &= hc\omega_3/KT \quad , & y_3 &= X_3 e^{-X_3}/(1 - e^{-X_3}) \end{aligned}$$

then,

$$\frac{T\partial S}{\partial T} = S(T)(X_o - 2 - y - 2y_1 - y_2 - y_3) \tag{B-23}$$

$$T^2 \frac{\partial^2 S}{\partial T^2} = -T\frac{\partial S}{\partial T} + T\frac{\partial S}{\partial T}(X_o - 2 - y - 2y_1 - y_2 - y_3) \cdot$$

$$\cdot \left[-X_o + y(1 - X - y) + 2y_1(1 - X_1 - y_1) + y_2(1 - X_2 - y_2) + \right.$$

$$\left. + \ y_3(1 - X_3 - y_3)\right] \tag{B-24}$$

These derivatives determine the sensitivity of the absorption to temperature and radiating species concentration fluctuations. The primary parameters are temperature and wavelength, but another important parameter is the energy of the lower state of the transition, E_o. The ratio, $hc\mathcal{E}_o/KT$, affects the temperature dependence of the absorption. It is possible for lines with different lower state energies to have opposite temperature sensitivities. Some examples are given in Figures B1 - B6 for typical temperatures found in the plume and for wavelengths near 4.5 μm. The plots are normalized by the absorption at the line center, k_o, and the wavenumber measured from the line center, $\Delta\omega = \omega - \omega_o$ is normalized by the half-width, $\alpha_i = \alpha$, evaluated at the temperature, T.

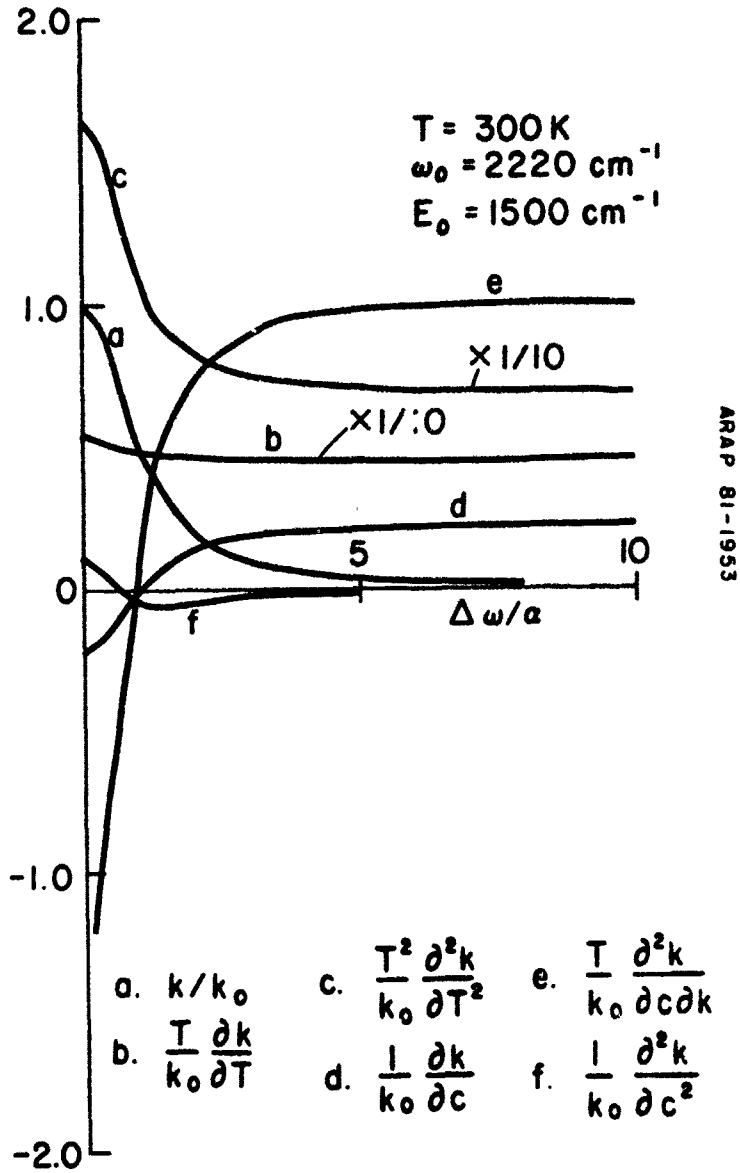

FIGURE B-1. Normalized Derivatives of the Spectral Absorption Coefficient: Single Line, Lorentz Line Shape, E_0 = 1500 cm^{-1}, T = 300 K.

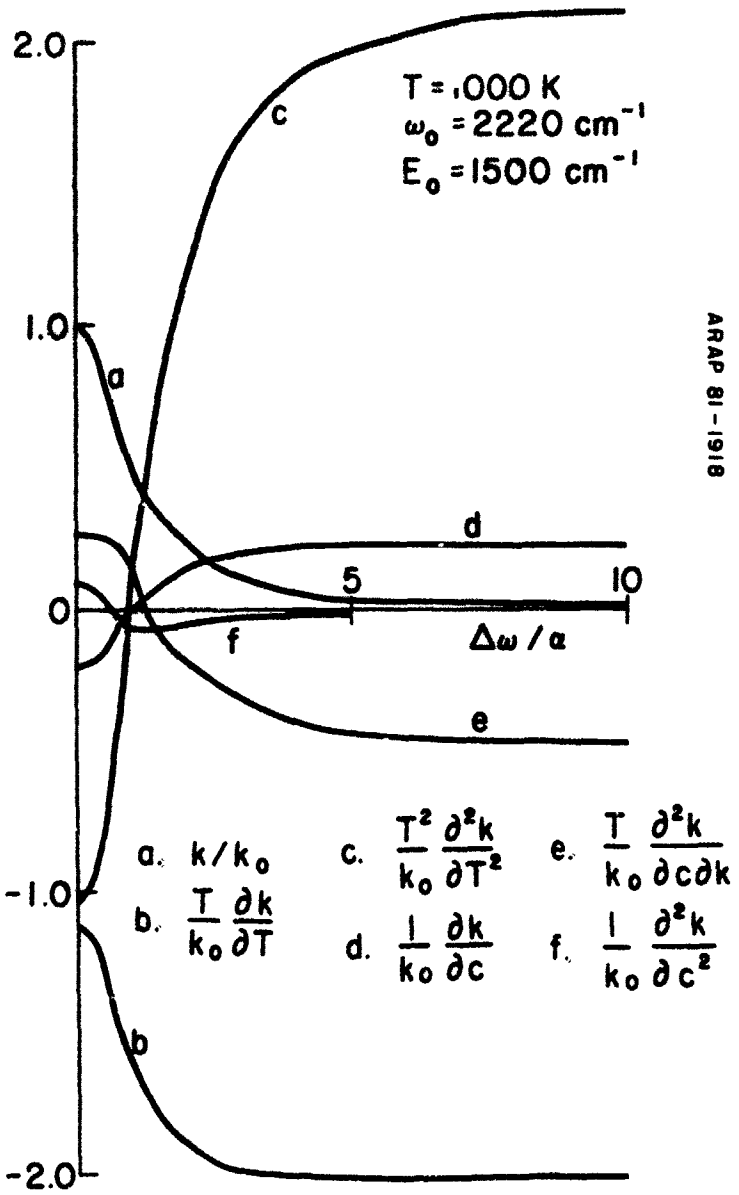

FIGURE B-2. Normalized Derivatives of the Spectral Absorption Coefficient: Single Line, Lorentz Line Shape, E_o = 1500 cm^{-1}, T = 1000 K.

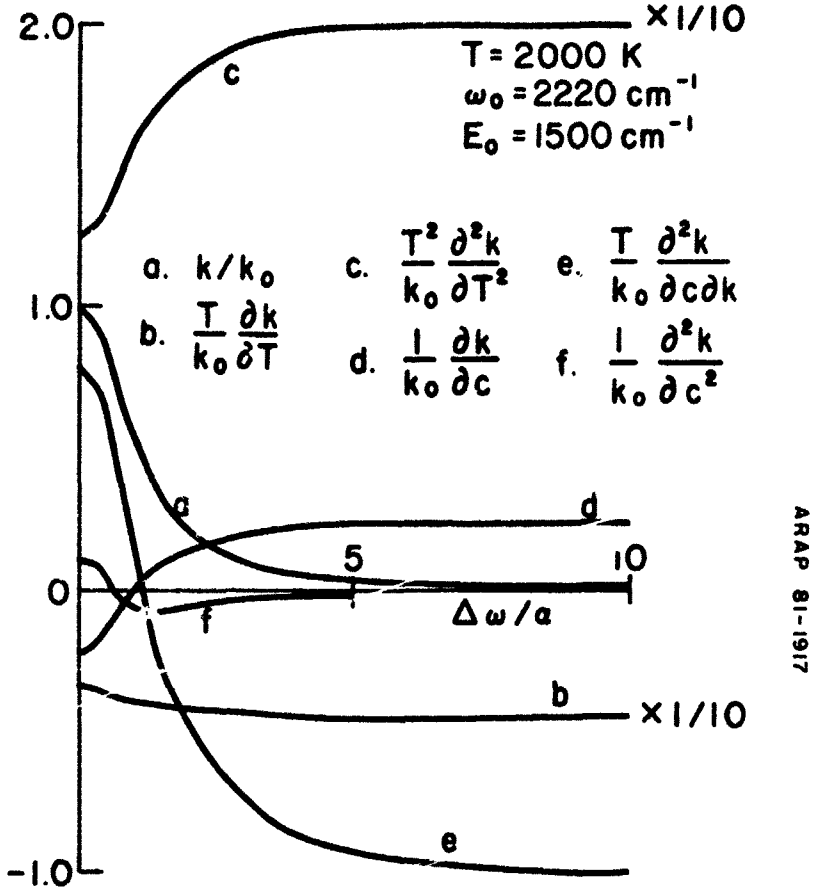

FIGURE B-3. Normalized Derivatives of the Spectral Absorption Coefficient: Single Line, Lorentz Line Shape, E_o = 1500 cm^{-1}, T = 2000 K.

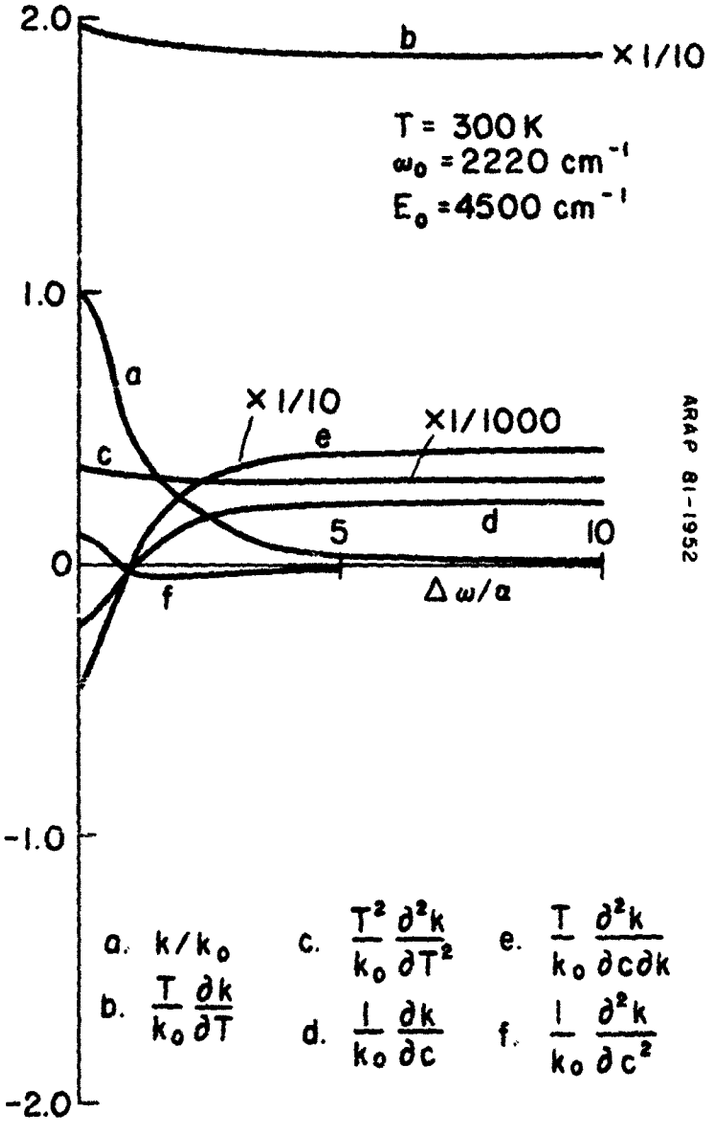

FIGURE B-4. Normalized Derivatives of the Spectral Absorption Coefficient: Single Line, Lorentz Line Shape, E_0 = 4500 cm^{-1}, T = 300 K.

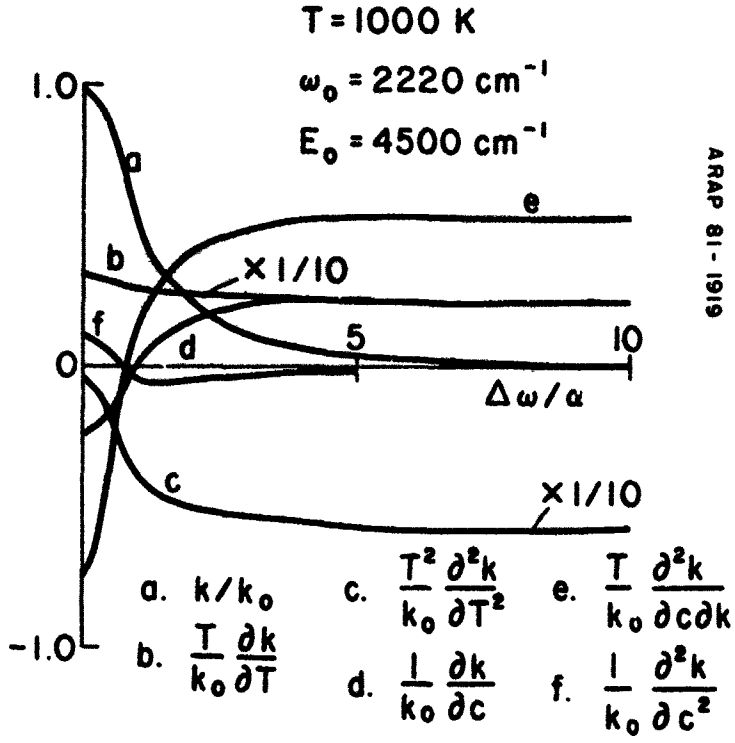

FIGURE B-5. Normalized Derivatives of the Spectral Absorption Coefficient: Single Line, Lorentz Line Shape, E_0 = 4500 cm^{-1}, T = 1000 K.

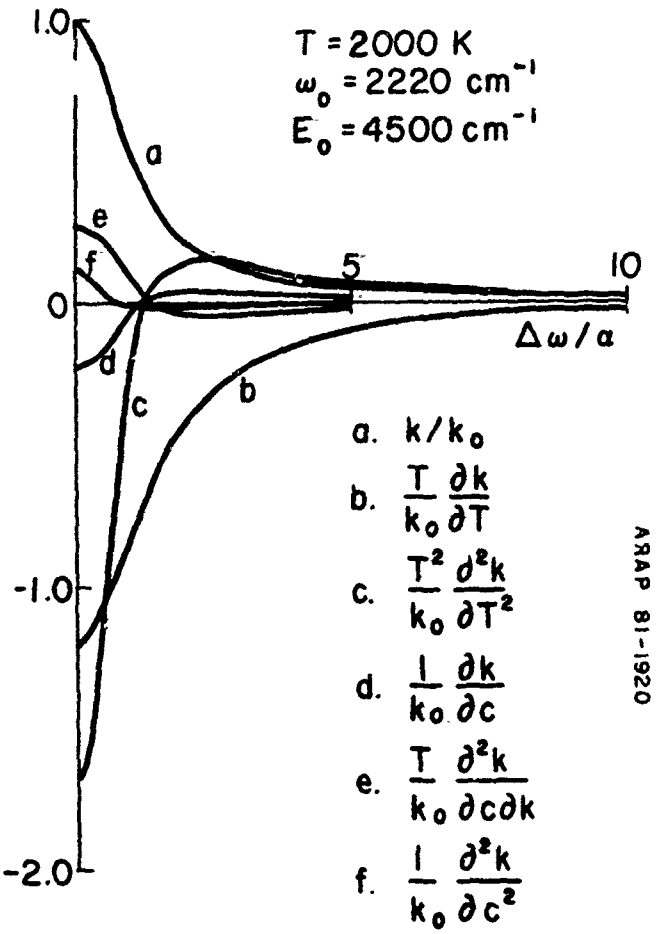

FIGURE B-6. Normalized Derivatives of the Spectral Absorption Coefficient: Single Line, Lorentz Line Shape, E_0 = 4500 cm^{-1}, T = 2000 K.

NOMENCLATURE

$B_\omega(T)$	Planck function, $B_o = B_\omega(\bar{T})$
C	Scale constant for turbulent length scale
C_1	Constant in Planck function, $C_1 = 1.19088 \times 10^{-12}$ ω-cm^2/str
c	Species mole fraction (primarily for the infrared active species CO_2)
$\tilde{c}$	Speed of light
E	Activation energy
$\hat{E}$	$E/R\bar{T}$
E_o	Lower energy level of transition for an individual spectral line
$F(\xi)$	Arbitrary function
$f(\alpha_i)$	Lorentz line shape function
H	enthalpy
h	Planck's constant
K	Boltzman's constant
k_f	Forward reaction rate coefficient
$k_\omega(T)$	Spectral absorption coefficient, $k_o = k_\omega(\bar{T})$, also denoted by k
L	Geometric length of optical path through plume
ℓ	Correlation length for scalar fluctuations
N	Number density of molecules
N_ω	Spectral radiance
p	Pressure

Q_V, Q_R	Vibrational and rotational partition functions
q^2	Mean square turbulence velocity
R	Universal gas constant
r	Radial coordinate
r_j	Exhaust nozzle radius
$r_p(x)$	Plume radius at axial location, x
r_{TT}, r_{cT}, r_{cc}	correlation coefficients between fluctuating temperature and species
S	Line strength
s	Distance along line of sight
T	Temperature
u	Mean axial velocity
u', v', w'	Turbulence velocities in x, r, θ direction
w_i	Weights for Gaussian Quadrature
x	Axial coordinate
α	Reactant mass fraction
α_i	Spectral line half-width
β	Reactant mass fraction
γ	Product mass fraction
γ_i	Collision broadening coefficient
ε	Turbulence energy dissipation
Λ	Turbulence velocity integral scale
τ	Optical depth
ρ	Fluid density

ω	Wavenumber
ξ	Variable of integration

Subscripts

jet,j	Jet exit
∞	Ambient
0	Reference condition or evaluated at mean temperature
pk	Peak value
m	Axis value
$\|_{s'}, \|_{s''}$	Evaluated at the location, s', s"
i,j	Chemical species i,j

Superscripts

$\overline{\quad}$	Mean (time-average)
'	Fluctuating (note the prime is also used to denote a dummy variable of integration

INITIAL DISTRIBUTION

14 Naval Air Systems Command
- AIR-00D4 (2)
- AIR-03A (1)
- AIR-03P22, A. R. Habayeb (1)
- AIR-330 (1)
- AIR-340C (1)
- AIR-370D, E. Hooper (1)
- AIR-512 (1)
- AIR-533 (1)
- AIR-533, E. Cosgrove (1)
- AIR-536 (2)
- AIR-53634F, D. Caldwell (1)
- AIR-5492, W. Whiting (1)

2 Chief of Naval Operations
- OP-35E, L. Triggs (1)
- OP-982F3, Capt. L. E. Pellock (1)

7 Chief of Naval Material
- MAT-08 (1)
- NSP-00 (1)
- NSP-01 (2)
- NSP-10 (1)
- NSP-20 (1)
- PM-22, High Energy Laser (HEL) Project Office (1)

3 Naval Electronic Systems Command
- NAVELEX-03G, R. Golding (1)
- NAVELEX-PME-107-52, A. Ritter (1)
- NAVELEX-PME-107, J. O'Brian (1)

9 Naval Sea Systems Command
- SEA-03D (1)
- SEA-62 (1)
- SEA-62R (1)
- SEA-62R1, T. Tasaka (1)
- SEA-62R2 (1)
- SEA-99612 (4)

1 Chief of Naval Research, Arlington (ONR-473)

1 Assistant Secretary of the Navy (Research, Engineering and Systems, Dr. Hubert Wang)

1 David Taylor Naval Ship Research and Development Center, Bethesda (Code 2833, R. Burns)

2 Naval Intelligence Support Center
- NISC-40, Perry Roberts (1)
- NISC-50, Hank Bowers (1)

2 Naval Ocean Systems Center, San Diego
- Code 133 (1)
- Code 532, Dr. J. H. Richter (1)

3 Naval Ordnance Station, Indian Head
- Code 5252, G. A. Buckle (1)
- Code DGS (1)
- Technical Library (1)

4 Naval Research Laboratory
  Code 1409, Dr. Kirshenstein (1)
  Code 5754, Dr. E. M. Alexander (1)
  Code 8320, L. Ruhnke (1)
  Technical Library (1)
2 Naval Surface Weapons Center, Dahlgren
  Dr. G. Moore (1)
  Technical Library (1)
2 Naval Surface Weapons Center Detachment, White Oak Laboratory, Silver Spring
  Code 213, A. Hirshman (1)
  Code KEM (1)
3 Pacific Missile Test Center, Point Mugu
  Code 0141.2, C. Elliott (1)
  Code 1233, Dr. N. Van Slyke (1)
  Code 1232, D. Stowell (1)
1 Assisstant Navy Deputy, SAM-D/ASMS Joint Project, Redstone Arsenal
1 Naval Plant Representative Office, Sunnyvale (Code SPL-3124)
1 Army Armament Materiel Readiness Command, Rock Island (DRSAR-LEM)
1 Army Armament Research and Development Command, Dover (B. Hornstein)
1 Army Ballistics Research Laboratories, Aberdeen Proving Ground (DRDAR-TSB-S (STINFO))
3 Redstone Arsenal
  AMCPM-MDER (1)
  AMSMI-RDD (1)
  AMSMI-RDK, Dr. B. Walker (1)
1 Army Missile Research & Laboratory Advanced Sensors Directorate, Redstone Arsenal (DRDMI-TEI, H. T. Jackson)
1 Night Vision Laboratory, Fort Belvoir (DRSEL-NV-VI, R. Moulton)
1 White Sands Missile Range (ERADCOM, DELAS-EO-MO, Atmospheric Sciences Laboratory, T. Hall)
1 Air Force Armament Laboratory, Eglin Air Force Base (AFATL/DLMT-3, Mack Gay)
3 Air Force Geophysics Laboratory, Hanscom Air Force Base
  OPA, R. Fenn (1)
  OPI, Stop 30, R. McClatchey (1)
  OPR, Stop 30, B. Sanford (1)
1 Air Force Rocket Propulsion Laboratory, Edwards Air Force Base (DACP, Dr. Andrepoint)
4 Air Force Rocket Propulsion Laboratory, Edwards Air Force Base (Plans and Programs Office)
2 Air Force Rocket Propulsion Laboratory, Edwards Air Force Base (Technical Library)
2 Air Force Wright Aeronautical Laboratories, Wright-Patterson Air Force Base
  AFWAL/AAWP, Dr. Richard Sanderson (1)
  AFWAL/PORA-1, J. Fultz (1)
2 Arnold Air Force Station
  Research Branch, Dr. W. K. McGregor (1)
  Special Projects, ETF-PO, C. R. Darlington (1)
1 Arnold Engineering Development Center, Arnold Air Force Station (Dr. Herman Scott)
1 Directorate of Armament Development, Eglin Air Force Base
1 Under Secretary of Defense for Research & Engineering, Electronics & Physical Sciences (J. MacCallum, Room 3D1079)
2 Defense Advanced Research Projects Agency, Arlington
  S. Zakanycz (1)
12 Defense Technical Information Center
1 Department of Defense Explosives Safety Board, Alexandria (6-A-145)

1 George C. Marshall Space Flight Center (S&E, Dr. T. Greenwood)
1 National Aeronautics and Space Administration (Code RP)
1 Aerodyne Research, Inc., Bedford, MA (Dr. Draper)
1 Aerojet Tactical Systems, Sacramento, CA (J. Coughlin), via AFPRO
2 Aeronautical Research Associates of Princeton, Inc., Princeton, NJ
    B. Pearce (1)
    Technical Library (1)
1 Atlantic Research Corporation, Alexandria, VA
2 Brigham Young University, Provo, UT
    Dr. D. L. Smoot (1)
    Dr. Lane Compton (1)
1 California Institute of Technology, Jet Propulsion Laboratory, Pasadena, CA
1 Calspan Corporation, Buffalo, NY (W. J. Sheeran)
1 Environmental Research Institute of Michigan, Ann Arbor (R. Legault)
1 General Applied Sciences Laboratory, Westbury, NY
1 General Dynamics Corporation, Pomona Division, Pomona, CA (E. Piesik)
1 General Research Corporation, McLean, VA (SWL Division, Russ Rollins)
2 Grumman Aerospace Corporation, Bethpage, NY
    Experimental Dymamics Research Group (1)
    Research Department, J. Selby (1)
1 Hercules Incorporated, Allegany Ballistics Laboratory, Cumberland, MD (G. Williams)
1 Hercules Incorporated, Magna, UT (R. J. Zeamer)
1 Hercules Incorporated, McGregor, TX
1 Hughes Aircraft Company, Culver City, CA
4 Institute for Defense Analyses, Arlington, VA
    L. Biberman (1)
    W. Holzer (1)
    Dr. R. Oliver (1)
    Dr. H. Wolfhardt (1)
1 Johns Hopkins University, Applied Physics Laboratory, Laurel, MD (H. Hall)
1 Lockheed Missiles and Space Company, Sunnyvale, CA (R. LeCount)
1 Martin-Marietta Corporation, Denver, CO (R. E. Compton, Jr.)
1 Martin-Marietta Orlando Aerospace, Orlando, FL (J. W. Fisher)
2 McDonnell Douglas Astronautics, Huntinton Beach, CA
    Advanced Propulsion Department, Department A-833, Group P-BBFO (1)
    D. Chow (1)
1 Northrop Corporation, Aircraft Division, Hawthorne, CA (Lloyd Tanabe)
1 Raytheon Manufacturing Company, Missile Systems Division, Bedford MA (B. DeRosa)
1 Rockwell International Corporation, Canoga Park, CA (R. A. Smith)
1 Science Applications, Inc., Gas Dynamics and Energy Division, Santa Ana, CA (R. J. Hoffman)
1 Science Applications, Inc., Princeton, NJ (H. Pergament)
1 Scientific Technology Associates, Inc., Princeton, NJ (CN 5203, Stokes Fishburn)
1 Spectral Science, Inc., Burlington, MA (Dr. D. C. Robertson)
1 Systems Planning Corp., Arlington, VA (D. Friedman)
1 TRW, Incorporated, Redondo Beach, CA (G. J. MacLeod)
1 The Boeing Company, Seattle, WA (Dr. J. M. Barton)
1 Thiokol Chemical Corporation, Huntsville Division, Huntsville, AL
2 Thiokol Chemical Corporation, Wasatch Division, Brigham City, UT
    N. Anderson (1)
    Webb (1)